# Analytical and Experimental Comparison of Deterministic and Probabilistic Optimization

by

*Eric Ponslet*

Dissertation submitted to the Faculty of the
Virginia Polytechnic Institute and State University
in partial fulfillment of the requirements for the degree of

DOCTOR OF PHILOSOPHY

in

Aerospace Engineering

APPROVED

Raphael T. Haftka, Co-Chairman

Harley H. Cudney, Co-Chairman

Efstratios Nikolaidis

Eugene M. Cliff

Rakesh K. Kapania

October, 1994

Blacksburg, Virginia

# Analytical and Experimental Comparison of Deterministic and Probabilistic Optimization

by

*Eric Ponslet*

Raphael T. Haftka & Harley H. Cudney, Chairs

Aerospace and Ocean Engineering

(ABSTRACT)

The probabilistic approach to design optimization has received increased attention in the last two decades. It is widely recognized that such an approach should lead to designs that make better use of the resources than designs obtained with the classical deterministic approach by distributing safety onto the different components and/or failure modes of a system in an optimal manner. However, probabilistic models rely on a number of assumptions regarding the magnitude of the uncertainties, their distributions, correlations, etc. In addition, modelling errors and approximate reliability calculations (first order methods for example) introduce uncertainty in the predicted system reliability. Because of these inaccuracies, it is not clear if a design obtained from probabilistic optimization will really be more reliable than a design based on deterministic optimization. The objective of this work is to provide a partial answer to this question through laboratory experiments – such experimental validation is not currently available in the literature.

A cantilevered truss structure is used as a test case. First, the uncertainties in stiffness and mass properties of the truss elements are evaluated from a large number of measurements. The transmitted scatter in the natural frequencies of the truss is computed and compared to experimental estimates obtained from measurements on 6 realizations of the structure. The experimental results are in reasonable agreement with the predictions, although the magnitude of the transmitted scatter is extremely small.

The truss is then equipped with passive viscoelastic tuned dampers for vibration control. The controlled structure is optimized by selecting locations for the dampers and for tuning masses added to the truss. The objective is to satisfy upper limits on the acceleration at given points on the truss for a specified excitation. The properties of the dampers are the primary sources

of uncertainties. Two optimal designs are obtained from deterministic and probabilistic optimizations; the deterministic approach maximizes safety margins while the probability of failure (i.e. exceeding the acceleration limit) is minimized in the probabilistic approach. The optimizations are performed with genetic algorithms. The predicted probability of failure of the optimum probabilistic design is less than half that of the deterministic optimum.

Finally, optimal deterministic and probabilistic designs are compared in the laboratory. Because small differences in failure rates between two designs are not measurable with a reasonable number of tests, we use antioptimization to identify a design problem that maximizes the contrast in probability of failure between the two approaches. The antioptimization is also performed with a genetic algorithm. For the problem identified by the antioptimization, the probability of failure of the optimum probabilistic design is 25 times smaller than that of the deterministic design. The rates of failure are then measured by testing 29 realizations of each optimum design. The results agree well with the predictions and confirm the larger reliability of the probabilistic design. However, the probabilistic optimum is shown to be very sensitive to modelling errors. This sensitivity can be reduced by including the modelling errors as additional uncertainties in the probabilistic formulation.

# Acknowledgements

I want to express my gratitude to Dr. Raphael T. Haftka for supervising this research for more than four years. His technical expertise, enthusiasm and imagination have been a constant encouragement throughout this project. This gratitude also extends to Dr. Harley H. Cudney and Dr. Stratos Nikolaidis for actively participating in this project for the last two years and making our weekly meetings so enjoyable and stimulating. Thanks also to Dr. William L. Hallauer for his help during my first few weeks in Blacksburg and for serving as my co-advisor during the first two years, and to Dr. Eugene M. Cliff and Rakesh K. Kapania for serving on my committee and reviewing the manuscript. I also want to acknowledge the collaboration of George Maglaras, also working towards his Ph.D. degree, during the last two years of the project. Thanks also to Pradeep Sensharma for his help with the experimental measurements.

Special thanks go to Dr. André Preumont of the Free University of Brussels, Belgium, without whom I would have never come to Blacksburg and started this Ph.D. I will always be grateful to him for this irreplaceable experience.

I also want to thank Dr. W. Keith Belvin for welcoming me at NASA Langley Research Center during the summer of 1991 and for later providing some of the experimental equipment used in this project, and Dr. Eric R. Johnson for his help with the MTS testing machine.

This research was funded in part by the National Aeronautics and Space Administration (NASA Grant NAG-1-224). This support is gratefully acknowledged.

Finally, and most importantly, I want to thank my parents for giving me a taste for learning and discovery, and my fiancée Lucie for her constant support and encouragement and for her invaluable help in preparing the manuscript during the few hectic weeks before graduation.

# Table of Contents

# List of Figures

# List of Tables

# Chapter 1
# Introduction

When designing a complex system, the designer typically has to statisfy a large number of requirements. Examples of such requirements include minimum levels of performance requested by a client, limits on the acceptable weight, size or manufacturing cost, the ability of the system to withstand mechanical loads, aggressive environmental conditions, or minimum fatigue life. A particular design can be accepted only if there is sufficient confidence that these requirements will be satisfied in the actual system. Today's design procedures have reached a high degree of sophistication and in many cases rely heavily on analytical and numerical models. These models predict the performance of the system based on given values of physical parameters like geometrical dimensions of components, material properties, ultimate stresses, and expected loads in operation, etc. Unfortunately, these parameters cannot realistically be given a unique, deterministic value. For example, the ultimate stress of a piece of structural steel depends on initial imperfections in the material, the production batch it came from, and the effects of corrosion and temperature, among other things. Similarly, the working loads on a civil engineering structure depend on the use of the structure (density of traffic on a bridge, occupancy in a building, ...), the wind velocity, the magnitude of seismic disturbances, etc... Most of these parameters are best described as random variables.

In view of such uncertainties, the designer has to take special precautions to minimize the risk of failure. Traditionally, this has been accomplished through the use of safety factors (or safety margins). In this approach, all values defining limit conditions are scaled by a given factor (or shifted by a given amount in the safety margin approach) and used as adjusted design requirements for the system. The resulting margins are supposed to "absorb" the effect of scatter in the parameters and "guarantee" adequate performance or safety of the system.

The values used for the safety factors can be adjusted based on sensitivity studies of the different performance requirements. Also, for traditional structures, these values have been continuously refined based on decades of experience. For components produced in large numbers, the history of their failures also provides valuable information to define adequate values of safety factors.

However, this approach suffers from the fact that safety factors have to be specified by the designer for each failure mode and typically each component of the structure beforehand. Even if we can relate safety factors to reliability at the component level[1], the reliability of the complete system is not explicitly evaluated. It has been shown (see for example Moses and Kinser[2]) that in order to arrive at the most reliable and least expensive system, the reliabilities of the different components have to be proportioned to their relative costs and impact on the overall reliability of the system. For complex systems this cannot be accomplished based on engineering judg'ment and experience alone.

Also, with the introduction of new technologies like composite materials (whose properties have large scatters), there is a lack of experience and data to determine appropriate values of safety factors. This leads to very conservative attitudes with respect to those technologies and reduces or even eliminates the potential weight savings that could otherwise be achieved.

Finally and most importantly, the ever increasing power of digital computers and the development of efficient optimization algorithms have led to a wide acceptance and use of automated design optimization techniques. These optimizations are almost always based on the classical deterministic design approach. As noted by Moses[3] this leads to a situation "in which each failure mode is shaved down until it is on the boundary of acceptability...[and] to a less safe design in which the probability of damage or failure is increased beyond what is usually obtained by the designer without the aid of programming methods". Moses and Kinser[2] also observe that this approach "causes so many failure modes to be constrained that conventional safety factors no longer produce the former levels of safety". These observations are supported by a number of studies. Thompson and Hunt[4] show that increasing degrees of optimization of buckling-critical structures creates increasingly severe coupling between different buckling modes which in turn leads to increased sensitivity to imperfections. Aubert *et al.*[5] studied the stability of an actively controlled truss with uncertainties in geometry, material properties and masses. They found that an optimal control scheme obtained from a deterministic formulation was unacceptably sensitive to uncertainties and easily destabilized by small perturbations in the structure. Haftka *et al.*[6] come to a similar conclusion in the case of a flexible structure with a minimum gain rate feedback control. They find that a very small mass perturbation (1% of the total mass of the structure) causes a 30% loss in damping ratio in one mode of the controlled structure.

In view of these difficulties, it is now widely recognized that a far more realistic and direct approach to design consists of explicitly including the uncertainties in a *reliability based optimization*. In this approach the scatter in the response quantities of the system is evaluated from statistical data about the scatter in the input quantities (like geometry, loading, material properties, etc.) using specialized analytical or numerical techniques. From the calculated response scatter, the probability of system and/or component failure is estimated and used in the objective function and/or constraints of an optimization formulation.

Note that there also exist intermediate techniques that optimize the system from a statistical point of view, but not as directly as the reliability based optimization approach. One such technique has been developed by Ponslet *et al.*[7] and is described in Appendix A. The approach followed there is to minimize the scatter in the most critical design requirement due to parametric uncertainties. The method is called *targeted robustness design* because it automatically selects the most critical response quantity for enhanced protection from uncertainties. The appendix presents applications of the targeted robustness technique to two active structure examples. Although the method effectively produces safer designs than deterministic optimization, it suffers from numerical conditioning problems. Also – like the safety factor approach – it does not directly minimize the probability of failure of the system. Another type of intermediate approach has been used by Bennet and Lust[8] and Parkinson *et al.*[9] for example. They perform the optimization in two steps. The first step is a conventional deterministic optimization without safety factors. Then, the sensitivities of the failure modes are computed at the optimal design point and the constraints are "padded" proportionally to their calculated sensitivities. The optimization is then repeated with the padded constraints to lead to the final design. This method assumes that the sensitivities of the constraints with respect to the uncertainties are invariant between the optimum points of the first and second step and is therefore limited to problems with nearly linear constraints.

The first direct reliability based formulation was reported by Charnes and Cooper[10] in 1958. They transformed the stochastic optimization problem into an equivalent deterministic formulation by linearly expanding the objective and constraints around the mean value of the random parameters. This approach was called *chance constrained programming technique* (CCP) and opened the door to the application of mathematical programming for the solution of reliability based optimization problems. In 1967, Moses and Kinser[2] used mathematical programming to minimize the weight of a ten-bar structure with a prescribed safety level. In 1974, Hasofer

and Lind[11] introduced a refined version of the first order reliability analysis by expanding the limit state functions around the most probable failure point (MPP) instead of the mean of the random parameters. This reduced the truncation errors due to the non-linearity of the response functions. The price paid for this improvement is a large increase in computational expense since iterations are needed to locate the MPP. Since then, the number of publications reporting optimal reliability-based design has increased exponentially, especially in the civil and ocean engineering communities. Works by Moses and Stevenson[12], Davidson, Felton and Hart[13,14], Parimi and Cohn[15,16], Frangopol[17,18,19,20], or Feng and Moses[21,22] in civil engineering, Sørensen and Christensen[23] or Baker and Vrouwenvelder[24] in ocean engineering, and Rao[25,26] in general engineering are only a few examples.

However, probabilistic optimization has not enjoyed the same popularity in the industrial world as deterministic optimization[19]. This lack of confidence is due to a number of factors. One is the long experience with the traditional safety factor approach and the lack of training of engineers in the statistical theory and its applications. Another is the fact that, in order to be accepted and used by engineers, the tools for probabilistic analysis and optimization must be integrated step by step around the existing deterministic tools[27]. It is interesting to note that, probably for that reason, the few industrial implementations have used Monte Carlo simulations to evaluate the statistics of the response (RASOS[24], developed by a European consortium and Probabilistic Design System (PDS) developed by Pratt & Whitney[27,28] for example). The FEBREL[29] package developed by Rockwell international, however, includes options for first and second order reliability methods in addition to Monte Carlo simulation. The obvious advantage of the Monte Carlo method is that it interfaces with existing design codes without requiring any modifications in these codes. The price to pay is of course the very significant and sometimes prohibitive amount of computational time needed for the analysis. In cases where the deterministic analysis is too expensive to be run repeatedly in Monte Carlo simulations, analytical response surfaces can be fitted to the results of a limited number of deterministic analyses corresponding to different combinations of parameter perturbations. Techniques from the design of experiments can be used to select these combinations in an optimal manner (see for example Fox[30]). The other advantage of Monte Carlo methods is that they provide full distributions of the output quantities (not just moments of those distributions) and that they are applicable to any problem, regardless of non-linearities.

However, the slow response of the industrial world can also be explained by a number of limitations of the probabilistic design methods:

1. There is rarely sufficient data available to accurately evaluate the statistics of the random parameters. In particular, the tails of the distributions correspond to extremely rare observations so that one never has substantial evidence to support the choice of one type of distribution or the other in the tail region. Unfortunately, in some cases the predicted probability of failure is very sensitive to this choice. Ben-Haim and Elishakoff[31] give an analytical expression for the predicted failure rate using a family of normal distributions with non-normal tails to describe the random parameters. They show that relatively small changes in the tail can lead to large changes in probability of failure. Fox and Safie[32] provide an extensive discussion of the rationale for choosing particular distributions. For a simple bar in traction with random load and random strength, they show that the probability of failure predicted using normal distributions for load and strength is almost four times less than using very similar Weibull distributions ($\beta = 2$, $\eta = 100$). Moses and Stevenson[12] and Khalessi *et al.*[29] however, conclude that the effect of the standard deviations used to model the uncertainties is larger than that of the choice of distribution. In any case, information about sensitivities of optimal probabilistic designs to the statistics of the input parameters is essential to the designer[33]. The type of assumption made on the scatter in design variables can also be important; using constant standard deviations or constant coefficient of variation (C.O.V.) can lead to different designs. As noted by Torng and Yang[34], when constant standard deviations are used, the design variables tend to reach their upper bound in the optimal design because this reduces the relative value of their scatter (i.e. the C.O.V.'s), which in turn reduces the scatter in the response quantities. Note that it is not necessarily easy to decide which option is most realistic in a practical situation.

2. When approximate analytical techniques (for example mean value based or advanced first order second moment methods) are used to evaluate the output scatter, the probability of failure can only be calculated by *assuming* a particular distribution for the output quantities. For nearly linear problems with numerous random parameters, the use of normal distributions is theoretically justified by the central-limit theorem. However, for problems with more pronounced non-linearities or when the effect of one or a small number of uncertainties dominates the output scatter, the distribution of response quantities can deviate

widely from normal. To avoid having to make an assumption, some optimization methods are based on safety indices (a normalized measure of the distance from the nominal design point to the most probable failure point) rather than probabilities of failure. Those methods are called *safety index optimization* (SIO). They present similarities with the conventional safety factor approach in that they do not explicitly optimize the reliability of the system. Applications of such methods can be found in Nikolaidis and Burdisso[35] and Reddy and Grandhi[36] for example.

3. The effect of modeling errors on the predicted reliability is also a major concern. A very good discussion of the effect of modeling errors can be found in the introduction of the book by Ben-Haim and Elishakoff[31]. They present examples of simple structures where the predicted failure rates depend largely on the theoretical assumptions used in modeling, the effect of initial imperfections, etc. For a simply supported beam under sudden loading and subject to a limit on the mid-span deflection, they show that the probability of failure evaluated from the classical Euler-Bernoulli theory (neglecting rotational inertia and shear deformations) is half the value predicted when the rotational inertia is included. When shear deformations are also included in the model, the predicted failure rate is an order of magnitude larger than predicted by the Euler-Bernoulli theory! In view of this, estimations of modeling errors should ideally be included in probabilistic formulations as additional uncertainties. However, evaluating the means, standard deviations and distribution shapes of modeling errors is extremely difficult. A realistic estimation would require data about analytical-experimental mismatch observed on a large number of systems of the same type. Such information will in general not be available. One study by Hasselman and Chrostowski[37,38] has accumulated some amount of data on modeling errors in dynamic analysis of conventional space structures. Statistics were compiled from about 22 sets of analysis/test data and grouped into pre-test and post-test data. However, the results are applicable only for the particular type of analysis and structure.

Considering these factors, it is clear that we can only predict an idealized, *nominal* probability of failure. This nominal probability can be significantly different from the actual one. It is not clear if probabilistic optimization based on that nominal value can still yield better designs than deterministic optimization. Validation is needed if the probabilistic approach is to gain wider

acceptance in the engineering community[39,40,41]. This validation can only be provided by actually measuring the rates of failure of deterministic and probabilistic optima corresponding to the same design problem. Although a number of studies have addressed experimental validation of deterministic optimizations (see the review by Adelman[42] or the work by Maghami *et al.*[43] for example), there has been no report of such validation in the field of probabilistic optimization. This is probably due to the large number of experiments needed to evaluate statistically the performance of a design. The goal of the present work is to fill this gap by providing a practical example of probabilistic optimization. Several realizations of two designs corresponding to the same problem will be tested in the laboratory and their respective rates of failure will be compared.

In order to compare the designs obtained from deterministic and probabilistic optimizations, we must use formulations that can be considered equivalent. The formulations of probabilistic optimization problems found in the literature belong to one of three distinct groups:

1. The most realistic formulation consists of minimizing the total expected cost of the system, which roughly speaking is the sum of the initial set up cost and the expected cost of repairs, periods of unavailability and possibly catastrophic failure. The difficulty with this approach is that it requires evaluating the cost of failures, which involve legal and sociological considerations. However, it is the most general approach in the sense that the optimization also determines optimum values for the safety levels associated with each type of failure. Examples of applications of this approach can be found in Cramer and Friis-Hansen[44] or Surahman and Rojiani[45] for example. There is no deterministic equivalent to this formulation however, since the deterministic approach does not explicitly consider the possibility of failure.

2. The second approach, which is also the most frequently used in the literature consists of minimizing the weight or initial cost of the system subject to constraints on the components and/or system reliabilities (the CCP approach of Charnes and Cooper belongs to this category). Note that constraints on component reliabilities are not necessary. If only the system reliability is specified, more costly/heavier components are automatically given a larger allowable failure probability than less expensive/lighter ones because the cost/weight penalty associated with improving their reliability is larger (see for example Moses and Kinser[2] or

Feng and Moses[22]). The result is an optimal distribution of allowable failure probabilities between the components of the system. Applications of this formulation are numerous in the literature; a few examples include studies by Moses and Stevenson[12], Davidson, Felton, and Hart[13], Frangopol and Rondal[46], Frangopol[17], and Lee and Kwak[47], among others. In those works, the weight or cost is calculated with all random parameters at their mean values. A slight variant of the same approach consists of minimizing the sum of the nominal weight and a portion of its standard deviation due to the uncertainties. This helps protect the objective itself against large variations from its nominal value. Rao[26] applied this technique to the minimum weight design of a cantilevered beam and a truss under random seismic excitation. He gives results for several variants of the objective function, using different multipliers of the mean and standard deviation of the weight. The deterministic equivalent to this formulation consists of minimizing weight or initial cost subject to deterministic constraints corresponding to the failure modes of the probabilistic formulation. Naturally, coefficients of safety or safety margins must be used to minimize failures. Deterministic designs obtained from this formulation cannot be easily compared to the probabilistic design, however. This is because the reliability is specified explicitly in the probabilistic formulation but only implicitly in the deterministic design (through somewhat arbitrary coefficients of safety). The relative performances and reliabilities of the designs obtained with each approach are then primarily dependent on the arbitrary choice of allowable failure probability and safety margins. This is made clear in reference [26] where minimum weight probabilistic and deterministic designs are compared for different values of the coefficients of safety and allowable probabilities of failure. Note, however, that a comparison could be performed with the following approach: an optimum deterministic design is obtained first and its reliability is evaluated; then, a minimum weight/cost probabilistic optimization is performed requiring the same value of system reliability. With this approach, the two optimal designs would have the same reliability but a different cost/weight.

3. Finally, the third approach lends itself to fair comparison between deterministic and probabilistic formulations. It consists of maximizing the system reliability (or minimizing the probability of failure) subject to a limit on the cost or weight. The deterministic equivalent

is to maximize the safety margins subject to the same limit. Although this approach is mentioned repeatedly in the literature, it has not seen many applications. Parimi and Cohn[16] apply it to the design of a reinforced concrete frame. In reference [[]48], Nikolaidis and Stroud consider the design of a ten bar truss with active and passive damping augmentation, with failure defined as the damping ratio of any of the first four vibration modes falling below a specified limit. The design they obtain from probabilistic optimization has almost half the failure rate of the deterministic design, with the same cost.

The third formulation is the best candidate for an experimental comparison of the deterministic and probabilistic approach. It is the formulation we adopted in this work. The experimental results will evaluate the actual difference in reliability between the two designs.

The particular structure used as the example throughout this work is a short cantilevered truss made of aluminum members and nodes. It is described in detail in Chapter 2. In the first part of the work (Chapter 2), we are interested in validating predictions of response scatter based on statistical information about uncertainties in the system.

As a first step, and in order to validate the finite element model of the truss and the statistical analysis technique, we consider the effect of large artificially produced uncertainties in node masses on the natural frequencies of the first three modes of the truss. In the experiments, the uncertainties are produced by attaching a random number of small masses (screws) to the nodes of the structure. The statistical description of these mass uncertainties is used to predict the transmitted scatter in the natural frequencies (using both a Monte Carlo simulation and a first order second moment technique). This scatter is then measured experimentally from 51 random realizations of the truss. The results are in excellent agreement with the predictions and confirm the validity of the models used.

Next, we eliminate the artificial uncertainties and evaluate the magnitude of the manufacturing scatter in the truss elements (member stiffnesses, node and member masses) by measuring the properties of a large number of those components. The resulting statistics are used to evaluate the transmitted scatter in the natural frequencies of the truss, using again a first order technique and a Monte Carlo simulation. The predicted values are compared to experimental measurements; for this, we use a "tinker toy" approach where we assemble several realizations of the same nominal truss from elements picked randomly from a pool. Each realization is tested in the laboratory,

and the results are used to evaluate the statistics (mean values and standard deviations) of the natural frequencies. The experimental results will be shown to be reasonably close to predictions (taking into account the uncertainties in the measured statistics due to the small sample size). However, we found that the transmitted scatter was extremely small. This is because the truss elements were specially manufactured for a NASA research project so that manufacturing uncertainties themselves are extremely small. Compared to deterministic optimization, the benefit of a probabilistic optimization based only on these manufacturing uncertainties would therefore also be small and could not be measured with a reasonably small number of experiments.

As a means to introduce more uncertainty in our system for the purpose of demonstration, we use passive tuned dampers to control the vibration of the truss. The dampers are made by hand from widely available plastic materials and viscoelastic foam. They are described in detail in Chapter 3. The choice of materials and the manual fabrication contribute to large manufacturing uncertainties. In addition, the performance of those dampers is controlled by the tuning of their natural frequency to a natural frequency of the truss. Away from tuning, the response of the damped truss is very sensitive to small changes in tuning. Unfortunately, it is also extremely non-linear and the performance function can have multiple most probable failure points so that first order second moment methods have to be abandoned and replaced by more expensive Monte Carlo simulation.

In Chapters 4 and 5, we consider the optimal design of the truss equipped with tuned dampers to control the amplitudes of forced vibrations. The uncertainties in the system are limited to the properties of the dampers. We manufacture a large number of dampers and measure their physical properties. Statistical descriptions of those properties are evaluated from the measurements. Because of manufacturing errors, the dampers are not perfectly tuned to the natural frequencies of the truss so that the amplitudes of vibrations are too high. To correct the mistuning, we add tuning masses to the truss. The added masses reduce the natural frequencies of the truss and can bring them closer to the resonant frequencies of the dampers (of course only if the dampers are undertuned, i.e. their natural frequencies are lower than that of the structure).

The optimization problem consists of finding the best locations on the truss for the tuning masses and for the tuned dampers. The total weight of the optimized structure is constrained by allowing the use of a maximum of 10 masses. The magnitude of those masses is assumed fixed

and deterministic. Because the scatter in the damper properties is much larger than the scatter in the masses and stiffnesses of the truss elements, the latter is neglected and the only uncertainties in the problem are the properties of the dampers. One damper per mode is used to control two modes of vibration of the truss. The design requirement is expressed as an upper limit on the response acceleration at two specific locations on the truss, for a given white noise excitation. The limit is set to the same value in two frequency ranges covering the two modes of interest. The system fails if the response acceleration exceeds the prescribed limit within the prescribed frequency ranges.

The probabilistic formulation minimizes the probability of failure while the deterministic formulation maximizes the safety margin between the response of the nominal damped structure (i.e., with all damper properties equal to their mean values) and the failure limit. The total weight constraint is implicitly satisfied in both formulations because of the limited number of masses.

Because the optimization problem described above is of combinatorial nature and uses only discrete design variables, a genetic algorithm is used to solve it. The algorithm is briefly described in Chapter 4; additional information can be found in Appendix D.

Chapter 4 compares analytically optimal designs obtained with both formulations. Based on Monte Carlo simulations, the probabilities of failure of the probabilistic and deterministic designs are 2.2% and 4.9%. Although the probabilistic design has less than half the probability of failure of the deterministic optimum, the difference is only about 2.7%. Measuring such a small difference would require a prohibitive number of experiments. If we want to be able to measure the difference in failure rates, we must find a design problem that leads to a much larger contrast. In Chapter 5, we formulate the contrast maximization as an additional optimization problem and solve it using another genetic algorithm. The variables used to describe the design problem are the statistics of the dampers and the magnitude of the failure limit imposed on the design. The contrast maximization procedure identifies a design problem that leads to a difference of about 14% between the probabilities of failure of the two designs. The dampers are then modified so that they exhibit the desired statistics. Their properties are remeasured and new probabilistic and deterministic designs are obtained. As expected, the simulated probabilities of failure of those two designs differ by more than 14.5%! To validate this last result experimentally, 29 realizations of each design are tested in the laboratory and the number of failures observed for each design are compared to the predictions. Excellent agreement is again observed.

Finally, Chapter 6 contains some concluding remarks and recommendations for future research.

**Note**: Part of the results presented in this dissertation are the fruit of a collaboration between the author and G. Maglaras, Ph.D. candidate in Aerospace Engineering. Some of those results are therefore liable to appear in G. Maglaras' dissertation.

# Chapter 2

# Predicting Scatter in the Response of a Truss: Experimental Validation

The use of probabilistic design techniques is based on the assumptions that the sources of uncertainties in the system can be identified and quantified and that statistical models can use that knowledge to predict the uncertainties in response quantities with sufficient accuracy. In this chapter, we attempt to provide an experimental verification of these hypotheses. For this, we selected the example of a small truss structure and consider its natural frequencies as the response quantities. Truss structures are ideal candidates for this type of experimental program because they are assembled from individual members and nodes. The uncertainties in the response of the truss are naturally attributed to scatter in the properties of these components (if we neglect other sources of uncertainties like imperfect assembly or boundary conditions). This scatter can be quantified from measurements on large numbers of elements. The response scatter can be measured in the laboratory using a "tinker-toy" approach, where several realizations of the same truss are assembled from members and nodes picked randomly from a pool of nominally identical components. The natural frequencies of each realization are then measured in the laboratory. Finally, the statistics of these measurements (mean values, standard deviations, etc...) are compared to analytical predictions.

In the next section, we describe in some detail the truss structure used for this study. The instrumentation used for the experimental modal analysis and the finite element model of the truss are also presented. The following two sections compare analytical predictions and experimental measurements of the uncertainties in the first 3 natural frequencies of the truss. In a first stage, we create large, artificial uncertainties in the node masses to evaluate the accuracy of the finite element and statistical models. The second stage is an attempt to predict the effect of manufacturing uncertainties in the truss components themselves. The statistics of those uncertainties are evaluated from stiffness and mass measurements on a large number of nodes and members. These data are used in conjunction with statistical models to predict scatter in the natural frequencies of the truss. Using the "tinker-toy" approach, we then experimentally evaluate the scatter and compare it to the analytical predictions.

## 2.1 Laboratory Truss

### 2.1.1 Description

The structure used in this study is shown in Fig. 2.1. It is a short, cantilevered beam-like truss structure assembled from 30 tubular aluminum members with steel end-fittings, connected through 12 solid spherical aluminum nodes.

All elements of the truss were obtained from NASA Langley Research Center. They were part of the phase-0 C.S.I. Evolutionary Model[49] of the Structural Dynamics Branch. The design of the members and nodes makes the truss relatively easy to assemble and disassemble (Fig. 2.2). Each member consists of a middle section of anodized aluminum tube and two end-fittings made of aluminum inserts supporting steel threaded rods (Fig. 2.3). The aluminum inserts are glued inside each end of the tube. The steel rods simply thread into holes of the aluminum nodes. These fittings are designed in a such a way that the threaded rods can collapse into the central tubular section for disassembly. This allows separating one member from a truss without perturbing the geometry of the structure.

Eighteen flat faces are machined on the spherical nodes; a 6.35 mm ($1/4$ in) threaded hole is drilled in the middle of each of these faces and accepts the steel threaded rods of the members.

The two middle bays of the truss are pyramids with a 0.254 m (10 in) square base. Two half bays attached to the ends of the middle section complete the structure. The 26 non-diagonal members are 0.254 m long from node center to node center, while the 4 diagonals are $\sqrt{2}$ times longer. The whole truss is about 1 m (40 in) long and weighs about 4.4 kg (9.6 lb). Three nodes are attached to a base made of thick steel and aluminum plates mounted on the laboratory wall.

Figure 2.4 shows a plot of the magnitude of a measured frequency response function (FRF) from excitation force to response acceleration for that truss. The first three modes are well separated and clearly identified. Their natural frequencies are about 100, 130 and 193 Hz. Local bending modes in the members occur at frequencies 280 Hz and higher, making a truss model useful only for the first three modes. For this reason, only the first 3 modes of the structure will be considered.

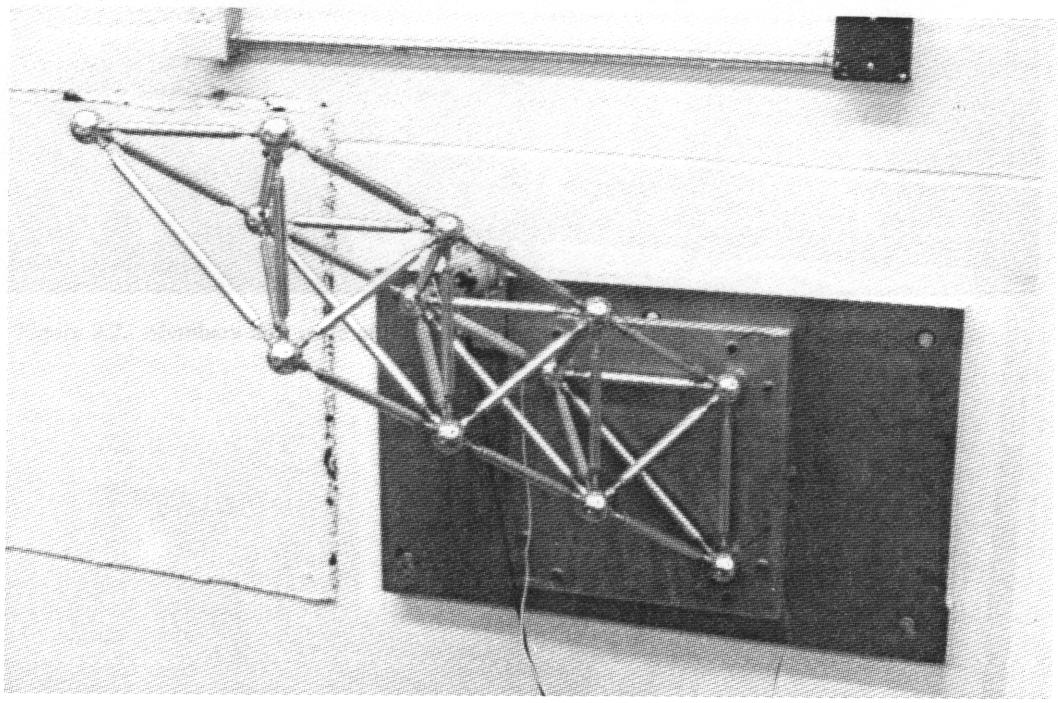

**Figure 2.1. Laboratory truss.**

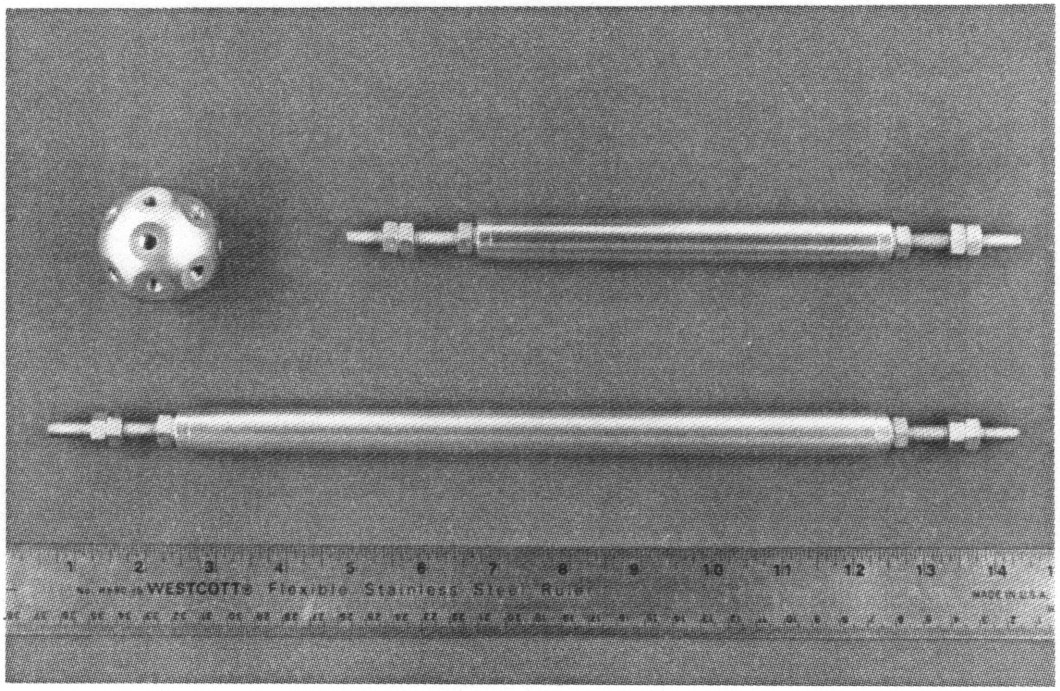


**Figure 2.2. Members and node of the laboratory truss.**

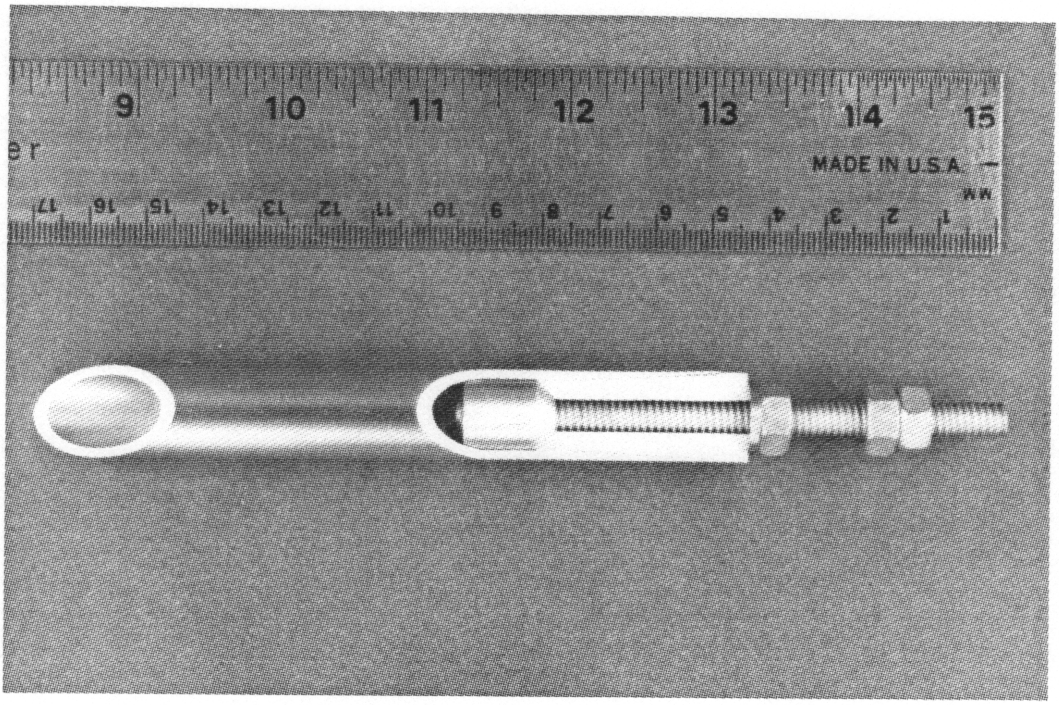


**Figure 2.3. Internal structure of a member's end-fitting.**

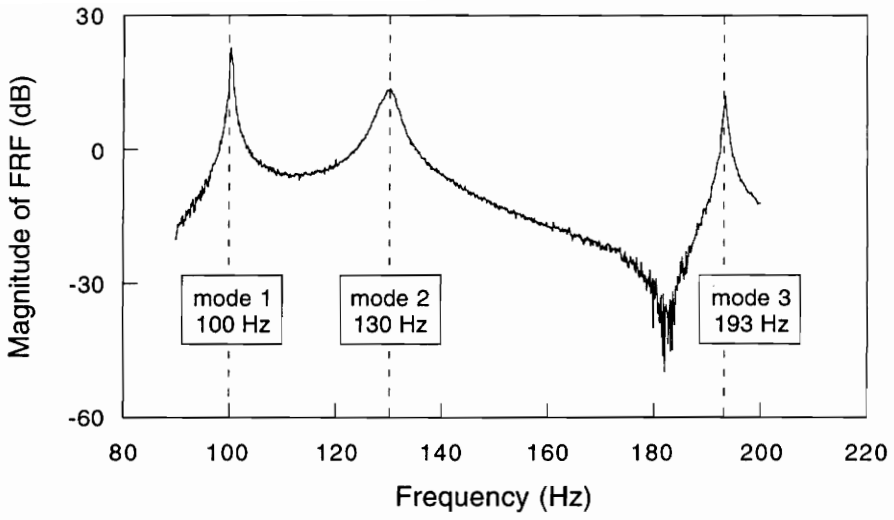


**Figure 2.4. Measured frequency response function of the laboratory truss (magnitude of acceleration per unit force).**

The first and third modes of the truss are very lightly damped; their measured damping ratios are only 0.13% and 0.08%, respectively. The damping ratio of the second mode is significantly higher (1.05%). This is believed to be due to coupling with the dynamics of the wall.

## 2.1.2 Instrumentation

For dynamic measurements, the excitation (Fig. 2.5) is provided by an electromagnetic shaker (Ling Dynamics, model 102) attached to the steel base plate and connected to a node of the truss through a stinger orthogonal to the wall. A piezoelectric load cell (PCB 208B) measures the excitation force.

The shaker is driven by the signal generator of a Tektronix 2630 FFT analyzer through a power amplifier (KEPCO, model BOP 50-2M). The response amplitude is measured by a subminiature accelerometer (PCB, model 303A03) attached to one of the tip nodes. The locations of the excitation and the response measurement were selected so that the first 3 modes could be identified simultaneously. The data acquisition and FFT analysis were performed on a Tektronix 2630, PC controlled analyzer.

## 2.1.3 Finite Element Model

The finite element model of the truss is shown in Fig. 2.6. We define a global axis system

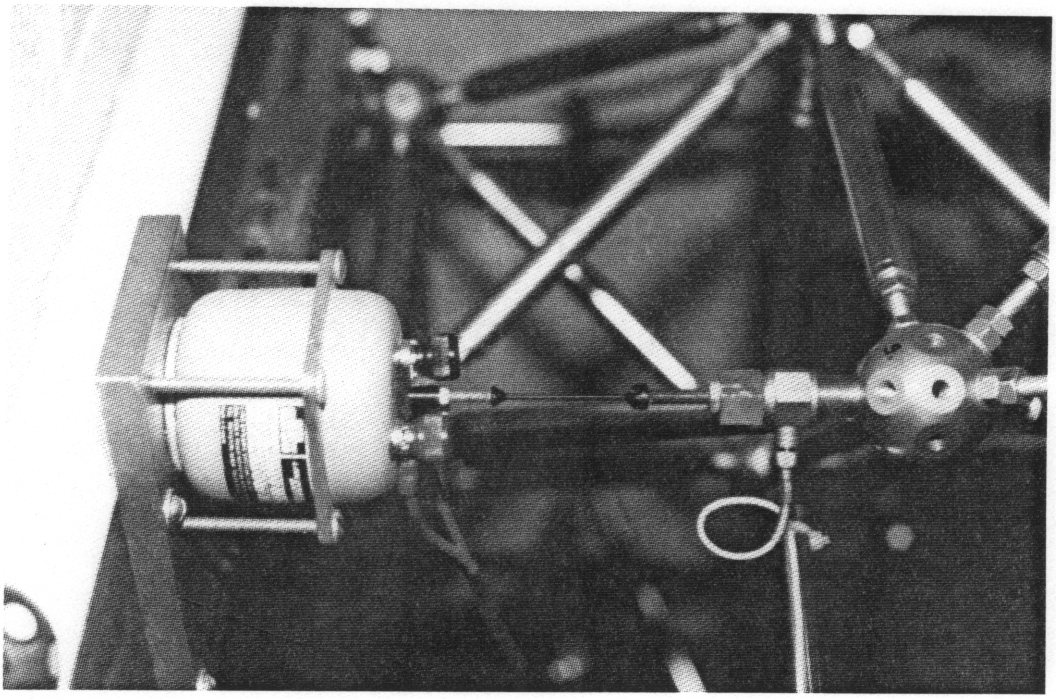

**Figure 2.5. Truss excitation setup.**

$\vec{1}_x$, $\vec{1}_y$, $\vec{1}_z$ as follows (see Fig. 2.6): $\vec{1}_z$ is pointing vertically up, $\vec{1}_x$ is orthogonal to and pointing away from the support plates and $\vec{1}_y$ completes the right-handed coordinate system.

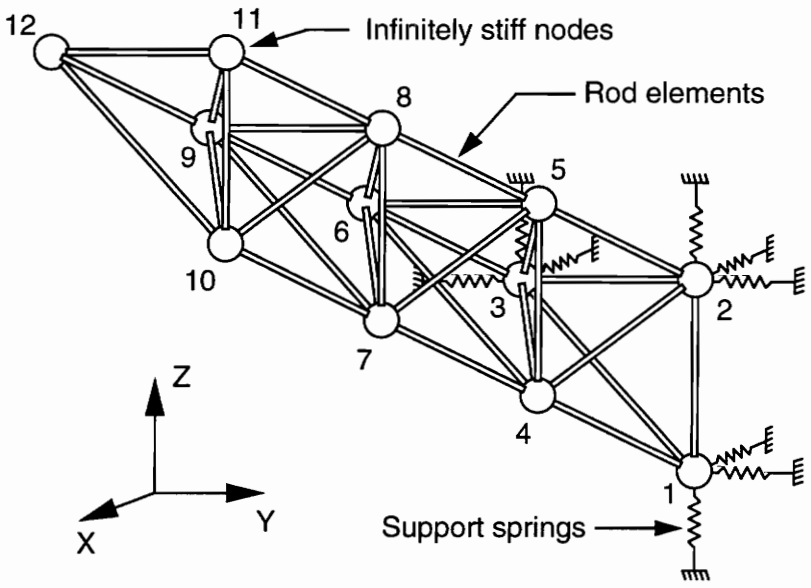


**Figure 2.6. Finite element model of the laboratory truss.**

Each member is modeled as a nonuniform, symmetric, straight, 6-degree of freedom, 3D rod finite element. This element is described in Appendix B. It is defined by its stiffness, mass and rotational inertia around its center of mass (which is the midpoint along the axis). The rotational inertias of the members were measured with the pendulum technique and assumed deterministic (i.e. any scatter in the value of the inertia was neglected). Each of the 12 nodes is modeled as an infinitely stiff concentrated mass.

The flat faces on the nodes are used to attach the accelerometers, load cells and other devices to the truss. The normals to those faces take only 9 distinct directions, denoted $\vec{1}$ to $\vec{9}$.

Their directional cosines are (in the global axis system of Fig. 2.6):

$$\begin{aligned}
\vec{1} &= (1,0,0) \\
\vec{2} &= (0,1,0) \\
\vec{3} &= (0,0,1) \\
\vec{4} &= (0, cos\,45^o, cos\,45^o) \\
\vec{5} &= (1, -cos\,45^o, cos\,45^o) \\
\vec{6} &= (cos\,45^o, 0.5, 0.5) \\
\vec{7} &= (cos\,45^o, -0.5, 0.5) \\
\vec{8} &= (-cos\,45^o, -0.5, 0.5) \\
\vec{9} &= (-cos\,45^o, 0.5, 0.5)
\end{aligned} \tag{2.1}$$

The model also includes 9 springs (3 per attached node, one into the base and two in the plane of the base) to simulate the flexibility of the base. The stiffnesses of those springs were roughly adjusted to minimize the experimental-analytical bias on the first three natural frequencies. With these springs, all nodes of the structure are free and the model contains 36 degrees of freedom. The analytical-experimental errors on the natural frequencies are less than 0.9%. Note that we measured experimentally the amplitudes of vibration at the 3 attached nodes and compared them to predictions from the adjusted model. Good agreement was observed. This shows that the spring stiffnesses used in the adjusted model actually represent the physics of the system and are not simply an artificial correction of the model.

Neglecting the small amount of damping, the free vibration equation is written using the system mass and stiffness matrices, $M$ and $K$, as:

$$M\ddot{x} + Kx = 0\,, \tag{2.2}$$

where $x$ is the vector of nodal displacements, and the dots denote differentiation with respect to time. The corresponding eigenvalue problem for free vibration is:

$$\left(-M\omega_j{}^2 + K\right) u_j = 0\,, \tag{2.3}$$

where $\omega_j$ is the natural frequency of the $j$th mode and $u_j$ is the corresponding vibration mode.

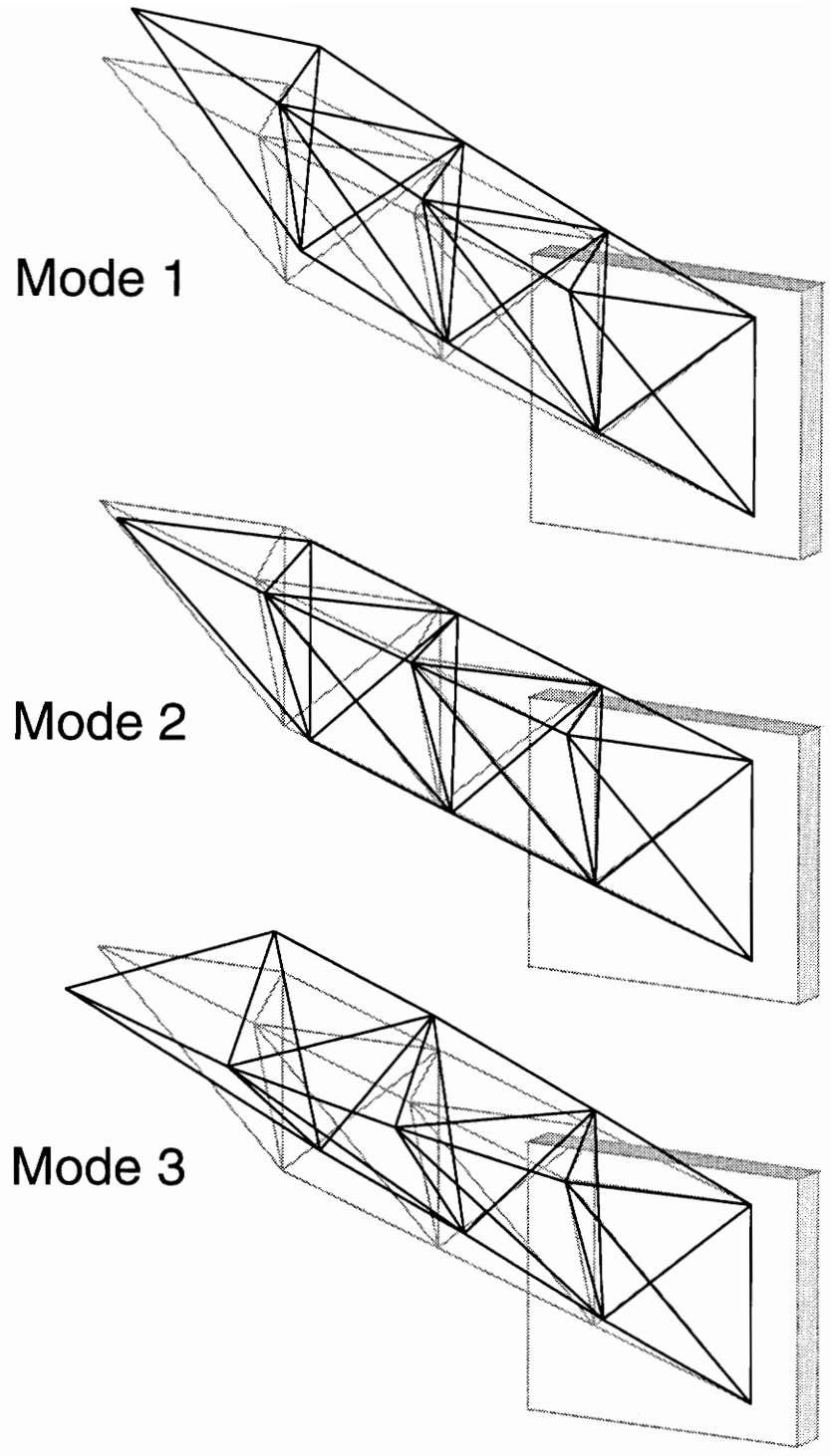


**Figure 2.7. First three mode shapes of the laboratory truss (from finite element analysis).**

Figure 2.7 shows the first three mode shapes of the truss as predicted by the model. The first and second modes are global bending modes; the third mode is a torsion of the beam-truss around its longitudinal axis. In all 3 modes, the largest amplitudes occur at the tip of the truss.

## 2.2 Prediction of Response Scatter

We are interested in evaluating the scatter in the natural frequencies of the truss due to scatter in the physical properties of its elements. The uncertainties are assumed to be limited to small variations in the masses of the members and nodes and in the stiffnesses of the members (special care was taken in the experimental procedure to minimize the uncertainty in the boundary conditions so that these were neglected). On the basis of this assumption, we approximate the $j^{th}$ natural frequency $\omega_j$ as:

$$\omega_j = \omega_j(\bar{k}, \bar{m}_m, \bar{m}_n) + \sum_{i=1}^{m} \left.\frac{\partial \omega_j}{\partial k_i}\right|_0 \Delta k_i + \sum_{i=1}^{m} \left.\frac{\partial \omega_j}{\partial m_{m_i}}\right|_0 \Delta m_{m_i} + \sum_{i=1}^{n} \left.\frac{\partial \omega_j}{\partial m_{n_i}}\right|_0 \Delta m_{n_i} + H.O.T., \tag{2.4}$$

where $\bar{k}$, $\bar{m}_m$, and $\bar{m}_n$ are the mean values of the member stiffnesses, member masses, and node masses, respectively, $\omega_j(\bar{k}, \bar{m}_m, \bar{m}_n)$ is the value of $\omega_j$ for the nominal structure, $m$ and $n$ are the numbers of members and nodes, respectively, $k_i$ and $m_{m_i}$ are the mechanical stiffness and mass of the $i^{th}$ member, $m_{n_i}$ is the mass of the $i^{th}$ node, the subscript 0 denotes derivatives taken with the stiffness and mass parameters at their mean values, and $\Delta$ represents deviations of these properties from their mean values.

In the experiments, we create each realization of the truss by picking members and nodes randomly, so that there is no correlation between properties of distinct nodes or members. However, we expect that the mass of a member is correlated with its stiffness. We account for this correlation in the formulation. All uncertainties are characterized by their standard deviations and correlation coefficients. Using the notation $\sigma$ for the standard deviation, $\bar{\omega}_j$ for the mean value of $\omega_j$ and $E$ for the expected value operator, the variance of the $j$th natural frequency is

$$\sigma^2(\omega_j) = E\left[(\omega_j - \bar{\omega}_j)^2\right] . \tag{2.5}$$

From Equation (2.4) the average frequency $\bar{\omega}_j$ is equal to $\omega_j(\bar{k}, \bar{m}_m, \bar{m}_n)$ . Substituting (2.4) into (2.5) and distributing terms, we obtain the following expression for the variance of the $j^{th}$ natural frequency due to stiffness and mass uncertainties:

$$\sigma^2(\omega_j) = \sum_{i=1}^{m} \left.\frac{\partial \omega_j}{\partial k_i}\right|_0^2 \sigma^2(k_i) + \sum_{i=1}^{m} \left.\frac{\partial \omega_j}{\partial m_{m_i}}\right|_0^2 \sigma^2(m_{m_i})$$
$$+2\sum_{i=1}^{m} \left.\frac{\partial \omega_j}{\partial k_i}\right|_0 \left.\frac{\partial \omega_j}{\partial m_{m_i}}\right|_0 \sigma(k_i)\sigma(m_{m_i})\rho(k_i, m_{m_i}) + \sum_{i=1}^{n} \left.\frac{\partial \omega_j}{\partial m_{n_i}}\right|_0^2 \sigma^2(m_{n_i}), \qquad (2.6)$$

where $\sigma(m_{m_i})$ and $\sigma(k_i)$ are the standard deviations of the mass and stiffness of the members, $\sigma(m_{n_i})$ is the standard deviation of the mass of the nodes, and $\rho(k_i, m_{m_i})$ is the coefficient of correlation between the stiffness and the mass of a member, defined as:

$$\rho(k_i, m_{m_i}) = \frac{\sigma(k_i, m_{m_i})}{\sigma(k_i)\sigma(m_{m_i})}, \qquad (2.7)$$

where $\sigma(k_i, m_{m_i})$ is the covariance between the stiffness and the mass of a member. All standard deviations and correlations in Eq. (2.6) have to be evaluated from measurements, or estimated using manufacturing tolerances for example.

The first partial derivatives of the natural frequencies in equation (2.6) can be evaluated using the frequencies and modes of the nominal structure. Differentiating the eigenvalue problem of Eq. (2.3) with respect to a mass parameter $m$ we have

$$K\frac{\partial u}{\partial m} - 2\omega\frac{\partial \omega}{\partial m}Mu - \omega^2\frac{\partial M}{\partial m}u - \omega^2 M\frac{\partial u}{\partial m} = 0. \qquad (2.8)$$

Premultiplying the last equation by $u^T$ and taking advantage of the symmetry of the system, we get[50]:

$$\frac{\partial \omega_j}{\partial m} = -\frac{\omega_j}{2}\frac{u_j^T \frac{\partial M}{\partial m} u_j}{u_j^T M u_j}. \qquad (2.9)$$

Similarly, the first derivative with respect to a stiffness parameter $k$ is

$$\frac{\partial \omega_j}{\partial k} = \frac{1}{2\omega_j}\frac{u_j^T \frac{\partial K}{\partial k} u_j}{u_j^T M u_j}. \qquad (2.10)$$

Note that the partial derivatives $\frac{\partial M}{\partial m}$ and $\frac{\partial K}{\partial k}$ of the mass and stiffness matrices involve only one member or one node at a time and are therefore very sparsely populated. This makes the estimation of the scatter in the natural frequencies computationally inexpensive.

## 2.3 *Effect of Large Artificial Uncertainties*

### 2.3.1 Characterization of Scatter

In order to evaluate the quality of the finite element and statistical models, we first performed some experiments with large artificially produced mass uncertainties. To create these uncertainties, steel screws are attached to the nodes of the truss. The number of screws at each node is random and varies between 0 and 4. There is equal probability (20%) for having 0, 1, 2, 3 or 4 screws at any given node. The mass of each screw was measured to 9.2 g (0.33 oz), so that the mass of each node increased by about 21% on average (the average number of screws per node is 2). The standard deviation of the node masses is 9.2 g $\times\sqrt{2}$ = 13 g (0.46 oz). The resulting distribution of the node masses is shown in Figure 2.8.

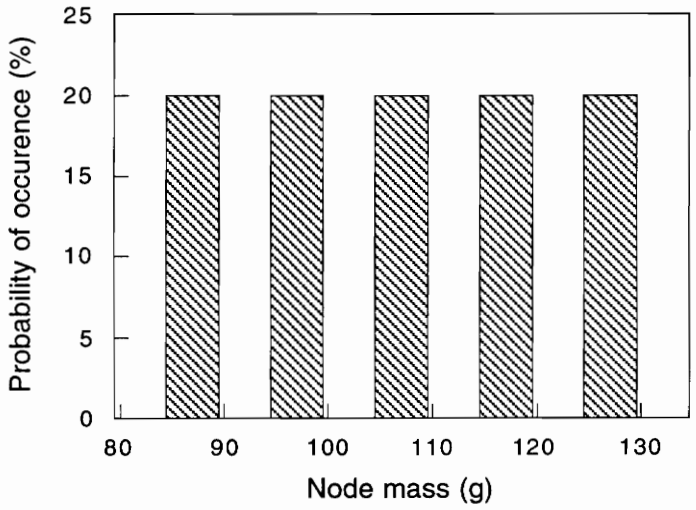


**Figure 2.8. Artificial uncertainties; distribution of node masses.**

### 2.3.2 Experimental Results

The effect of artificial node mass scatter was checked on a single realization of the truss, so that the effect of natural variations in mass and stiffness could be ignored. We generated 51 random configurations of mass perturbations on a computer and computed their natural frequencies

with the finite element model (since the uncertainties are artificial, we know the exact amount of mass added to the nodes in each realization). The 51 configurations were then assembled one after the other and their natural frequencies were measured in the laboratory. The experimental results are plotted versus analytical predictions in Fig. 2.9. The solid lines in the figures represent ideal one to one correspondence between experimental and F.E.M. results. The figure shows the good quality of the measurements (analytical-experimental correlation coefficients are better than 99% in all 3 modes). However, there is a small residual bias in the analytical results. It is due to the fact that the truss model has not been adjusted to match exactly the measured natural frequencies of the original truss. The average slope of the experimental-analytical curve is also slightly less than the ideal value of 1 (i.e., our model overestimates the *change* in natural frequency due to the added masses). This also results in overestimations of the scatter in natural frequencies due to scatter in mass properties.

**Table 2.1. Effect of artificial scatter in node masses on first 3 natural frequencies of the truss (all values in Hertz).**

| | Experiment | | Simulation | | Monte Carlo* | | Linear approx. | |
|---|---|---|---|---|---|---|---|---|
| i | $\bar{\omega}_i$ | $s(\omega_i)$ [95% confidence interval for $\sigma$] | $\bar{\omega}_i$ | $s(\omega_i)$ | $\bar{\omega}_i$ | $s(\omega_i)$ | $\bar{\omega}_i$ | $s(\omega_i)$ |
| 1 | 95.68 | 0.68 [0.57...0.84] | 95.15 | 0.75 | 95.28 | 0.75 | 95.28 | 0.76 |
| 2 | 123.49 | 0.85 [0.71...1.06] | 122.38 | 1.00 | 122.57 | 1.00 | 122.56 | 1.01 |
| 3 | 182.98 | 1.34 [1.12...1.66] | 180.92 | 1.53 | 181.21 | 1.54 | 181.18 | 1.56 |

* 5000 replications.

Table 2.1 compares the means and standard deviations of the first three natural frequencies obtained by 4 approaches: 51 experiments, finite element analysis of the 51 configurations, Monte Carlo simulation with 5000 random replications and the linear approximation of section 2.2. We also included in the table 95% confidence intervals for the standard deviation $\sigma$, evaluated from the experimental sample deviation $s$ as [51]

$$\sqrt{\frac{(n-1)s^2}{\chi^2_{1-\alpha/2,n-1}}} \leq \sigma \leq \sqrt{\frac{(n-1)s^2}{\chi^2_{\alpha/2,n-1}}}, \tag{2.11}$$

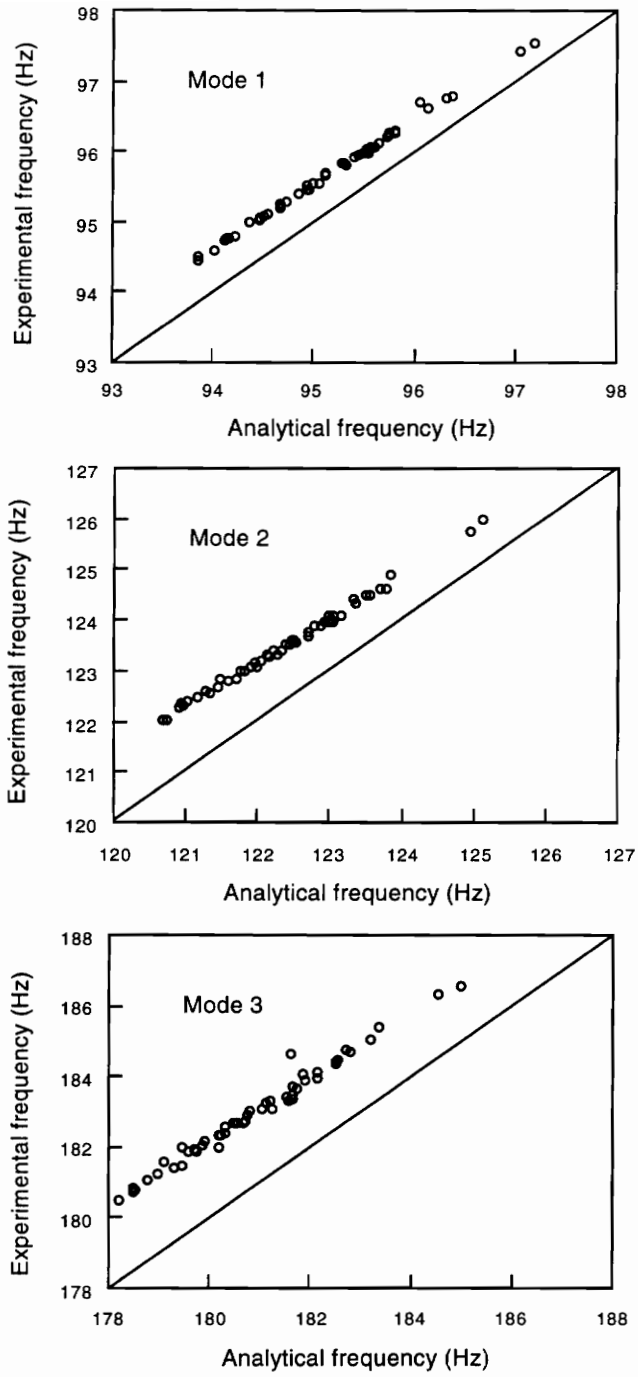


**Figure 2.9. Effect of artificial uncertainties; experimental natural frequencies of three first modes versus analytical predictions (the solid lines represent an ideal one to one correspondence.**

where $n$ is the sample size, $\alpha$ is the significance level (1 minus the confidence level), $\chi^2_{\beta,m}$ denotes the value for which the area to its right under the chi-square distribution with $m$ degrees of freedom is equal to $\beta$, and the distributions of natural frequencies are assumed normal. For 95% confidence and 51 experiments, $\alpha = 0.05$ and $n = 51$.

The results from the 51 analyses, Monte Carlo simulation and linear approximation are in excellent aggreement. This demonstrates the usefulness of the first order expansion of Eq. (2.4), even for relatively large mass perturbations. The experimental results compare favorably with the predictions although the experimental estimates of the standard deviations are 9% to 15% lower than the predicted values. However, all predicted values fall within the 95% confidence intervals evaluated from the experiment.

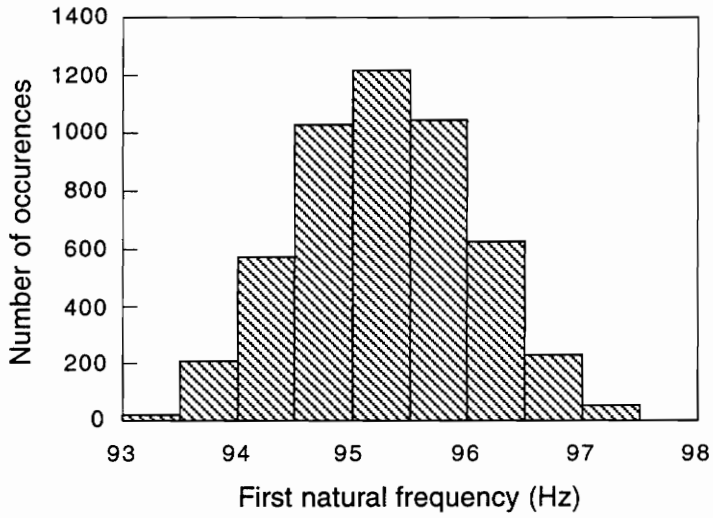


**Figure 2.10. Effect of artificial uncertainties; distribution of the first natural frequency (5000-points Monte Carlo simulation).**

Figure 2.10 shows the distribution of the first natural frequency in the Monte Carlo simulation. Note that although the distribution of the mass uncertainty is far from normal (see Fig. 2.8), the resulting distribution of natural frequencies appears very close to normal. This is expected from the central-limit theorem since the natural frequencies of the truss depend on the cumulated effects of masses added at all nodes.

## 2.4 *Effect of Manufacturing Uncertainties*

The results presented in the previous section for artificial uncertainties have demonstrated the quality of the truss model and the validity of the assumptions used in the statistical analysis. In this section, we study the effect of manufacturing uncertainties on the scatter in the natural frequencies of the same truss. The uncertainties are assumed to be limited to the masses of the nodes and the masses and stiffnesses of the members. The statistics of these parameters are evaluated from measurements on randomly selected samples. Predicted values for the scatter in the natural frequencies of the truss are then compared to measurements on 6 realizations of the truss.

### 2.4.1 Characterization of Scatter

#### *2.4.1.1 Node Masses*

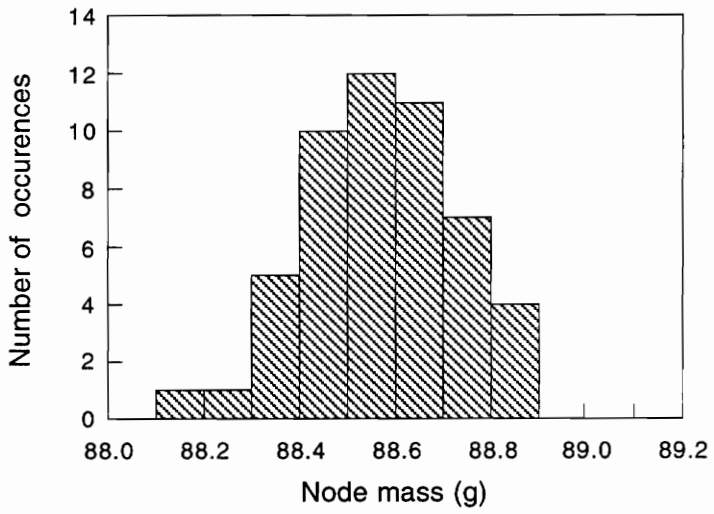


**Figure 2.11. Distribution of measured node masses (51 nodes).**

We measured the masses of a sample of 51 nodes, selected randomly out of a pool of about 100. The measurements were taken using a digital scale with a resolution of 0.1 g (0.035 oz). The distribution of measured masses is shown in Fig. 2.11. The mean, standard deviation,

and coefficient of variation (C.O.V., equal to the standard deviation divided by the mean) of the sample are listed in Table 2.2.

### *2.4.1.2 Member Masses*

We measured the masses of 58 diagonal members and 99 short members. The distributions of the results are shown in Fig. 2.12 for the short members (non diagonal members) and in Fig. 2.13 for the diagonals. The averages, standard deviations and coefficients of variation are listed in Table 2.2.

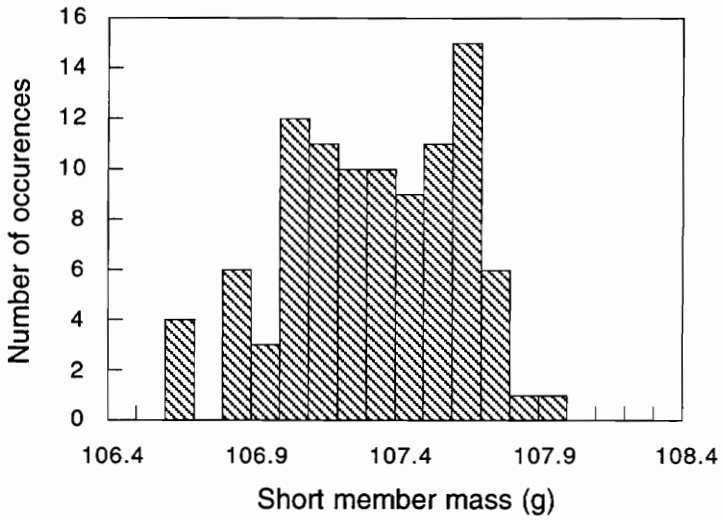


**Figure 2.12. Distribution of measured member masses (99 short members).**

### *2.4.1.3 Member Stiffnesses*

The stiffnesses of the short members were measured statically, using a computer-controlled servo-hydraulic testing machine (MTS, 819 series, model 319.50). Each member was connected in series with one node so that the measured stiffness was effectively an approximation of the stiffness from node center to node center as modeled in the F.E.M. Solid steel cylindrical end-pieces are attached to each end of the member-node assemblies (Fig. 2.14). Those steel cylinders were locked into the two hydraulic grips of the testing machine.

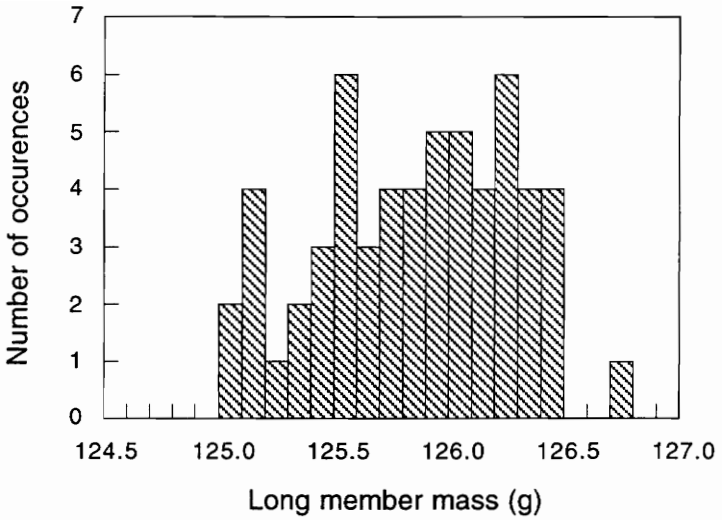


**Figure 2.13. Distribution of measured member masses (58 diagonal members).**

The member-node combinations were selected randomly. A static axial traction load of 2224 Newtons (500 lbf) was applied to the member-node assembly and measured by the load sensors located in the upper grip of the testing machine (resolution 4.5 N or 1 lbf). The resulting axial deformation was measured with an external rocker arm LVDT (Linear Variable Displacement Transformer) displacement gage (MTS model 632.06, resolution 0.25 $\mu$m ($10^{-5}$ in)) mounted on a U beam attached to the lower grip (see Fig. 2.15). The gage measures the change in the distance between the two grips of the testing machine. If no slip occurs in the grips, this is equivalent to measuring the deformation of the member-node assembly. The sensor's readings before and after loading and unloading the test sample were compared to verify the no-slip condition. We also measured the amount of non-linearity at the 2224 N (500 lbf) level. The non-linear component of the elongation was found to be less than 2% of the total elongation. The resolution of the stiffness measurement with this set up is about 0.4%.

These stiffness measurements were performed on 25 randomly selected node-member assemblies. Each assembly was measured twice for protection against experimental errors. Figure 2.16 shows the distribution of the stiffnesses, averaged between the 2 tests. The mean value, standard deviation and coefficient of variation are listed in Table 2.2.

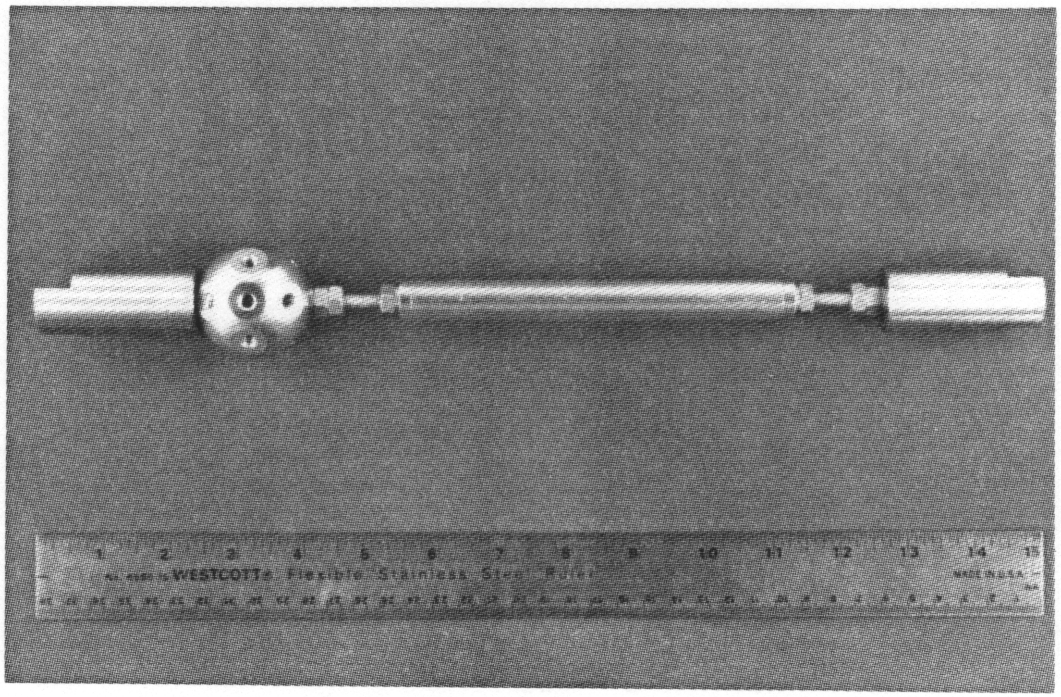


**Figure 2.14. Member-node assembly ready to be tested. The steel cylinders at each end go into the grips of the testing machine.**

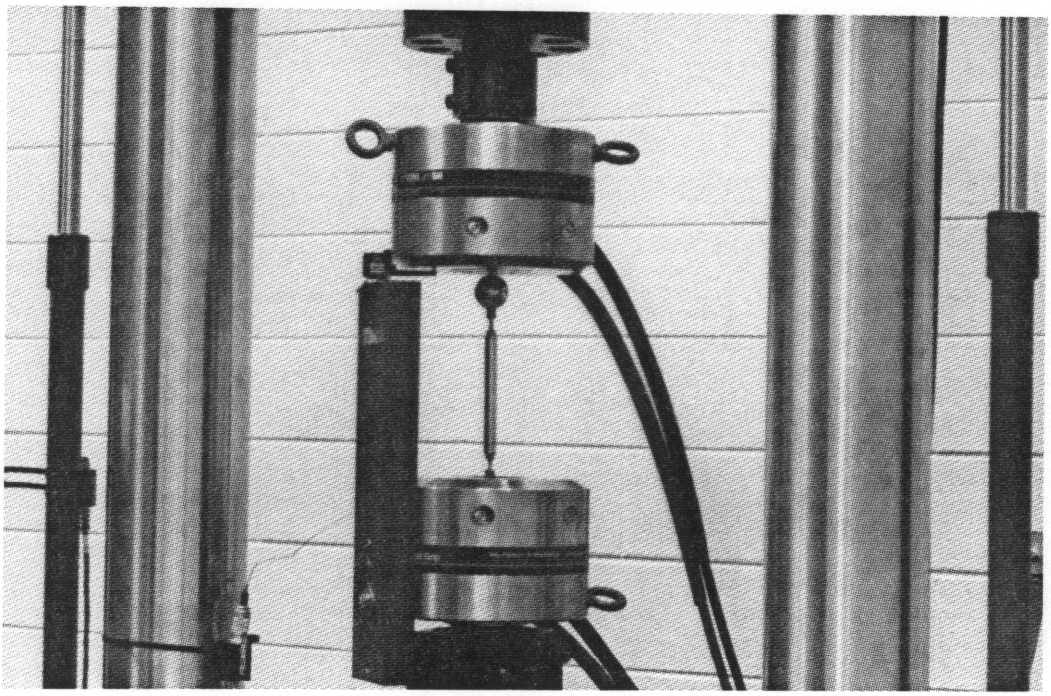

**Figure 2.15. Mechanical stiffness measurement set up.**

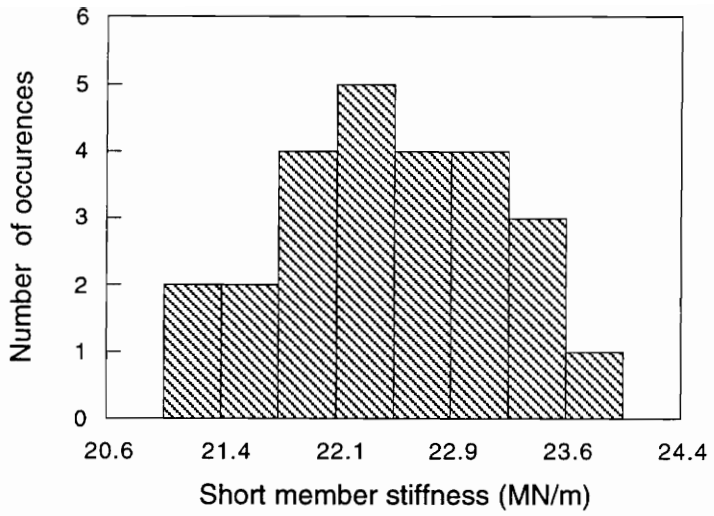


**Figure 2.16. Distribution of measured member stiffnesses (25 short members, average of two measurements).**

**Table 2.2. Manufacturing uncertainties in masses and stiffnesses of truss elements.**

| parameter | mean value | standard deviation | coefficient of variation | sample size |
|---|---|---|---|---|
| Node mass [g] | 88.62 | 0.16 | 0.18% | 51 |
| Short member mass [g] | 107.37 | 0.30 | 0.28% | 99 |
| Diagonal member mass [g] | 125.91 | 0.42 | 0.33% | 58 |
| Short member stiffness [MN/m] | 22.51 | 0.69 | 3.08% | 25 |
| Diagonal member stiffness [MN/m] | 14.82* | — | 3.08%* | — |

* Estimated.

We did not repeat the same procedure to measure the stiffness of the diagonal members. Instead, we assumed the same value of the coefficient of variation as reflected in Table (2.2). The mean stiffness $k_d$ of the diagonal members was extrapolated from that of the short members ($k_s$) as follows. A member can be considered as a series of three springs (Fig. 2.17): a middle spring of stiffness $k^{al}$ that represents the tubular part of the member and two identical end springs of stiffnesses $k^e$ that represent the stiffness from one end of the tube to the center of the node.

The only difference between the short and diagonal members is the length of the tubular part. Those lengths are denoted $l_s$ and $l_d$ for the short and diagonal members, respectively. The

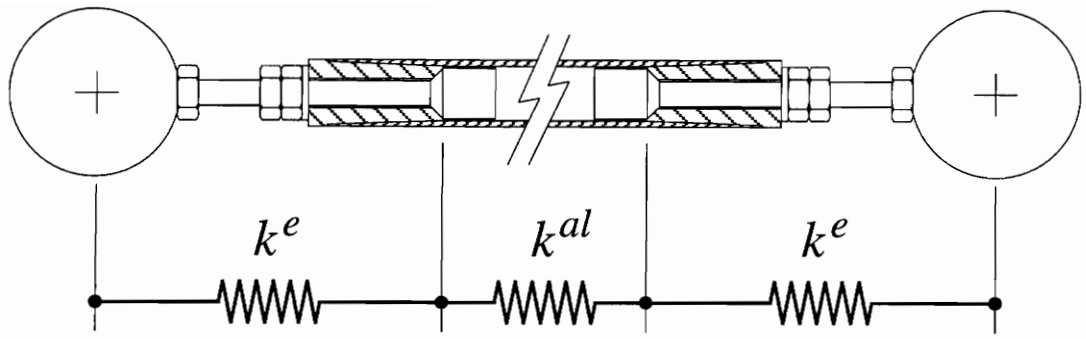


**Figure 2.17. Member stiffness model used to evaluate the mean stiffness of the diagonal members.**

stiffnesses of $k_s^{al}$ and $k_d^{al}$ of the tubular parts of the members are

$$k_s^{al} = \frac{E\,A}{l_s}, \qquad k_d^{al} = \frac{E\,A}{l_d}, \tag{2.12}$$

where $A$ and $E$ are the cross-sectional area and elastic modulus of the the aluminum tube. The value of $k^e$ is the same for both types and is evaluated from the measured stiffness $k_s$ of the short members as

$$k^e = 2\left(\frac{1}{k_s} - \frac{1}{k_s^{al}}\right)^{-1}. \tag{2.13}$$

That value is then used to evaluate the stiffness of the diagonal members

$$K_d = \left(\frac{2}{k^e} + \frac{1}{k_d^{al}}\right)^{-1}. \tag{2.14}$$

Notice that the coefficients of variation (C.O.V.) of the manufacturing uncertainties in table 2.2 are extremely small. Since the truss elements were carefully manufactured for a scientific experiment, those values are probably not representative of the magnitude of uncertainties in mass production items.

### *2.4.1.4 Member Stiffness - Mass Correlation*

Physically, we should expect some correlation between the mass of a member and its stiffness because a heavier member should have more load-carrying material. To verify this, we plotted in Fig. 2.18 the stiffnesses of the 25 short members of the previous sample versus their

measured mass. The figure shows that the mass and stiffness of a member are indeed positively correlated. The result of a least square linear fit is also plotted in the figure. The coefficient of correlation $R$ is about 0.547. The same value of the coefficient of correlation was assumed for the diagonal members.

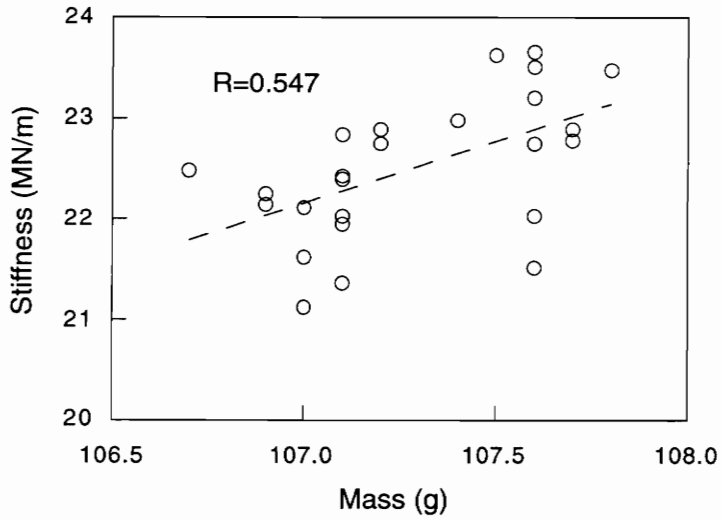


**Figure 2.18. Mass stiffness correlation (25 short members).**

## 2.4.2 Experimental Results

We measured the natural frequencies of the first 3 modes of 6 nominally identical realizations of the cantilevered truss. We actually used only three distinct structures but created two realizations with each of them, by clamping them once from one end and once from the other end. This creates two independent realizations because the significant uncertainties are different when the structure is clamped from one end or the other: the scatter in mass properties has a significant effect only for nodes and members close to the tip of the truss (where accelerations are large), while the effect of scatter in stiffnesses is significant only for members close to the root of the truss (where the elastic energy is large).

The only differences between these 6 realizations are due to uncertainties in physical properties of the elements (and possibly other unmodeled effects). The mean values $\bar{\omega}_i$, standard deviations $s(\omega_i)$ and coefficients of variation (C.O.V.) of the first 3 natural frequencies for this

sample of 6 experiments are listed in the first columns of Table 2.3. Confidence intervals at 95% confidence level are also given in the table. They were evaluated from the sample deviations $s$ according to Eq. (2.11) with $n = 6$ and $\alpha = 0.05$.

**Table 2.3. Effect of manufacturing uncertainties on first 3 natural frequencies of the truss (all values in Hertz).**

| | Experiment | | | Linear approximation | | | Monte Carlo* | | |
|---|---|---|---|---|---|---|---|---|---|
| i | $\bar{\omega}_i$ | $s(\omega_i)$ | C.O.V. | $\bar{\omega}_i$ | $s(\omega_i)$ | C.O.V. | $\bar{\omega}_i$ | $s(\omega_i)$ | C.O.V. |
| | [95% conf. interval for $\sigma$] | | | | | | | | |
| 1 | 99.68 | 0.43 | 0.43% | 100.35 | 0.61 | 0.61% | 100.31 | 0.61 | 0.61% |
| | [0.27. . .1.06] | | | | | | | | |
| 2 | 129.57 | 0.23 | 0.18% | 129.23 | 0.72 | 0.56% | 129.19 | 0.72 | 0.56% |
| | [0.15. . .0.57] | | | | | | | | |
| 3 | 192.55 | 0.61 | 0.32% | 192.15 | 0.81 | 0.42% | 192.07 | 0.81 | 0.42% |
| | [0.38. . .1.49] | | | | | | | | |

* 5000 replications.

Table 2.3 also shows the mean values, standard deviations and coefficients of variation of the natural frequencies computed using the linear approximation of section 2.2. These results are also compared to estimates from a 5000 point Monte Carlo simulation performed assuming normal distributions of the uncertainties. The distribution of the first natural frequency in the Monte Carlo simulation is shown in Figure 2.19. The Monte Carlo simulation was repeated using other assumptions on the distributions of uncertainties (i.e. uniform distributions) and the results were essentially identical (largest difference was 3% on the standard deviation of the second mode). This was again expected from the central limit theorem since the natural frequency depends on a large number of random properties.

The results from the first order analytical prediction and the Monte Carlo simulation are practically identical. However, the experimental estimates of the standard deviations are surprisingly low compared to analytical predictions. Because of experimental errors and the possible existence of unmodeled uncertainties, one would expect that experimental estimates of the scatters in natural frequencies would exceed predicted values. Note however that the sample size (6) is very small. This makes the sample to sample variation of the sample deviation rather large as

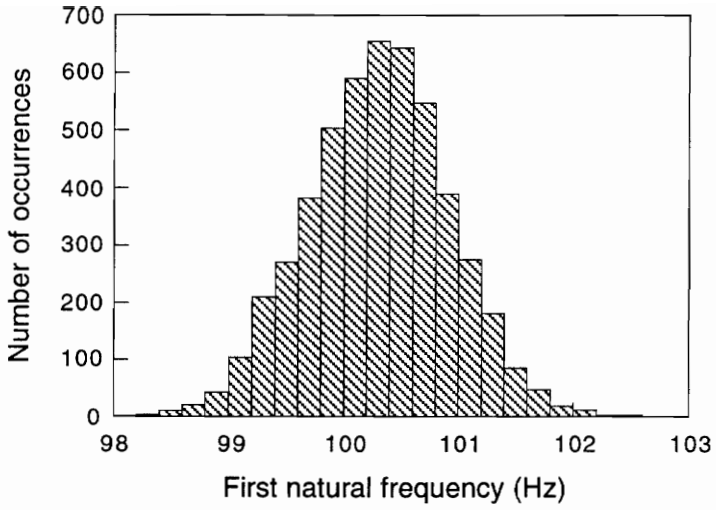


**Figure 2.19. Effect of natural uncertainties; distribution of the first natural frequency (5000-points Monte Carlo simulation).**

evidenced in the size of the confidence intervals of Table 2.3. Notice that the analytical results for mode 1 and 3 fall within the 95% confidence intervals. This however is not true for mode 2. We think that the apparent discrepancy between analytical and experimental results may be due to the fact that, because of limited resolution of the testing machine, the member stiffnesses were measured at load levels (2224 N or 500 lbf), that are much larger than the loads experienced by the members during the forced vibration measurements (estimated to about 22 N (5 lbf) for mode 2 and 133 to 178 N (30 to 40 lbf) for modes 1 and 3). This could have led to an over-estimation of the scatter in the stiffnesses and could explain the discrepancy.

Finally, we note that the scatter in the physical properties of the elements of this truss is extremely small so that the resulting scatter in the natural frequencies is also very small and extremely difficult to measure. For this reason, the "tinker-toy" approach relying on manufacturing uncertainties in this truss is not a feasible approach to compare experimentally the reliabilities of designs obtained from deterministic and probabilistic optimizations. If we want to be able to obtain measurable differences in reliability between two designs, we need to work with systems that contain much larger uncertainties but retain the convenience of being assembled from discrete components.

One category of systems that present these characteristics consists of trusses equipped with viscoelastic tuned dampers. The uncertainties in the damped response of these systems depend

on the scatter in the properties of the dampers. Because the damping effect from a tuned damper is critically dependent on the tuning of the damper (i.e., how well its natural frequency matches that of a target mode of the structure), small deviations in the damper properties tend to create large deviations in the response of the truss. Also, tuned dampers are easily manufactured and cheap (which is important since we need large numbers of them for the statistical analysis), and even small dampers can produce very significant amounts of damping.

These observations led us to choose the design of trusses equipped with tuned dampers as a test case for comparing deterministic and probabilistic optimization approaches. Chapter 3 describes the viscoelastic tuned damper we designed for this study as well as the associated models and analysis techniques. This tuned damper is then used in the analytical and experimental comparisons of deterministic and probabilistic design presented in Chapters 4 and 5.

Note that, as will be shown in Chapter 3, the use of tuned dampers creates very non-linear relations between the system's parameters and its response. Because of this, first order second moment techniques such as derived in section 2.2 will have to be abandoned. The statistical analysis in Chapters 4 and 5 will be done by Monte Carlo simulation. Also, the strong non-linearities and high sensitivities of the damped truss make it very sensitive to modeling errors. This makes the design of the damped truss a realistically difficult problem.

# Chapter 3
# Viscoelastic Tuned Dampers

Viscoelastic tuned dampers were designed and manufactured to increase the amount of damping in the laboratory truss. These dampers will be used in the optimization problems of Chapters 4 and 5. This chapter provides general information about the design of the dampers, the 4-parameter analytical model that describes them, the experimental techniques used to identify these parameters, and a finite element representation. Measures of the magnitude of the damped response for a truss with tuned dampers are also discussed as well as the approximate analytical technique used to compute those measures. Finally, the effect of the different parameters on the performance of the damper is also discussed.

## *3.1 Damper Design*

The tuned dampers (Fig. 3.1) consist of symmetric cantilevered beams, attached at their midpoint to a node of the structure and carrying tip masses at an adjustable distance from the midpoint. The first bending mode of the beams is tuned to a natural frequency of the truss to obtain a tuned damper behavior.

Figure 3.2 shows a schematic sketch of the tuned damper. The beam is a sandwich of 2 thin plastic sheets and an inner core of viscoelastic acrylic foam (3M, product number 4205). This viscoelastic foam is commercially available in the form of a 1.14 mm (0.045 in) thick, double sided self-adhesive tape, which is very convenient for the fabrication of sandwich beams. The same material has been used in passive members for the PACOSS experiment[52]. A 6.35 mm ($1/4$ in) hole is drilled in the middle of the sandwich plate. The damper is attached to a node of the structure with a 6.35 mm ($1/4$ in) nylon screw passing through that hole. A brass washer is embedded in place of the foam around the hole to prevent crushing the damping layer with the attachment screw.

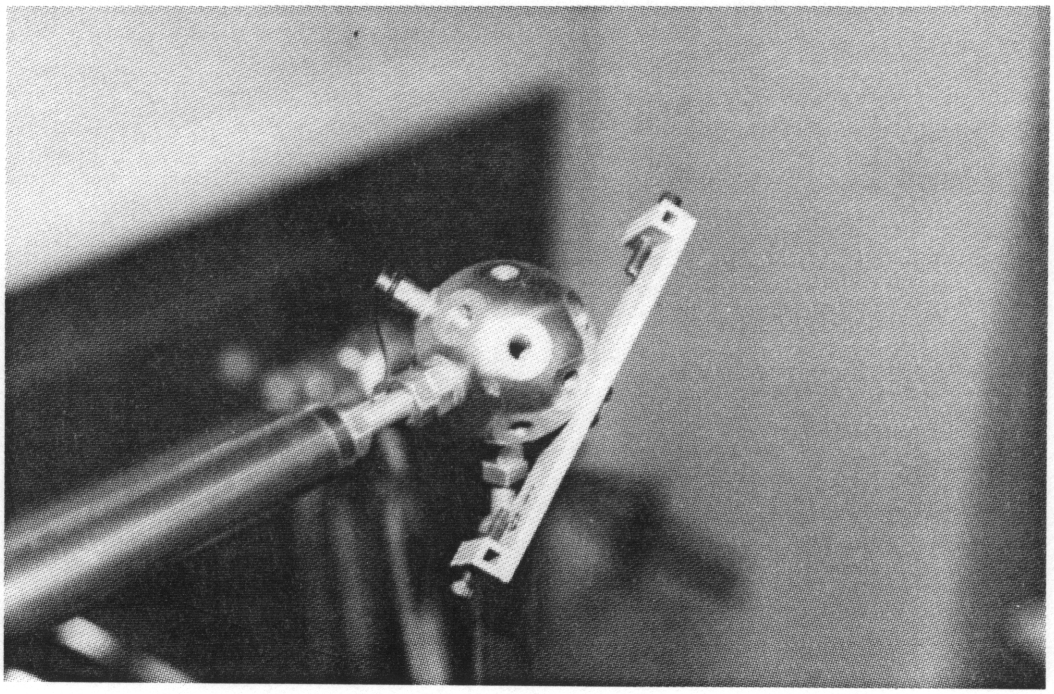

**Figure 3.1. Tuned damper attached to the truss.**

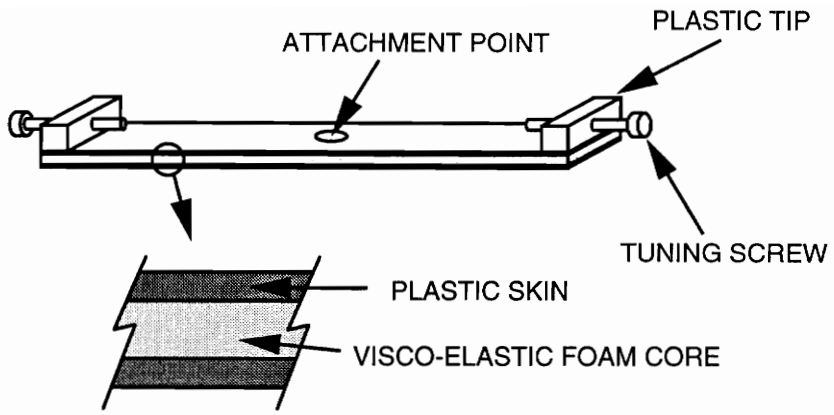


**Figure 3.2. Design of the tuned damper.**

This sandwich design with a relatively thin core induces large shear deformations in the viscoelastic foam, even for small deflections of the beam. The tuned damper is therefore highly damped (the measured loss factor is greater than 10%). This guarantees significant damping to the structure in a relatively wide bandwidth around perfect tuning (see section 3.4).

A plastic tip block is glued to one of the plastic layers at each end of the beam. A steel tuning screw is threaded into each of these blocks. This allows the fundamental frequency of the damper to be adjusted by moving the center of gravity of the tip masses in and out.

Two slightly different versions of this design (we will refer to them as *type 1* and *type 3*) are used to target the first and the third natural frequency of our laboratory truss structure. The dampers of type 1 – used for damping the first mode of the truss – use 0.55 mm ($1/48$ in) thick plastic sheets and are 108 mm ($4\,1/4$ in) long (from tip to tip) and 25.4 mm (1.0 in) wide. The design used for damping the third mode (type 3) is slightly shorter (92.3 mm ($3\,3/4$ in) from tip to tip) and uses thicker plastic skins (0.82 mm or $1/32$ in). This difference in design shifts the damper frequencies to the neighborhoods of their respective target modes. Then the frequencies can be fine-tuned by the tuning screw. Type 1 can be adjusted from about 98 Hz to about 116 Hz; the range for type 3 is about 170 Hz to 204 Hz.

The fabrication of these dampers does not require any particular tooling, and the materials used are widely available and inexpensive. This allows us to manufacture cheaply a large number of each type of damper as needed for the experimental study presented in Chapter 5.

The masses of the dampers are very small compared to the mass of the structure. Both types weigh about 10 grams, which represents about 0.2% of the total mass of the truss. Despite their size, these dampers provide very significant damping to the truss.

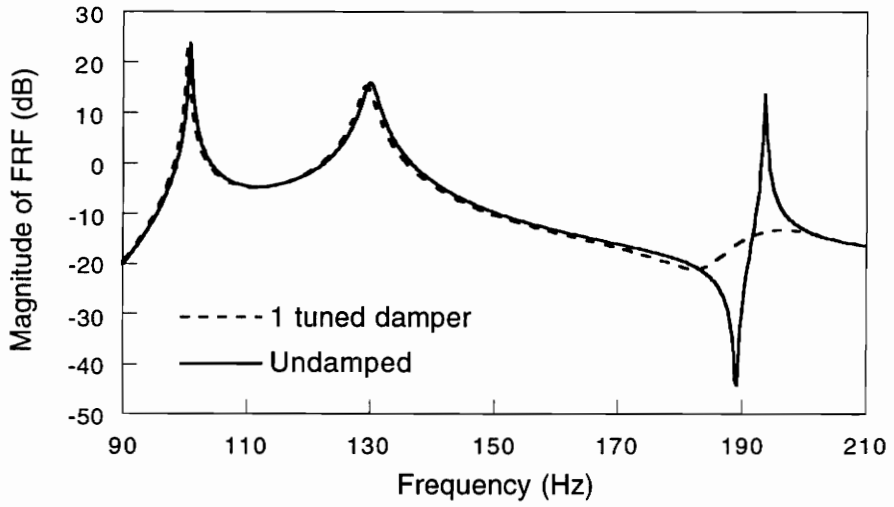


**Figure 3.3. Effect of a type 3 tuned damper on the response of the laboratory truss (the damper is at the most effective location on the truss).**

Figure 3.3 shows the frequency response function (FRF) of a tip node acceleration, before and after adding one type-3 damper to the structure in a quasi-optimal manner (i.e., tuned to the frequency of mode 3 and located at the node and in the direction that correspond to the largest amplitude of vibration in the third mode shape). The reduction in amplitude achieved in mode 3 is more than 25 dB.

Note that the tuned damper does not significantly affect the other modes of the truss because the natural frequencies of these other modes are far from the tuned frequency of the damper, preventing any significant exchange of energy between the truss and the damper (see section 3.4). The very small effect visible on the figure is due to the slight change in the natural frequency of the truss due to the mass of the damper. This implies that at least one damper per target mode is needed.

## 3.2 Modeling

### 3.2.1 Four Parameter Simplified Model

The following simplifying assumptions are made about the dampers. First, the attachment point is assumed to move in pure translation, neglecting any rotation of the supporting node (note that our truss model does not include these rotations). Second, the two halves of the damper are assumed identical, so that their deflections are identical in magnitude and phase, and the contributions from the two halves can be superposed. Finally, the damper is assumed to deform only in its first bending mode (higher modes are neglected as well as torsion along the axis of the beam).

With these simplifications, the damper can be represented as a two degree of freedom system, consisting of an infinitely stiff and massless lever of length $d$, simply supported but elastically restrained at the base by a torsional spring $k_\alpha$, and carrying a concentrated mass $m$ at the tip and $m_0$ at the base (Fig. 3.4).

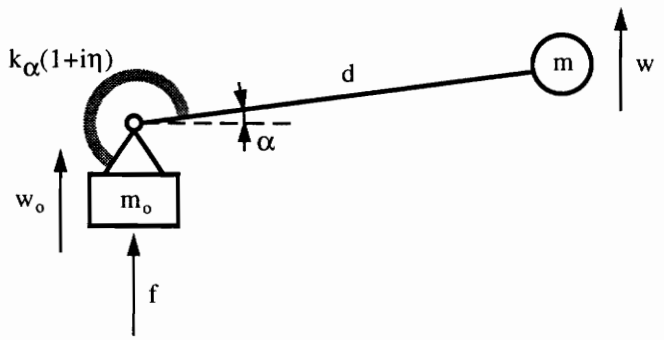


**Figure 3.4. Tuned damper, two degrees of freedom lever model.**

This single lever models the combined effects of both halves of the damper. The damping from the viscoelastic material is modeled using a complex stiffness value for the elastic restraint spring $k_\alpha(1 + i\eta)$ where $\eta$ is the loss factor. The use of complex stiffness is a typical choice to model the internal damping of viscoelastic materials. Parin *et al.*[52] have measured the physical properties of the particular foam (3M-4205) as a function of frequency and temperature. Their

results indicate that the loss factor of this material is almost constant between 100 and 200 Hz (the variation is less than 20%; it would be 100% for viscous damping). Also, we initially used a model that contained both viscous and complex stiffness damping. The parameter identification procedure described in section 3.2.2 consistently converged to zero viscous damping and confirmed the final assumption of pure complex stiffness damping. The equations of motion of the system of figure 3.4 with base excitation are

$$md^2\ddot{\alpha} + md\ddot{w}_0 + k_\alpha(1 + i\eta)\alpha = 0\,, \tag{3.1}$$

$$m_0\ddot{w}_0 + m\ddot{w} = f\,, \tag{3.2}$$

where $d$ is the length of the lever, $\alpha$ measures its angle of rotation, $w_0$ and $w$ measure the vertical displacements of the base and tip, and $f$ is the force applied to the base of the damper, and the dots represent differentiation with respect to time. For small deflections, the angle $\alpha$ is related to $w$ and $w_0$ according to

$$\alpha = \frac{w - w_0}{d}\,. \tag{3.3}$$

Substituting this relation in the first equation of motion (3.1) and dividing by $d$ we get

$$m\ddot{w} + \frac{k_\alpha}{d^2}(1 + i\eta)(w - w_0) = 0\,. \tag{3.4}$$

Note that this system can be represented as a simple linear spring-mass system as shown in Fig. 3.5, where the stiffness of the spring is

$$k = \frac{k_\alpha}{d^2}\,. \tag{3.5}$$

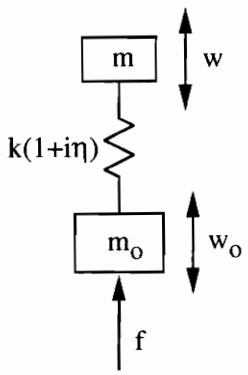


**Figure 3.5. Tuned damper, spring-mass model.**

This model is entirely defined by four parameters. Several different combinations can be used; we chose the tip mass $m$, the total mass $m_T = m + m_0$, the natural frequency $\omega_n = \sqrt{\frac{k_a}{m d^2}}$ and the loss factor $\eta$.

Assuming $w = We^{i\omega t}$, $w_0 = W_0 e^{i\omega t}$, and $f = Fe^{i\omega t}$ we obtain the equations of motion in the frequency domain as

$$-\omega^2 W + \omega_n^2(1 + i\eta)(W - W_0) = 0\,, \tag{3.6}$$

$$-\omega^2(m_0 W_0 + mW) = F\,. \tag{3.7}$$

Using the first equation (3.6), we express $W$ in terms of $W_0$ as

$$W = \frac{\omega_n^2(1 + i\eta)}{\omega_n^2(1 + i\eta) - \omega^2} W_0\,, \tag{3.8}$$

then substitute (3.8) into (3.7) to get a single-input single-output transfer function that relates the acceleration of the base (that is, the acceleration of the supporting node) to the force transmitted to the base as

$$H = \frac{F}{-\omega^2 W_0} = \frac{\omega_n^2(m + m_0)(1 + i\eta) - m_0\omega^2}{\omega_n^2(1 + i\eta) - \omega^2}\,. \tag{3.9}$$

The net amount of energy $D$ absorbed by the damper in one cycle at frequency $\omega$ determines the amount of damping provided to the structure. It can be computed as

$$D = \int_{t_o}^{t_o+T} f(t)\dot{w}_0(t)\,dt\,, \tag{3.10}$$

where $t_o$ is an arbitrary initial time and $T = 2\pi/\omega$ is the duration of a cycle. Substituting $f(t) = \Re(Fe^{i\omega t})$ and $w_0(t) = \Re(W_0 e^{i\omega t})$, where $\Re$ stands for the real part operator, and carrying out the integration we find

$$D = -\pi\Im(FW_0^*)\,, \tag{3.11}$$

where the superscript $^*$ denotes the complex conjugate and $\Im$ the imaginary part operator. Replacing $F$ by its expression in terms of $W_0$ and the transfer function $H$

$$F = -\omega^2 W_0 H\,, \tag{3.12}$$

we find

$$D = -\pi\omega^2 \|W_0\|^2 \Im(H)\,. \tag{3.13}$$

The imaginary part of the frequency response function $H$ is therefore of particular interest because it is directly related to the net amount of energy dissipated in the damper in one cycle. Extracting the imaginary part of (3.9) we find

$$\Im(H) = -\eta m \frac{\omega^2/\omega_n^2}{(1-\omega^2/\omega_n^2)^2 + \eta^2}. \tag{3.14}$$

and finally

$$D = \pi\omega^2 \|W_0\|^2 \eta m \frac{\omega^2/\omega_n^2}{(1-\omega^2/\omega_n^2)^2 + \eta^2}. \tag{3.15}$$

The energy absorbed per cycle is dependent on the damper location (through $\|W_0\|^2$). This implies that optimum locations for the damper maximize the magnitude of the component of displacement orthogonal to the sandwich plate. Also, $D$ depends linearly on the tip mass $m$. The tip mass should be thought of as the "size" of the damper. It acts as a scaling factor on the damping provided to the structure. The dependencies on the loss factor $\eta$ and the frequency ratio $\omega/\omega_n$ are somewhat more complicated. Figure 3.6 shows the effect of those two parameters on the normalized energy dissipation $D^\star$ defined as

$$\begin{aligned} D^\star &= \frac{D}{\omega^2 \|W_0\|^2 m} \\ &= \pi\eta \frac{\omega^2/\omega_n^2}{(1-\omega^2/\omega_n^2)^2 + \eta^2}. \end{aligned} \tag{3.16}$$

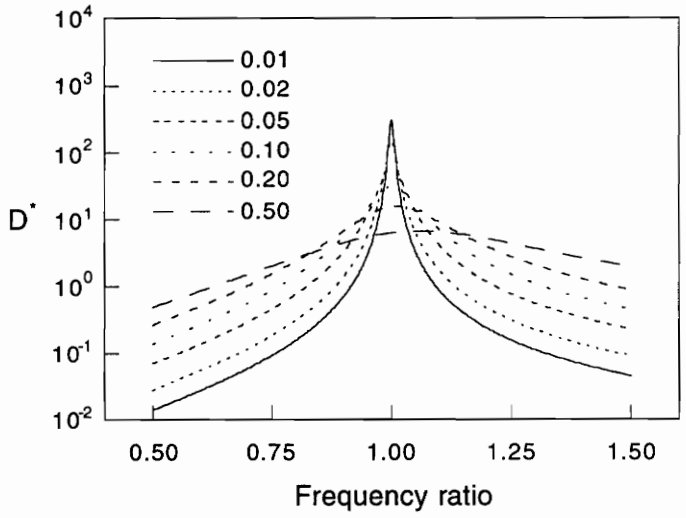


**Figure 3.6. Effect of frequency ratio on normalized energy absorption; the 6 curves correspond to different values of the loss factor.**

This function presents a peak around a frequency ratio of 1. The frequency $\bar{\omega}$ that maximizes the energy $D$ absorbed per cycle should be considered as the tuning frequency. Adjusting that frequency to match the natural frequency of the structure maximizes the damping obtained in the structure-damper system. That frequency is easily found to be,

$$\bar{\omega} = \omega_n \sqrt{1 + \eta^2} \,. \tag{3.17}$$

### 3.2.2 Experimental Identification of Damper Parameters

The parameters used to describe the damper ($m$, $m_T$, $f_n$ and $\eta$, see section 3.2.1) are derived from the description of a complex physical system (the sandwich beam in flexure) by a simple model (the spring-mass system of Fig. 3.5), and are therefore not directly measurable. Instead, they have to be identified from the response of the damper. The transfer function $H$ defined in the previous section is an ideal candidate. Note that this transfer function measures the excitation force per unit base acceleration; it is the inverse of the mechanical impedance. It can be easily measured and the parameters of the damper can then be identified by curve fitting the analytical transfer function predicted from the model of Fig. 3.5 to the experimental measurement.

The experimental set up used for measuring the transfer function is shown in Fig. 3.7. The damper is attached to the moving coil of an electromagnetic shaker (MB Electronics, model EA1500). The lateral stiffnesses of this shaker are large enough that the motion of the base of the damper can be considered unidirectional. A piezoelectric load cell (PCB 208A) measures the force applied to the base of the damper and an accelerometer (PCB 353B17), located inside the shaker-load cell adapter measures its acceleration. An aluminum adapter is mounted on top of the load cell and accepts the 6.35 mm (¼ in) nylon screw holding the damper. The tightness of that screw was determined to have a large effect on the behavior of the damper. To ensure repeatability of the measurements, the screw was tightened with a fixed torque by a torque-metering screwdriver.

The signal generator of a Tektronix 2630 FFT analyzer is used to drive the shaker through a power amplifier (KEPCO BOP 50-2M). The transfer function from base acceleration to base force is measured using a sine dwell technique. The amplitude of the excitation signal is adjusted so that the amplitude of vibration of the tuned damper on the shaker is of the same order of

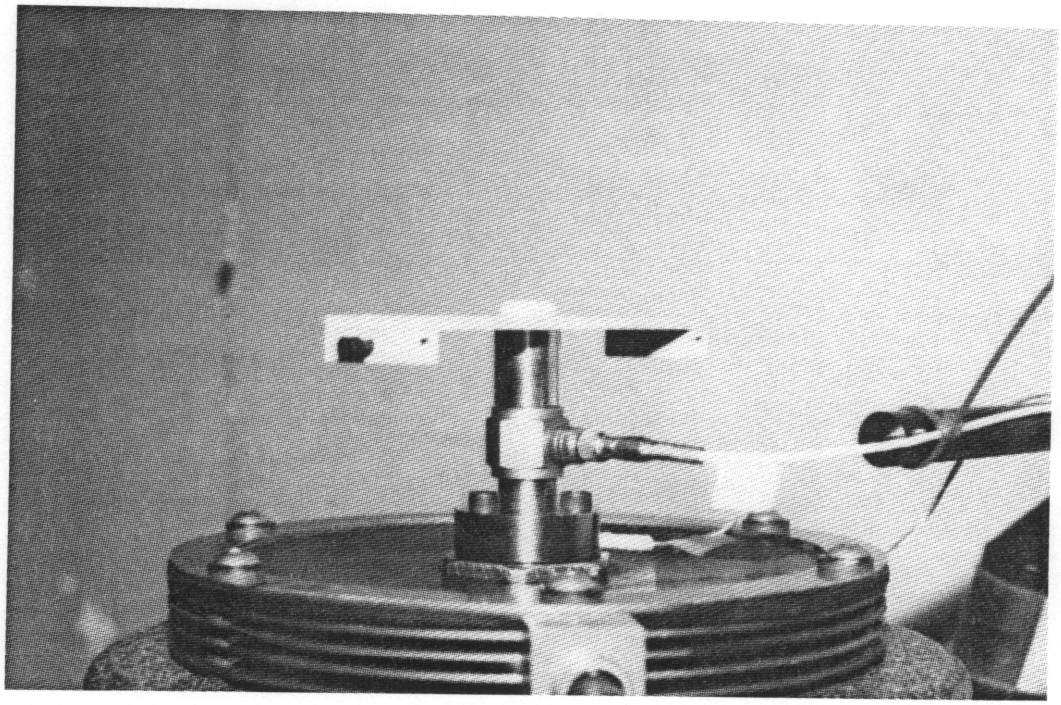

**Figure 3.7. Measurement of damper parameters: experimental set up.**

magnitude as on the damped structure. This is done to minimize the effect of any non-linear behavior.

Because the total mass of the damper affects the natural frequencies of the structure, it is desirable that the value of $m_T$ used in the model be equal to the actual mass of the damper, measured on a scale. Also, when measuring the transfer function on the shaker set up, the magnitude of the base mass $m_0$ is contaminated by the mass of the adapter and part of the mass of the load cell. In addition, we have shown in section 3.2.1 that the imaginary part of the transfer function from base force to base acceleration is independent of $m_0$ and is directly related to the energy dissipated by the damper in one cycle, which in turn is directly related to the amount of damping introduced in the truss structure.

Considering these factors, we decided to curve fit only the imaginary part of the transfer function which depends only on the 3 parameters $m$, $\omega_n$, and $\eta$, see Eq. 3.14. The base mass $m_0$ does not appear in the expression so that the masses of the load cell and adapter do not have to be considered.

The data acquisition and post-processing were entirely automated in MATLAB[53]. A 3 parameter least square fit is performed on the imaginary part of the measured transfer function and provides estimates for $m$, $f_n$, and $\eta$. The remaining parameter $m_T$ is measured on a scale. Note that the effects of the 3 parameters are clearly decoupled (section 3.4), so that the identification procedure is numerically very stable. Figure 3.8 shows a typical result of the identification procedure for a damper of type 1. The points represent the imaginary part of the measured transfer function (only a few of the experimental points are shown for clarity) and the solid line corresponds to the identified model. The least square fit used the data measured from 50 to 150 Hz. The values of the identified parameters are also listed in the figure.

Because the dampers use a viscoelastic foam, their characteristics are strongly dependent on temperature. The effect of temperature on the identified parameters was measured to be about 9% per $^o$C (5% per $^o$F) on the loss factor, -0.9% per $^o$C (-0.5% per $^o$F) on the natural frequency, and 0.7% per $^o$C (0.4% per $^o$F) on the identified tip masses. To protect ourselves from this effect, we use a temperature stabilization system that maintains the temperature of the laboratory at 24.4$^o$C (76$^o$F) on average with a rapid oscillation of $\pm$0.8$^o$C ($\pm$1.5$^o$F). The period of that oscillation is

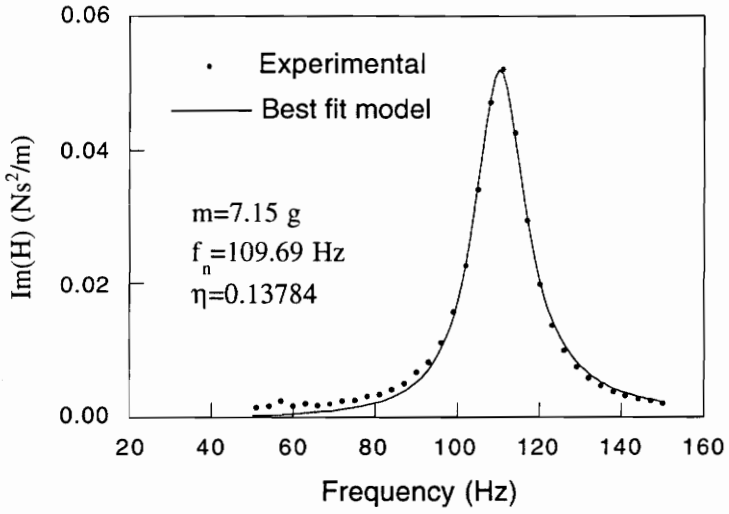


**Figure 3.8. Result of a damper parameter identification (type 1 damper).**

about 15 minutes. All measurements are repeated 3 times and averaged to reduce the effect of the small temperature oscillation and other measurement errors.

Also, the deformations and temperature perturbations introduced in the sandwich beams when manipulating the dampers were found to affect the identified parameters if the dampers were not allowed to rest on the set up for a few minutes before taking the measurements. A 5 minute waiting time was found sufficient to allow the damper to return to its undeformed state at room temperature. With the very large number of measurements needed for statistical evaluation, this waiting time considerably lengthened the experimental program.

### 3.2.3 Tuned Damper Finite Element

The damper is intended to be attached to a truss structure. The truss model has only translation degrees of freedom. In this section, we derive a finite element that models the interaction between the truss and the damper.

The damper is defined by its four parameters: the total mass $m_T$, a tip mass $m$, the natural frequency $f_n$, and the loss factor $\eta$ (see Fig. 3.9). The base mass $m_0$ and the stiffness $k$ are related to these 4 parameters according to

$$m_0 = m_T - m\,, \tag{3.18}$$

and

$$k = m\omega_n^2 \,, \tag{3.19}$$

where $\omega_n = 2\pi f_n$.

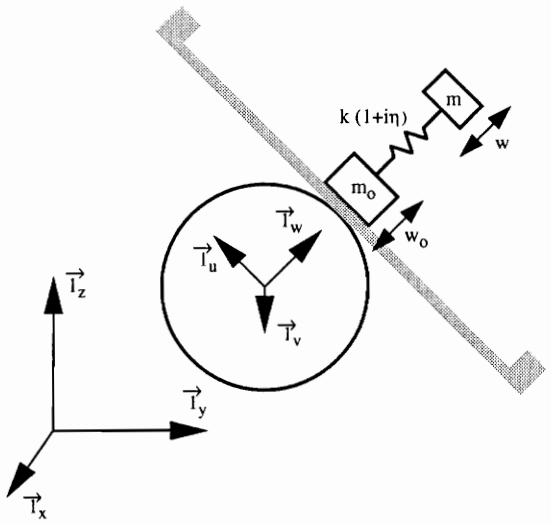


**Figure 3.9. Tuned damper finite element.**

We define a local rectangular reference frame $(\vec{1}_u, \vec{1}_v, \vec{1}_w)$ where $\vec{1}_w$ is aligned with the direction of the normal to the physical sandwich plate. As shown below, the choice of $\vec{1}_u$ and $\vec{1}_v$ does not affect the finite element matrices, and so is left unspecified. The components of the motion of the base node in that local frame are $u_0$, $v_0$, $w_0$. The tip mass $m$ is constrained to move along $\vec{1}_w$ with respect to the base node so that its components of displacement are $u_0$, $v_0$, $w$. With this assumption the equations of motion are

$$(m + m_0)\ddot{u}_0 = f_u \,, \tag{3.20}$$

$$(m + m_0)\ddot{v}_0 = f_v \,, \tag{3.21}$$

$$m_0\ddot{w}_0 + k(1 + i\eta)(w_0 - w) = f_w \,, \tag{3.22}$$

$$m\ddot{w} + k(1 + i\eta)(w - w_0) = 0 \,, \tag{3.23}$$

where $f_u$, $f_v$, $f_w$ are the components in the local frame of the force transmitted by the structure to the base of the damper. These equations are put in matrix form as

$$M_d \frac{d^2}{dt^2} \begin{Bmatrix} u_0 \\ v_0 \\ w_0 \\ w \end{Bmatrix} + K_d \begin{Bmatrix} u_0 \\ v_0 \\ w_0 \\ w \end{Bmatrix} = \begin{Bmatrix} f_u \\ f_v \\ f_w \\ 0 \end{Bmatrix} \,, \tag{3.24}$$

where

$$M_d = \begin{bmatrix} m_T & 0 & 0 & 0 \\ 0 & m_T & 0 & 0 \\ 0 & 0 & m_0 & 0 \\ 0 & 0 & 0 & m \end{bmatrix}, \tag{3.25}$$

and

$$K_d = \begin{bmatrix} 0 & 0 & 0 & 0 \\ 0 & 0 & 0 & 0 \\ 0 & 0 & k(1+i\eta) & -k(1+i\eta) \\ 0 & 0 & -k(1+i\eta) & k(1+i\eta) \end{bmatrix}. \tag{3.26}$$

We now express the degrees of freedom $u_0$, $v_0$, and $w_0$ in terms of the nodal displacements $x$, $y$, and $z$ in global axes $\vec{1}_x$, $\vec{1}_y$, $\vec{1}_z$ using the transformation

$$\begin{Bmatrix} u_0 \\ v_0 \\ w_0 \\ w \end{Bmatrix} = T \begin{Bmatrix} x \\ y \\ z \\ w \end{Bmatrix}, \tag{3.27}$$

where

$$T = \begin{bmatrix} R & 0_{3\times 1} \\ 0_{1\times 3} & 1 \end{bmatrix}, \tag{3.28}$$

and R is a $3 \times 3$ rotation matrix that brings $\vec{1}_x, \vec{1}_y, \vec{1}_z$ on $\vec{1}_u, \vec{1}_v, \vec{1}_w$ i.e.

$$R = \begin{Bmatrix} \vec{1}_u^T \\ \vec{1}_v^T \\ \vec{1}_w^T \end{Bmatrix}_G, \tag{3.29}$$

where the subscript $G$ indicates that the unit vectors are expressed in the global reference frame $\vec{1}_x, \vec{1}_y, \vec{1}_z$. Using the same transformation for the forces and substituting in (3.24) we get, after premultiplying by $T^T$ (T is orthogonal)

$$M \frac{d^2}{dt^2} \begin{Bmatrix} x \\ y \\ z \\ w \end{Bmatrix} + K \begin{Bmatrix} x \\ y \\ z \\ w \end{Bmatrix} = \begin{Bmatrix} f_x \\ f_y \\ f_z \\ 0 \end{Bmatrix}, \tag{3.30}$$

where $f_x$, $f_y$, $f_z$ are the components in global axes of the force exerted by the structure on the base of the damper, and

$$M = T^T M_d T \tag{3.31}$$

$$\text{and} \qquad K = T^T K_d T, \tag{3.32}$$

are the mass and stiffness matrices of the damper in global axes. We carry out these transformations by first decomposing $M_d$ into $M_{d1}$ and $M_{d2}$,

$$M_d = M_{d1} - M_{d2}\,, \tag{3.33}$$

with

$$M_{d1} = \begin{bmatrix} m_T & 0 & 0 & 0 \\ 0 & m_T & 0 & 0 \\ 0 & 0 & m_T & 0 \\ 0 & 0 & 0 & m \end{bmatrix}, \tag{3.34}$$

and

$$M_{d2} = \begin{bmatrix} 0 & 0 & 0 & 0 \\ 0 & 0 & 0 & 0 \\ 0 & 0 & m & 0 \\ 0 & 0 & 0 & 0 \end{bmatrix}. \tag{3.35}$$

Since $R$ is an orthogonal matrix, $M_{d1}$is unchanged in the transformation,

$$T^T M_{d1} T = \begin{bmatrix} m_T R^T R & 0_{3\times 1} \\ 0_{1\times 3} & m \end{bmatrix} = M_{d1}\,, \tag{3.36}$$

while the second matrix $M_{d2}$ is changed into

$$T^T M_{d2} T = \begin{bmatrix} m\vec{1}_w \vec{1}_w^T & 0_{3\times 1} \\ 0_{1\times 3} & 0 \end{bmatrix}. \tag{3.37}$$

The transformed damper mass matrix in global axes is then

$$M = \begin{bmatrix} m_T I_{3\times 3} - m\vec{1}_w \vec{1}_w^T & 0_{3\times 1} \\ 0_{1\times 3} & m \end{bmatrix}. \tag{3.38}$$

The same transformation is applied to the stiffness matrix $K_d$ to give the damper stiffness matrix in global axes as

$$K = \begin{bmatrix} k(1+i\eta)\vec{1}_w \vec{1}_w^T & -k(1+i\eta)\vec{1}_w \\ -k(1+i\eta)\vec{1}_w^T & k(1+i\eta) \end{bmatrix}. \tag{3.39}$$

Matrices $M$ and $K$ are then assembled to the model of the truss. Each added damper increases the number of degrees of freedom in the system by 1. As can be seen from Eqs. (3.38) and (3.39), the choice of $\vec{1}_u$ and $\vec{1}_v$ does not affect the finite element model. This also means that the model is insensitive to rotations of the dampers about the screws used to attach them to the truss. In other words, only the direction of the normal to the sandwich plane matters (in the model). Note that in reality, the orientation of the damper about the normal has a small effect on the damper performance. This is due to coupling with small amounts of node rotation and was

confirmed by a more detailed finite element analysis. However, this effect is small enough to be neglected.

## 3.3 Analysis of a Truss with Tuned Dampers

In the analysis of space structures, the damping ratios associated with the vibration modes are often used as measures of the damping available to the structure. However, the use of tuned dampers produces pairs of very closely spaced natural modes. Around the natural frequency of a damped mode, the response of the truss corresponds to the superposition of these 2 modes (and of course smaller contributions from the other modes). The superposition of these two modes results in only one identifiable resonance peak in the response of the truss. Furthermore, the damping ratios associated with two closely spaced modes are very sensitive to small changes in the properties of the system. In these conditions, the damping ratios of the individual modes are not a good measure of the damped response of the structure. Other measures are more appropriate.

For a given location of the excitation, one such measure is the largest magnitude (over a frequency range) of the transfer function between the excitation force and the response acceleration at specified points on the structure as illustrated in Fig. 3.10. This measure will be referred to as *peak acceleration* and denoted $H_{max}$.

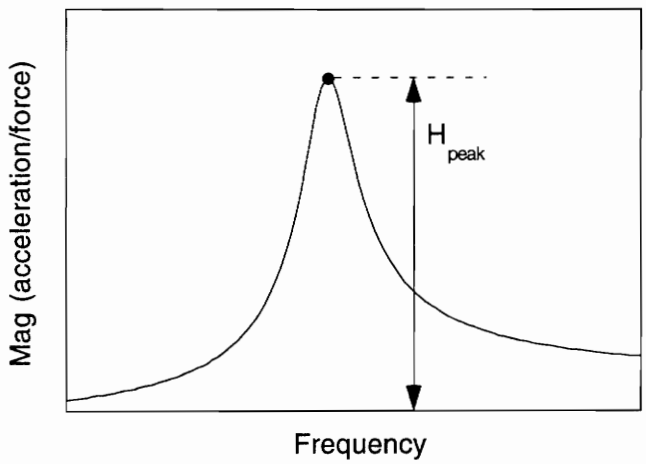


**Figure 3.10. Peak acceleration of a damped mode.**

To evaluate the peak acceleration, the magnitude of the transfer function is evaluated numerically with a relatively coarse step size within the frequency window of interest. The peak is first located approximately using a simple slope reversal search. The location of the peak and the corresponding value of the FRF are then refined by second order interpolation between the approximate peak and the 2 neighboring points in the FRF. This technique requires the calculation of the transfer function. The next 2 sections describe a full order analysis that uses the classical mode superposition method and a very fast reduced order approximation that uses a closed form analytical expression of the transfer function.

### 3.3.1 Full Order Analysis

Since we are concerned with damping, the model of section 2.1.3 is extended to account for the inherent damping in the truss. For consistency with the model of the dampers, we also used complex stiffness to model the inherent damping in the truss. Each member is given a complex stiffness $k(1 + i\eta_s)$ where $\eta_s$ is a loss factor. With this, the stiffness matrix $K$ and the displacement vector $x$ are complex and the free damped vibration equation of the truss equipped with tuned dampers is

$$M\ddot{x} + Kx = 0\,, \tag{3.40}$$

where $M$ and $K$ are the mass and stiffness matrices and $x$ is the vector of nodal displacements and damper deflections. The order of this system is equal to the number of degrees of freedom of the clamped truss (36) plus the number of dampers attached to the truss. The eigenvalue problem corresponding to (3.40) is

$$Ku = -\lambda^2 Mu\,, \tag{3.41}$$

where $u$ is the eigenvector and $\lambda$ the eigenvalue. Equation (3.41) is a generalized complex eigenvalue problem that is solved numerically. The transfer function is then evaluated using the mode superposition method[54]

The design optimizations of Chapters 4 and 5 will be performed using genetic algorithms. Being a random search technique, a genetic algorithm uses a very large number of analyses. Moreover, in the probabilistic approach, the probabilities of failure will be evaluated using Monte Carlo simulations. In that context, the computational burden associated with the solution of (3.41)

is prohibitive. The next section describes an approximate, semi-analytical technique to evaluate the transfer function.

### 3.3.2 Semi-Analytical Approximation

The method described here is designed to evaluate the transfer function of a truss equipped with no more than one damper for each elastic mode. The frequencies of the different elastic modes of the undamped truss are assumed well separated, so that each mode can be considered separately. With these assumptions, each resonance of the damped truss can be analyzed with a one degree of freedom (d.o.f.) model of the structure attached to a 1 d.o.f. model of the damper. The resulting model has only 2 d.o.f.'s so that a closed form analytical expression can be derived for the transfer function (if more than 1 damper was used for a particular mode, the resulting system would have more than 2 d.o.f.'s and a different — and more complicated — analytical expression would have to be derived). That analytical expression replaces the solution of the eigenvalue problem and the mode superposition method.

Starting from the mass and stiffness matrices of the truss without tuned damper, the first step consists of adding the dead mass effect of the tuned damper to the mass matrix of the truss (the dead mass is $m_0$ in the damping direction and $m_T$ in directions orthogonal to the damping direction). The resulting modified mass matrix is denoted $M'$; the stiffness matrix $K$ remains unchanged. Let us denote by $x$ the vector of nodal displacements of the truss. We define three vectors $\vec{1}_d$, $\vec{1}_f$ and $\vec{1}_a$ that determine the locations and orientations of the damper, excitation force and response acceleration measurement with respect to the degrees of freedom of the truss. The vectors contain zeros at all degrees of freedom except for the node to which the damper is attached or at which the excitation force is applied or the acceleration measured; the 3 non-zero components corresponding to that node contain the directional cosines of the damping, forcing or measurement direction, expressed in the global axis system. In the case of $\vec{1}_d$, these non-zero components are the directional cosines of the normal to the damper plane ($\vec{1}_w$). With these definitions, the motion $w_0$ of the base of the damper is $w_0 = \vec{1}_d^T x$ and the equation of motion of the damped truss

$$M'\ddot{x} + Kx = -\vec{1}_d\, k\,(1 + i\eta)\,(\vec{1}_d^T x - w) + f\,\vec{1}_f\,, \tag{3.42}$$

where $k$ is the stiffness of the damper, equal to $m\omega_n^2$. The motion $w$ of the tip of the damper is described by the equation (see Eqs. 3.4 and 3.5)

$$m\ddot{w} + k(1+i\eta)(w - \vec{1}_d^T x) = 0\,. \tag{3.43}$$

The measured acceleration $a$ can be obtained by multiplying the vector $\ddot{x}$ of nodal accelerations by $\vec{1}_a$ as

$$a = \vec{1}_a^T \ddot{x}\,. \tag{3.44}$$

We now reduce the degrees of freedom of the truss to only one mode shape $u$. We define the scalar reduced coordinate $q$ according to

$$x = uq\,. \tag{3.45}$$

Substituting (3.45) into (3.42), (3.43), and (3.44) and premultiplying by $u^T$ we get

$$u^T M u\,\ddot{q} + u^T K u\, q = -u^T \vec{1}_d\, k\,(1+i\eta)\,(\vec{1}_d^T uq - w) + u^T f\,\vec{1}_f \tag{3.46}$$

$$m\ddot{w} + k\,(1+i\eta)\,(w - \vec{1}_d^T uq) = 0 \tag{3.47}$$

$$a = \vec{1}_a^T\, u\,\ddot{q} \tag{3.48}$$

Assuming $q = Qe^{i\omega t}$, $f = Fe^{i\omega t}$, $w = We^{i\omega t}$, and $a = Ae^{i\omega t}$, where Q, F, W and A are complex numbers, and substituting $k = m\omega_n^2$ we rewrite those equations in the frequency domain as

$$-\mu\omega^2 Q + \kappa Q = -\delta\,\omega^2\, m\,(1+i\eta)\,(\delta Q - W) + \varphi\, F \tag{3.49}$$

$$-\omega^2 W + \omega_n^2\,(1+i\eta)\,(W - \delta Q) = 0 \tag{3.50}$$

$$A = -\alpha\omega^2 Q \tag{3.51}$$

where $\delta$ is the modal amplitude at the damper location, $\alpha$ and $\varphi$ are the modal amplitudes at the acceleration pickup and forcing points, and $\kappa$ and $\mu$ are the modal stiffness and mass corresponding to mode $u$, repectively. They are defined as

$$\delta = u^T \vec{1}_d\,, \tag{3.52}$$

$$\alpha = u^T \vec{1}_a\,, \tag{3.53}$$

$$\varphi = u^T \vec{1}_f\,, \tag{3.54}$$

$$\kappa = u^T K u\,, \tag{3.55}$$

$$\mu = u^T M u\,, \tag{3.56}$$

From equation (3.50) we find

$$W = \frac{\delta\omega_n^2\,(1+i\eta)}{\omega_n^2(1+i\eta)-\omega^2}\,Q\,. \tag{3.57}$$

Substituting this last expression into (3.49) we finally get the frequency response function

$$\begin{aligned} H(\omega) &= \frac{A}{F} = -\alpha\omega^2\frac{Q}{F} \\ &= \alpha\,\varphi\,\omega^2\,\frac{\omega_n^2\,(1+i\eta)-\omega^2}{\omega^2\,(\kappa-\mu\omega^2)+\omega_n^2\,(1+i\eta)\,(\mu\omega^2+m\delta^2\omega^2-\kappa)}\,. \end{aligned} \tag{3.58}$$

This expression replaces the mode superposition method and the solution of the generalized eigenvalue problem of Eq. (3.41). To evaluate the accuracy of this approximation, we computed the peak acceleration of the truss equipped with one tuned damper in a near-optimal location (one that maximizes $\delta$), as a function of the natural frequency of the damper. The results from the approximation are compared to those of a full order analysis. Figure 3.11 gives the results for a type-1 damper while Fig. 3.12 corresponds to a type 3 damper.

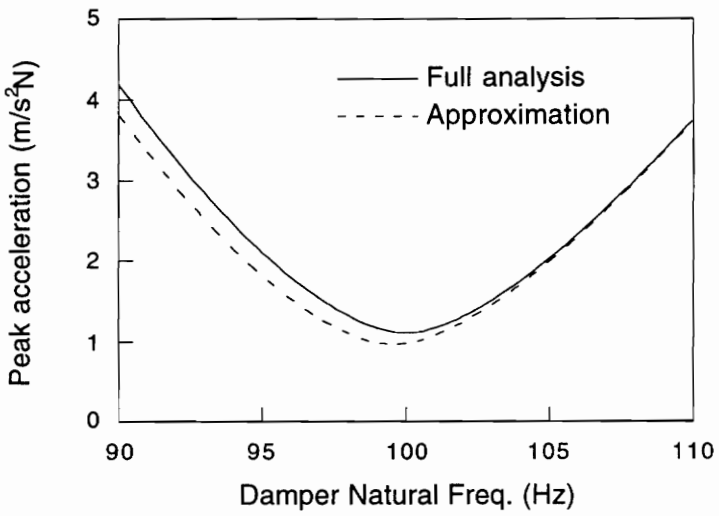


**Figure 3.11. Peak acceleration of of the first mode as a function of the natural frequency of the damper (damper of type 1, $m$=7g, $m_T$=10g, $\eta$=0.15 at node 12, direction 4).**

In the range of mistuning considered, the error in the approximation goes up to about 16% for type 1 and 4% for type 3. Also, the frequency for minimum peak acceleration differs slightly

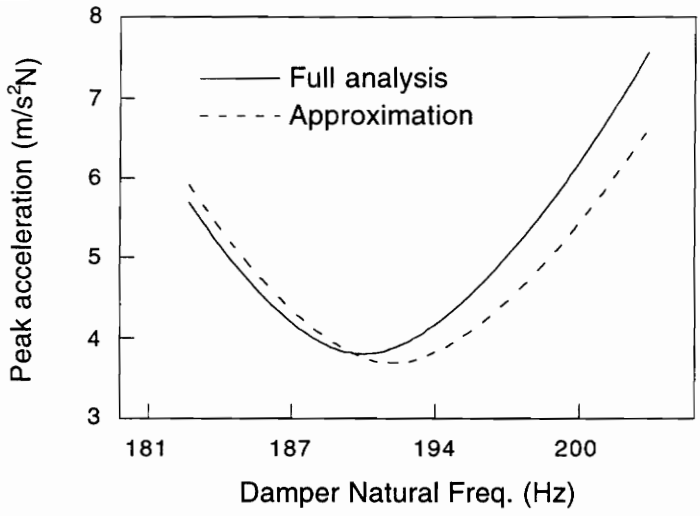


**Figure 3.12. Peak acceleration of of the third mode as a function of the natural frequency of the damper (damper of type 3, $m$=7g, $m_T$=10g, $\eta$=0.15 at node 11, direction 8).**

between the two analyses. However, we consider the accuracy of the approximation sufficient for use in the optimizations. The design obtained from an optimization using the approximation will probably be slightly sub-optimal when evaluated with the full analysis. The difference is expected to be small, however, and will be ignored. Also, the probabilities of failure of the optimal designs will be predicted based on the full analysis for comparison with experimental results.

## *3.4 Performance: Effect of Different Parameters*

With the model of section 3.2.1, a damper is entirely defined by the value of its 4 parameters: the tip mass $m$, the total mass $m_T$, the natural frequency $f_n$ and the loss factor $\eta$. Each of these parameters influences the performance of the damper. In the same section, a study of the energy absorption has already shown that the tip mass acts somewhat like a scaling factor on the effectiveness of the damper (when the other 3 parameters are kept constant). Here, we investigate the effect of the parameters on the peak acceleration of a target mode of the damped truss.

We define the *tuning ratio* $r$ as the natural frequency of the damper divided by the natural frequency of the target mode of the original truss (undamped and without the dead mass effect

of the damper). When $r$ is equal to 1, the damper is perfectly tuned to the undamped truss. The damper will be said *overtuned* when $r > 1$ and undertuned when $r < 1$. We will see that the effect of the damper parameters on the peak acceleration is highly dependent on the value of the tuning ratio.

The total mass $m_T$ of the tuned damper is responsible for a slight shift in the natural frequency of the target mode: adding the tuned damper to a node of the truss increases the dead mass at that node which in turn decreases the natural frequencies of the structure. This change in natural frequency of the truss modifies the relative tuning of the damper and truss. The effect of the shift on the peak acceleration of the truss depends on the initial tuning of the damper: for $r \geq 1$ the peak amplitude increases with $m_T$ because the dead mass effect brings the natural frequency of the truss away from that of the damper; for $r < 1$ the effect is reversed.

The curves in Fig. 3.13 represent the effect of $m_T$ on the peak amplitude of the third mode of our laboratory truss (natural frequency before adding the damper is 193 Hz). The three curves correspond to different values of the initial tuning ratio (5% undertuned, perfectly tuned, and 5% overtuned). The other 2 parameters are kept constant. Their values are listed in the figure.

The effects of the damper loss factor and natural frequency are illustrated in Figs. 3.14 and 3.15. The curves in Fig. 3.14 show the effect of the tuning ratio on the peak amplitude for different values of the loss factor. In Fig. 3.15, the effect of the loss factor is plotted for different values of the tuning ratio.

For perfect tuning, the performance of the damper is better (the peak acceleration is smaller) when its loss factor is smaller. When the tuning is imperfect, however, this effect is reversed and a damper with a larger loss factor is more effective. In other words, a lightly damped tuned damper is potentially more effective than a more heavily damped design, but only if it can be very accurately tuned. A damper with a relatively high loss factor is less effective at perfect tuning but is more tolerant to tuning errors and therefore more appropriate in cases where the natural frequencies of the truss are not completely predictable or likely to change over time.

Finally, Fig. 3.16 shows the effect of the damper tip mass on the peak acceleration of the truss. As mentioned before and as expected from the expression of the absorbed energy, the effect of the tip mass is not strongly dependent on the tuning range: increasing $m$ is like using a larger tuned damper and always results in a decreased value of the peak amplitude.

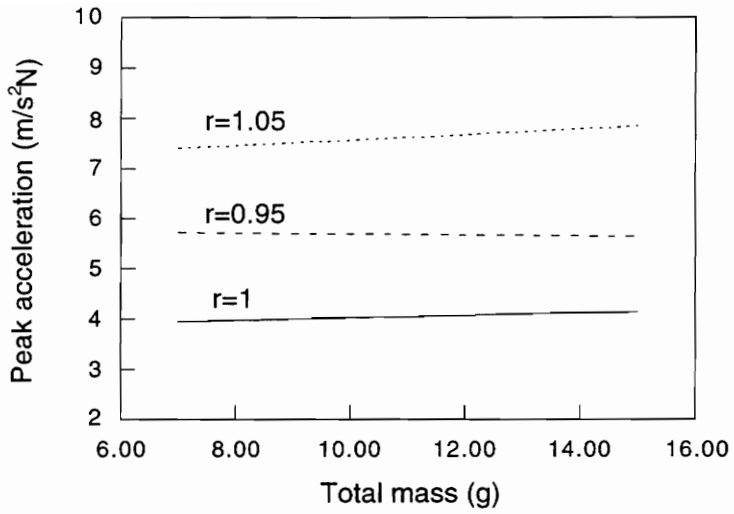


**Figure 3.13.** **Effect of the damper total mass on the peak acceleration of the third mode of the laboratory truss. The three curves correspond to different values of the tuning ratio ($m$ =7 g, $\eta$ =0.15).**

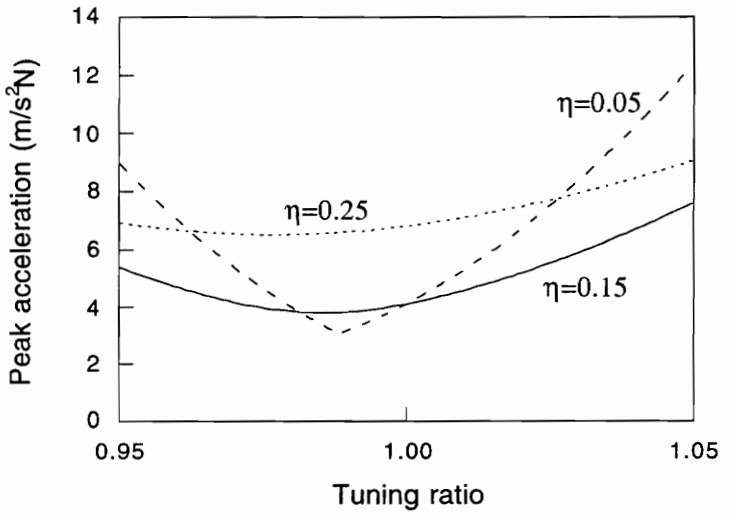


**Figure 3.14.** **Effect of the tuning ratio on the peak acceleration of the third mode of the laboratory truss. The three curves correspond to different values of the damper loss factor ($m$ =7 g, $m_T$ =10 g).**

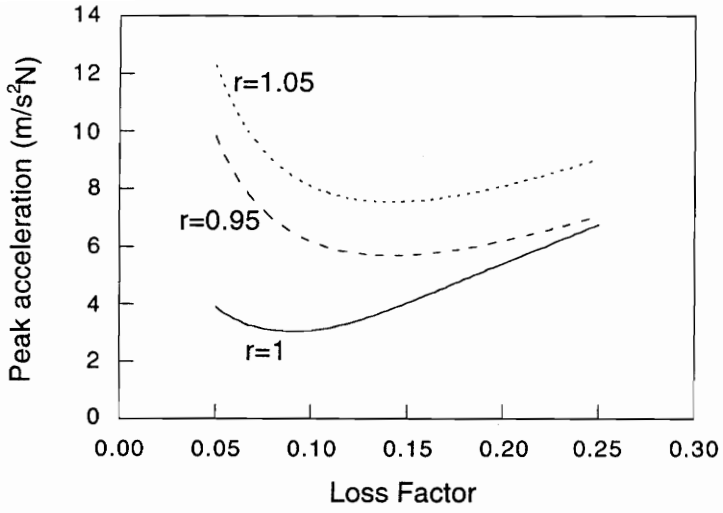


**Figure 3.15.** Effect of the damper loss factor on the peak acceleration of the third mode of the laboratory truss. The three curves correspond to different values of the tuning ratio ($m$ =7 g, $m_T$ =10 g).

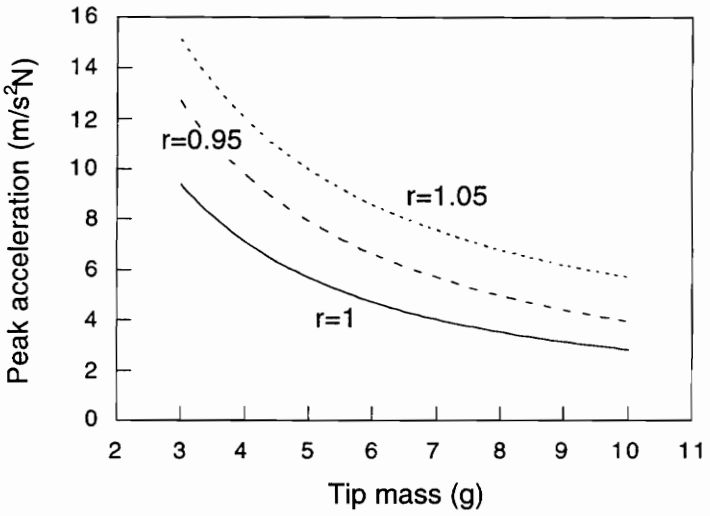


**Figure 3.16.** Effect of the damper tip mass on the peak acceleration of the third mode of the laboratory truss. The three curves correspond to different values of the tuning ratio ($m_T$ =10 g, $\eta$ =0.15).

# Chapter 4

# Deterministic and Probabilistic Optimization of a Damped Truss

In Chapter 2, we have shown that reasonable estimates of the scatter in the response of a truss can be obtained if sufficient knowledge is available about the nature and magnitude of the uncertainties in the system.

In this chapter, we will use this capability to design a damped truss subject to limits on the amplitude of response to a given dynamic excitation. The probability of exceeding these limits will be minimized by a design optimization procedure. To assess the potential advantage of the probabilistic methods, a design obtained from such probabilistic optimizations will be compared to one obtained from a deterministic approach to assess the potential advantage of the probabilistic methods,

In the next section, we take a general look at the design of damped structures. The design requirements are defined and the formulations of the deterministic and probabilistic approaches are presented. We then address the specific design of the laboratory truss of Chapter 2, equipped with tuned dampers. The optimizations are performed with a genetic algorithm, described in section 4.5. Finally, the deterministic and probabilistic designs are obtained and compared on the basis of numerical simulations.

## *4.1 Deterministic and Probabilistic Approaches*

We consider the design of truss structures with damping augmentation systems where the main source of response uncertainty is the variability in the properties of the nominally identical damping devices. The uncertainties are quantified by measuring the properties of a large number of dampers. We compare the probabilities of failure of two alternative designs: one obtained from deterministic optimization and the other from probabilistic optimization. The two designs are subject to the same requirements and resource limits.

The design requirements are expressed as upper limits on the acceleration at given points on the structure and within prescribed frequency ranges, for a given dynamic excitation. These requirements can be formulated as a series of upper limits $A_{lim}^{(m)}$ on the acceleration at prescribed locations within a series of $n_m$ frequency "windows". This is illustrated in Fig. 4.1. The locations, frequency ranges and amplitudes of the excitation forces are assumed to be specified.

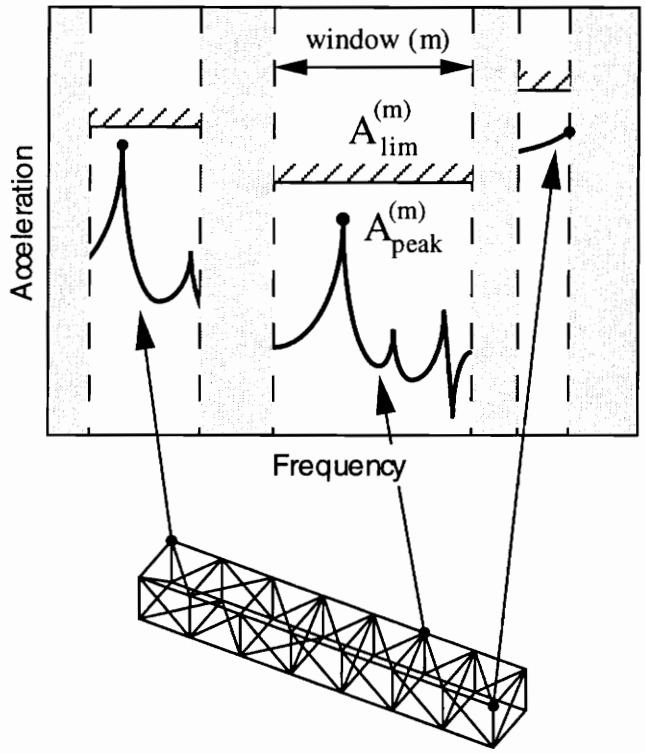


**Figure 4.1. Performance requirements for a damped truss.**

Note that the locations on the structure where acceleration limits are specified need not be the same in each window. This is the case, for example, when sensitive devices are attached at different locations on a structure; each device could be sensitive to a particular range of frequencies. The frequency windows where the limits are specified can also overlap.

The design variables $x$ can include design parameters of the damping devices and the truss itself, as well as the locations of the damping devices on the structure. In actual structures some or all design variables as well as other parameters $p$ of the model are uncertain. They are considered

random variables in the probabilistic approach. Only the nominal (mean) values $\bar{x}$ and $\bar{p}$ of the design variables $x$ and model parameters $p$ are used in the deterministic approach.

The design problem consists of bringing the peak acceleration $A_{peak}^{(m)}$ in each window $m$ below the prescribed limit $A_{lim}^{(m)}$ by adjusting the design variables between the bounds $x_l$ and $x_u$ while satisfying $r$ resource limits $g_i \leq 0,\ i = 1, \ldots, r$ (for example, limit on the total weight of the structure, limit on gains in active systems, etc.). We will refer to a situation where any of the peak accelerations exceeds its limit as "failure". With these notations and assuming a uniform safety margin $\alpha$, we formulate a **deterministic** optimization problem as

$$\begin{aligned} \underset{\bar{x}}{\textbf{Maximize}} \quad & \alpha\,, \\ \textbf{such that} \quad & A_{peak}^{(m)}(\bar{x},\bar{p}) + \alpha \leq A_{lim}^{(m)}, \qquad m = 1, \ldots, n_m\,, \\ \textbf{and} \quad & x_l \leq \bar{x} \leq x_u\,, \\ \textbf{and} \quad & g_i(\bar{x},\bar{p}) \leq 0, \quad i = 1, \ldots, r\,. \end{aligned} \tag{4.1}$$

where all parameters of the system are assumed to take nominal values, and the safety margin $\alpha$ is expected to "absorb" uncertainties and prevent failure.

If the main sources of uncertainties are known and if their statistical distributions can be measured or estimated with sufficient accuracy, then the probability of failure can be computed from a model and minimized by optimization. A **probabilistic** optimization that minimizes the probability that the amplitudes will exceed the limits (hence failure) can then be formulated as

$$\begin{aligned} \underset{\bar{x}}{\textbf{Minimize}} \quad & P_f = P\big(A_{peak}^{(m)}(x,p) \geq A_{lim}^{(m)}\big), \qquad m = 1, \ldots, n_m\,, \\ \textbf{such that} \quad & x_l \leq \bar{x} \leq x_u\,, \\ \textbf{and} \quad & g_i(\bar{x},\bar{p}) \leq 0, \quad i = 1, \ldots, r\,. \end{aligned} \tag{4.2}$$

Note that the same resource limits are used in both formulations. Our goal is to evaluate the potential gain in reliability (reduction in probability of failure) when using the probabilistic formulation (4.2) instead of the deterministic optimization (4.1) for the truss design problem.

## 4.2 Problem Description

We use again the short truss structure of section 2.1, this time equipped with the specially designed viscoelastic tuned dampers described in Chapter 3. As mentioned in Chapter 2, the

damping in the second mode of the truss is about one order of magnitude larger than in modes 1 and 3, probably because of coupling with the dynamics of the support plates and wall. Since this is not included in our finite element model, we will ignore the second mode completely so that we only try to control modes 1 and 3. Also – for simplicity – only one tuned damper will be used for each controlled mode. Note that the approximate analysis of section 3.3.2 is valid only under this condition. The total number of dampers added to the truss will therefore be 2: one damper of type 1 to control the first mode and one of type 3 for the third mode.

### 4.2.1 Uncertainties

Since manufacturing uncertainties in the truss elements were found to have a very small effect in our laboratory truss (see Chapter 2), we eliminate them completely by using the same truss for all realizations of the complete system and only take into account the much larger uncertainties in the properties of the tuned dampers (see Tables 4.1 and 4.2 in section 4.6). With this assumption, the parametric uncertainties in the system are limited to scatter in the properties of the tuned absorbers. These can be characterized by measuring samples of each type of damper.

### 4.2.2 Design Requirements

The locations and directions of the excitation and the response measurements used in this study are shown in Fig. 4.2. The locations of the response measurements ($u^{(1)}$ and $u^{(3)}$) were chosen at the nodes and in the directions that correspond to the largest amplitudes in the first and third modes, respectively, in the original undamped truss (node 12, direction $\vec{1}_4$ for $u^{(1)}$ and node 11, direction $\vec{1}_8$ for $u^{(3)}$; refer to figure 2.6 and Eq. (2.1) for the definition of these nodes and directions)

The excitation is assumed to have a flat spectrum and a unit amplitude. This allows us to use transfer functions from excitation force to response accelerations as a substitute for the accelerations themselves. The transfer functions $H^{(1)}$ and $H^{(3)}$ corresponding to the two measurement points are defined as

$$H^{(1)}(i\omega) = \frac{\ddot{u}^{(1)}(i\omega)}{f(i\omega)}, \tag{4.3}$$

$$H^{(3)}(i\omega) = \frac{\ddot{u}^{(3)}(i\omega)}{f(i\omega)}, \tag{4.4}$$

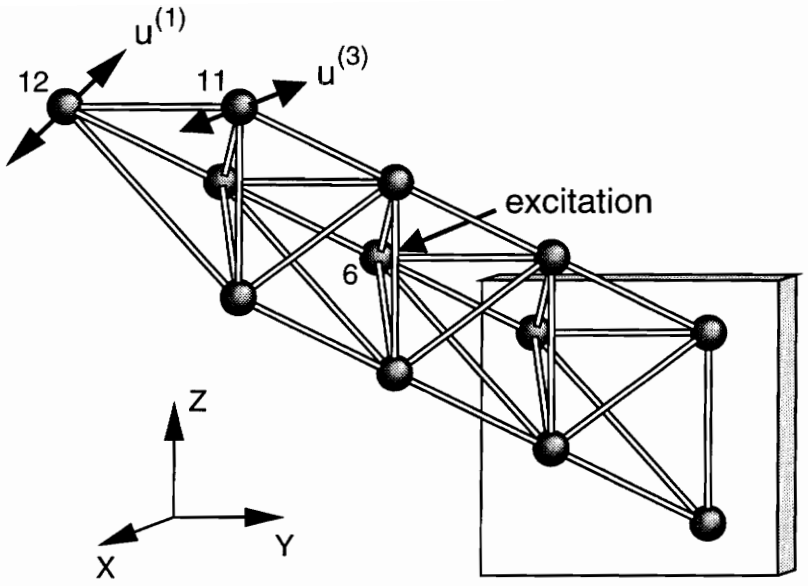


**Figure 4.2. Locations of excitation and response measurements on the laboratory truss.**

where $u^{(1)}$ and $u^{(3)}$ are displacements, $f$ is the excitation force, $\omega$ is the frequency, $i = \sqrt{-1}$, and a dot denotes differentiation with respect to time.

The upper limits on $H^{(1)}$ and $H^{(3)}$ are set to the same level $H_{lim}$ (i.e., $H^{(1)}_{lim} = H^{(3)}_{lim} = H_{lim}$) in two frequency windows, covering the two modes of interest (mode 1 and mode 3). This is illustrated in Fig. 4.3.

### 4.2.3 Optimization Scenario and Design Variables

We consider the following scenario: the truss has been designed with one damper for each mode (modes 1 and 3 only) to limit dynamic response accelerations. A large number of trusses and dampers have been manufactured and samples have been tested. The tests have revealed a significant mistuning of the dampers that will result in poor overall performance of the damped structure. The mistuning consists of a substantial shift in the average frequencies of the dampers. We assume that the dampers cannot be modified to improve their tuning. However, *tuning masses* can be easily added to the nodes of the truss to modify its natural frequencies and improve tuning. These tuning masses have a fixed magnitude (16.6 g or 0.59 oz) and – in order to limit the added weight – a maximum of 10 masses can be used. Also, the locations of the 2 dampers on the

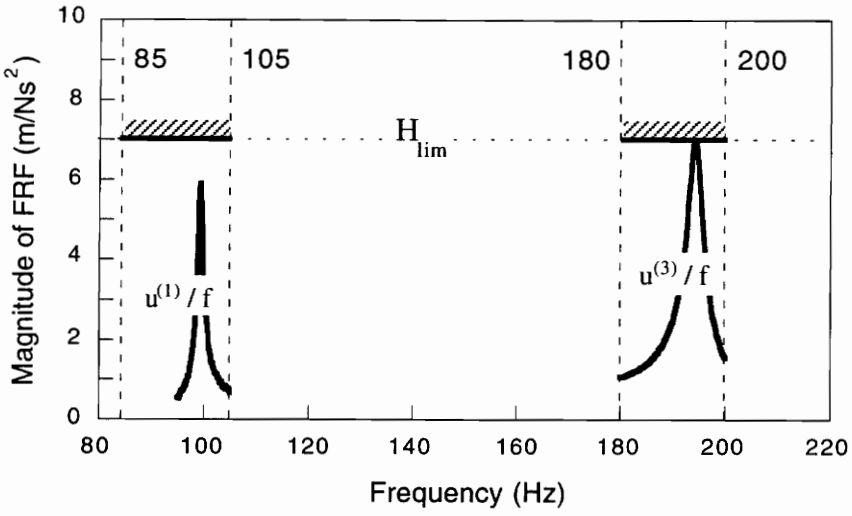


**Figure 4.3. Frequency windows and amplitude limits.**

structure can be modified. The problem consists of optimally redesigning the system by adding tuning masses and moving the dampers to ensure satisfactory performance.

This problem can be solved with two different approaches. In a deterministic approach, the properties of the dampers will be assumed equal to a nominal value and the peak amplitudes of the two modes will be minimized to create the largest possible margin between the nominal peak acceleration and the required upper limit. In a probabilistic approach, the statistics of the damper properties are evaluated from measurements of samples of dampers. These properties are then used in conjunction with analytical models to predict — and minimize — the probability of violating the requirements. The properties of the truss and tuning masses are assumed deterministic.

## *4.3 Deterministic and Statistical Analyses*

The truss is modeled as described in section 2.1.3. The initial damping is added to the model through the use of complex stiffnesses $k(1 + i\eta_s)$ for the members, assuming a uniform value of the loss factor $\eta_s$ for all members of the truss. The values used in the model for the masses of the nodes and the masses and stiffnesses of the members are the mean values of the series of measurements described in section 2.4.1.

As before, the model contains 9 support springs to model the flexibility of the wall. These 9 springs have also been given complex stiffnesses. The values of those stiffnesses are determined using a least square fit procedure described in Appendix C. This procedure ensures that the resulting model of the original truss predicts its natural frequencies and damping ratios exactly. This is necessary because of the very high sensitivity of the tuned dampers to the relative tuning of the truss and dampers.

With 2 dampers added to the truss, the number of degrees of freedom is 38. Also, with the use of complex stiffnesses, the dynamics of the damped truss is described by a generalized complex eigenvalue problem. The full order analysis involves solving for the eigenvalues and eigenvectors of the damped structure and evaluating the transfer function with a mode superposition method as explained in section 3.3.1. Solving this eigenvalue problem is computationally expensive, particularly in the context of genetic optimization. The complete full order analysis of the design (i.e., solving for the eigenvectors, applying the mode superposition method and evaluating the peak amplitudes of modes 1 and 3) takes about 0.5 second of CPU time on an IBM3090 in vectorized mode.

To reduce the computational burden, the peak accelerations are evaluated using the semi analytical approximation of section 3.3.2. To account for the effect of the tuning masses, a first order expansion technique is used to approximate the mode shapes of the truss with tuned masses from the mode shapes of the original truss. Those approximate mode shapes are then used in the analytical expression. The eigenvectors of the original truss and their sensitivity derivatives with respect to node masses needed for that expansion are evaluated only once, before the beginning of the optimization. The effect of the mode shape correction is illustrated in Fig. 4.4. The figure shows analytical results for the peak magnitude of the first mode of the truss equipped with 1 damper of type 1 attached at node 12, direction $\vec{1}_4$. The horizontal axis corresponds to an increasing amount of mass added at node 12 (from 0 to 155 grams). The three curves on the plot were obtained from full analysis and approximate analysis with and without mode shape update. We see that, for an added mass of 100 grams (about 6 tuning masses of 16.6 g each) for example, the approximation is in error by 9% compared to the full analysis when no update is used. This error is reduced to about 1% when the mode shapes are first updated for the effect of the added mass. The gain is of course less significant for smaller amounts of added mass.

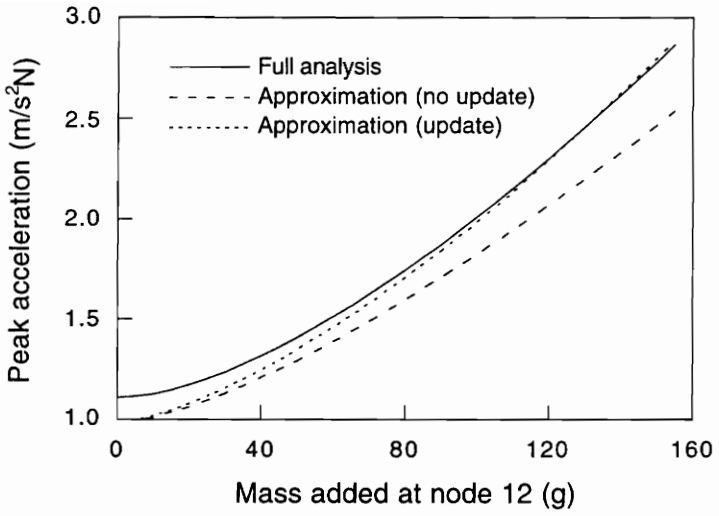


**Figure 4.4. Effect of mode shape correction on approximate analysis; truss equipped with damper type 1 at node 12, direction 4.**

This semi analytical approximation is implemented in FORTRAN on an IBM 3090 in vectorized mode and uses about 12 milliseconds of CPU time. This is about 40 times faster than the full order analysis.

For the probabilistic optimization, we need to evaluate repeatedly the probability of failure of the system (i.e., the probability for $H^{(1)}_{peak}$ or $H^{(3)}_{peak}$ to exceed $H_{lim}$). It is clear that the amplitude (or acceleration) of vibration near resonance of a structure is highly non-linear in the structural parameters. For that reason, a mean value based first order covariance propagation method cannot be used[55]. In addition, because of the complex, non-linear relationship between the parameters of a tuned damper and the magnitude of the peak response of a truss equipped with that tuned damper (section 3.4), there are multiple local maxima of the probability of failure in the space of random variables (multiple "most probable failure points"). This is illustrated in Fig. 4.5.

The figure shows a hypothetical distribution of the natural frequency of a tuned damper. The other curve in the figure shows the peak amplitude of the structural mode as a function of the damper natural frequency. We can see that failure occurs at both tails of the damper distribution. This may cause a second moment method to grossly underestimate failure probabilities. For this reason, we used Monte Carlo simulation to evaluate the probabilities of failure. A sample size

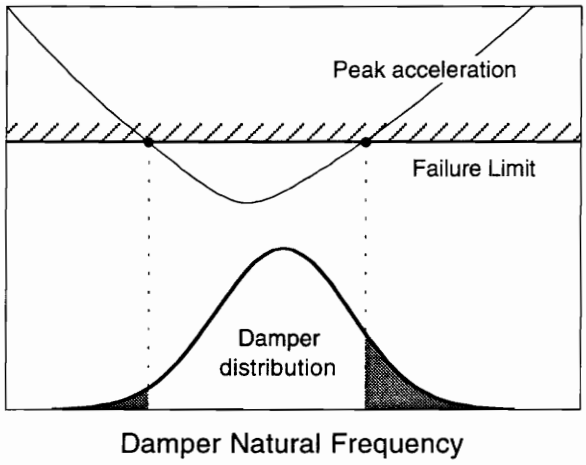


**Figure 4.5. Existence of multiple failure points for a truss equipped with tuned dampers with random parameters.**

of 1000 was chosen. Because the total mass of the dampers was found experimentally to have very little scatter, it is assumed deterministic in the simulations. The 3 remaining parameters (natural frequency ($f_n$), tip mass ($m$) and loss factor ($\eta$)) of each damper were assumed normally distributed, correlated random variables. A complete 1000 point Monte Carlo simulation uses about 12 seconds of CPU time with the semi-analytical approximation (using an IBM 3090 in vectorized mode).

## *4.4 Formulations of the Deterministic and Probabilistic Optimizations*

As explained in section 4.2.2, the design requirements consist of an upper limit $H_{lim}$ on the peak accelerations of mode 1 ($H^{(1)}_{peak}$) and mode 3 ($H^{(3)}_{peak}$). The deterministic and the probabilistic optimizations use the same design variables: the locations of the 2 dampers ($a_1$ and $a_3$ for the type 1 and type 3 damper, respectively), the orientations of these 2 dampers on the node ($d_1$ and $d_3$), and the locations of a maximum of 10 masses ($m_1, \ldots, m_{10}$), for a total of 14 design variables.

The locations of the masses and dampers are restricted to the nodes of the truss. Moreover, to limit the size of the design space and reduce the CPU time needed for the optimizations, we

restricted the candidate locations for the masses and dampers to subsets of the 12 nodes of the truss. The dampers were only allowed to be attached to nodes 10, 11, and 12 at the tip of the beam-truss. The masses can be attached to nodes 7 to 12. Note that these subsets include the most effective locations for the masses and dampers (the nodes where the amplitudes of motion under modes 1 and 3 are largest). Since a total of up to 10 masses can be attached to 6 locations, any node can support more than one mass at a time. For convenience in the optimization algorithm, we assumed that all 10 masses are always used but that unused masses are attached to a *fictitious* node (number 0). We use the standard mounting holes of the nodes to attach the dampers. Those holes are aligned in the 9 discrete directions defined in section 2.1.3. Note that all 14 design variables are discrete. Discrete variables are not handled easily by conventional gradient-based optimization methods, so we used a genetic algorithm as the optimizer.

With these variables, the deterministic optimization problem of Eq. (4.1) is reformulated as

$$\begin{aligned} \underset{a_1,d_1,a_3,d_3,m_1,\ldots,m_{10}}{\textbf{Maximize}} \quad & \alpha \\ \textbf{where} \quad & \alpha = H_{lim} - max\left(H^{(1)}_{peak}, H^{(3)}_{peak}\right) \\ \textbf{such that} \quad & a_1, a_3 \in \{10,11,12\}, \\ & d_1, d_3 \in \{1,2,3,4,5,6,7,8,9\}, \\ & m_1,\ldots,m_{10} \in \{0,7,8,9,10,11,12\}, \end{aligned} \tag{4.5}$$

where $H^{(1)}_{peak}$ and $H^{(3)}_{peak}$ are evaluated for nominal (mean) damper properties. A negative value of the safety margin $\alpha$ corresponds to a design that violates at least one of the constraints on response accelerations even without considering uncertainties in parameters. Note that with the expression used in (4.5) for the safety margin, the explicit constraints on accelerations of Eq. (4.1) have been eliminated. The use of the *max* function creates kinks in the objective function that would cause numerical difficulties with gradient-based optimizers. However, such discontinuities are not a problem when genetic algorithms are used for the optimization.

The corresponding probabilistic formulation minimizes the probability of failure $P_f$, which is the probability that the design will violate the requirements due to scatter in the damper

properties

$$\begin{aligned} \underset{a_1,d_1,a_2,d_2,m_1,\ldots,m_{10}}{\textbf{Minimize}} \quad & P_f = P\left(H^{(1)}_{peak} \geq H_{lim} OR \quad H^{(3)}_{peak} \geq H_{lim}\right) \\ \textbf{such that} \quad & a_1, a_3 \in \{10,11,12\}, \\ & d_1, d_3 \in \{1,2,3,4,5,6,7,8,9\}, \\ & m_1,\ldots,m_{10} \in \{0,7,8,9,10,11,12\}. \end{aligned} \tag{4.6}$$

The genetic algorithms used to solve problems (4.5) and (4.6) are described in the next section.

## 4.5 Implementation: Genetic Algorithm

Genetic algorithms mimic the principle of Darwin's theory of evolution through survival of the fittest. Developed by Holland [56] in 1975, they simulate the mechanics of natural genetics. By contrast with classical optimization methods, genetic algorithms work with a *population* of designs that "evolve" from one *generation* to the next in response to an artificial environment. This environment is the counterpart of the natural environment of Darwin's theory and favors designs that maximize the value of a *fitness function*. The fitness is the equivalent of the objective function of an unconstrained optimization problem. Designs that have a high fitness are given more chances of breeding and thereby transmitting their characteristics to future generations. The algorithms use operators that simulate the natural mechanisms of genetics on the chromosomal strings that occur in biological reproduction. The mechanics of those operators result in structured yet randomized exchange of genetic information (i.e., useful traits) between the reproducing parents. Classical operators consist of *selection*, *crossover* and occasional *mutation* of the chromosomal strings. Other operators, for example *inversion* or specialized mutations are also used.

Because a genetic algorithm is a random search technique, its outcome is also random and has only a probability of being close to optimal. However, the fact that the algorithm works with a population rather than a single design has two advantages: first, it has less of a tendency to get stuck at local optima than gradient-based techniques, and second, the designer is left with a choice between several designs with similar performances in the final population. In addition, genetic algorithms are ideally suited for problems where the variables are required to take discrete or integer values.

However, the price we pay for these advantages is the very large number of fitness function evaluations required to obtain convergence. Also, because the result of the search is random, the algorithm must be run more than once to increase the reliability of the optimization.

The application of genetic algorithms to optimum location problems is addressed in the second part of Appendix D. The reader is referred to that appendix for a more complete discussion. We used genetic algorithms to solve the discrete optimization problems of Eqs. (4.5) and (4.6). All variables in these formulations decide the locations of discrete devices on our laboratory truss (tuned dampers, masses). There are several possible ways in which a design can be coded into a string of numbers to be used as the chromosome for the genetic search. The choice of a coding can determine the efficiency of the search. In Appendix D, we present a comparison of different coding options for optimum location problems. The integer coding described in the next section has the advantage of simplicity and has been shown to perform satisfactorily.

We use the same genetic algorithm for the solution of the deterministic and probabilistic design problems; only the objective function differs. We use a string of 14 integer numbers as the chromosome of the genetic search. Each gene in the chromosome stores the value of one of the 14 design variables. Symbolically, the string can be written

$$\text{Chromosome} = [a_1|d_1|a_3|d_3|m_1|\ldots|m_{10}]\,, \tag{4.7}$$

where $a_1$ and $a_3$ are the locations of the type-1 and type-3 dampers, respectively, $d_1$ and $d_3$ are the directions of the same dampers, and $m_1, \ldots, m_{10}$ are the locations of the 10 tuning masses. The ranges of these variables are

$$\begin{aligned} a_1, a_3 &\in \{10, 11, 12\} \\ d_1, d_3 &\in \{1, 2, 3, 4, 5, 6, 7, 8, 9\} \\ m_1, \ldots, m_{10} &\in \{0, 7, 8, 9, 10, 11, 12\}\,. \end{aligned} \tag{4.8}$$

With these ranges, the size of the design space is approximately equal to $2 \times 10^{11}$.

In the implementation of the algorithm, the values of the genes are all integer numbers varying from 1 to the number of possible physical values of the corresponding design variable. For the damper locations, for example, the genes $a_1$ and $a_3$ in the chromosome actually take the

values 1, 2, or 3 instead of 10, 11, and 12. This simplifies the genetic operators described further. A correspondance table is used to convert gene values into values of the design variables.

The algorithm uses the three classical genetic operators (selection, crossover, and mutation) and an elitist strategy. The selection picks two parents in the current population. The chromosomes of those parent designs are then combined by crossover to create an offspring. Random mutations may then be applied to the offspring chromosome before it is stored in the next generation. This process is repeated until the new generation has the required number of individuals. In addition, the best individual of each generation is always cloned into the new population. A flow chart of the algorithm is shown in Fig. 4.6.

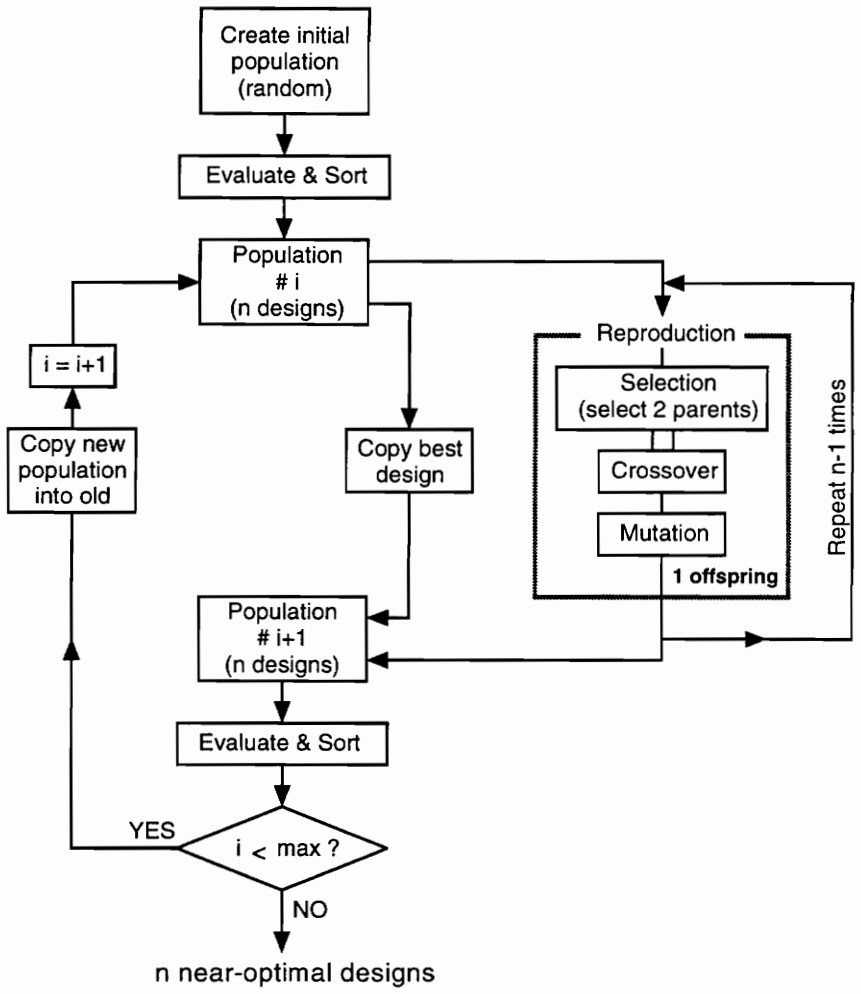


**Figure 4.6. Flow chart of genetic algorithm.**

**Elitist Strategy** The elitist strategy consists of always cloning the best individual of the current population into the next population. This guarantees that the best design found will never be lost in later stages of evolution.

**Selection** The selection uses the ranking technique. The designs are first evaluated and sorted in decreasing order of fitness. The probability $P_s$ of selection of a particular design is then linearly dependent on its rank $r$ in the population according to

$$P_s = 2\,\frac{1+n-r}{n^2+n}\,, \tag{4.9}$$

where $n$ is the size of the population. Portions proportional to $P_s$ are allocated to each design on a biased roulette wheel. The wheel is spun twice to select two parents for reproduction. These parents are then subjected to crossover and mutation to create a design for the new population.

**Crossover** We use a one-point averaging crossover. A continuous, real random number is used as the cutting point; the parts of the strings on either side of the cutting point are exchanged between parents and the remaining gene is generated as a weighted average of the two parent genes. For example, assume the following two parent chromosomes have been selected for reproduction

parent 1: 2 7 1 9 7 7 5 1 7 8 3 1 4 3
parent 2: *1 2 1 5 3 1 1 4 2 2 7 1 4 5*

Further assume that we have picked a random cutting point equal to 4.31. An offspring chromosome is formed using genes 1 to 4 from parent 1, and genes 6 to 14 from parent 2. The value of gene number 5 is computed as a weighted average

$$0.31 \times 7 + 0.69 \times 3 = 4.24 \tag{4.10}$$

and rounded to 4. Note that this operation is capable of introducing gene values that were not present in any of the parents. Creating new genetic information is vital to avoid creating "blind spots" in the design space. The resulting offspring chromosome is then

offspring: 2 7 1 9 **4** *1 1 4 2 2 7 1 4 5*

The offspring has some of the characteristics of each parent design and also some new features (gene 5). The crossover is performed with a given probability $P_c$. If crossover is not used, one of the 2 parent chromosomes is chosen randomly and cloned into the new population.

**Mutation** The mutation is a classical gene by gene random mutation: for each gene in the string, a probability of mutation is applied. If mutation occurs, a random value with uniform distribution within the range of the particular gene is substituted to the current value of that gene. The role of the mutation is to introduce new genetic information in the population and prevent premature convergence of the search. Without mutation, the population would very rapidly become uniform, preventing the algorithm from sufficiently exploring the design space.

Besides the choice of a particular coding, the values of the probability of mutation $P_m$ and the population size $n$ are the most important parameters that affect the convergence and reliability of the search. Unfortunately, there are no general rules defining appropriate values for these parameters. In fact, their optimum values are so dependent on the particular optimization problem that they have to be determined by trial and error. This is an expensive proposition, since it requires a large number of runs to determine the average performance as a function of the parameters.

Since the genetic algorithm itself is not the purpose of this study but rather a tool, we did not try to finely optimize these parameters. We did however experiment with a few different values, running the algorithm 10 times for each combination of parameters. The values that roughly maximized the reliability of the search (i.e., the probability of getting close to the optimum in one search) were retained. The total number of analyses per search was set to 1200 to limit the computational expense. The population size and mutation and crossover probabilities, were set to $n = 20$ individuals and $P_m = 6\%$ and $P_f = 95\%$, respectively. This implies that 60 generations can be performed with 1200 analyses. The probability that an individual design will undergo at least one mutation is $1 - 0.94^{14} = 0.58$.

Because genetic algorithms (GA) are random search techniques, a single search does not reliably provide an optimum design. Instead, it provides a design that has only a probability of falling within a range of the optimum. Clearly, the reliability can be considerably improved by running the genetic search a few times on any given problem (with different seeds used in the random number generators). The best design of those multiple searches has a higher probability of being very close to optimum: if $r$ is the reliability of a single search (i.e., the probability that the final design is within specified margin from the actual optimum), then the reliability of $n$ searches is

$$r_n = 1 - (1 - r)^n . \tag{4.11}$$

This shows that the reliability of the genetic optimization grows very fast as the number of searches goes up. For our problem we evaluated the reliability of a single search to about 30% (designs were considered acceptable if the value of their objective function was within 1% of the best known design). Since the deterministic optimization is cheap, we can run it 10 times and achieve a reliability of about 97%. The probabilistic optimization on the other hand, includes Monte Carlo simulations and is therefore much more expensive. We cannot afford to run it 10 times. However, with 3 runs, the reliability is already about 67%.

## 4.6 Results: Optimum Deterministic and Probabilistic Designs

We manufactured 29 dampers of each type. The properties of these dampers were measured using the procedure described in section 3.2.2. To reduce the effect of measurement errors and temperature variations, the dampers were measured 3 times and the average of those 3 measurements was used to evaluate the mean values, standard deviations and correlation coefficients of the parameters. Those statistics are listed in tables 4.1 and 4.2.

**Table 4.1. Type 1 dampers, statistics of parameters (sample of 29).**

| Parameter: | $m$ | $f_n$ | $\eta$ | $m_T$ |
|---|---|---|---|---|
| Mean | 6.942 g | 105.08 Hz | 0.11934 | 10.811 |
| St. dev. | 0.108 g | 3.1950 Hz | 0.00681 | — |
| C.O.V. | 1.55% | 3.00% | 5.71% | — |
| Correlation coefficients | | | | |
| $m$ | 1.000 | | | |
| $f_n$ | 0.804 | 1.000 | | |
| $\eta$ | 0.729 | 0.491 | 1.000 | |

The deterministic optimization is based on the mean values of the parameters. For the probabilistic design, we assume normally distributed, correlated parameters, with the statistics of Table 4.1 and 4.2 (the uncertainties on the mean values and standard deviations themselves due

**Table 4.2. Type 3 dampers, statistics of parameters (sample of 29).**

| Parameter: | $m$ | $f_n$ | $\eta$ | $m_T$ |
|---|---|---|---|---|
| Mean | 7.613 g | 198.08 Hz | 0.14722 | 11.528 |
| St. dev. | 0.0700 g | 2.1750 Hz | 0.008120 | — |
| C.O.V. | 0.91% | 1.10% | 5.52% | — |
| Correlation coefficients | | | | |
| $m$ | 1.000 | | | |
| $f_n$ | 0.218 | 1.000 | | |
| $\eta$ | 0.692 | 0.055 | 1.000 | |

to the limited sample sizes were ignored). The failure limit $H_{lim}$ is set to $6.0\,m/s^2N$ and the mass of each of the 10 tuning masses is equal to 16.6 g. The deterministic design is obtained from the best of 10 runs of the genetic algorithm. Only 3 runs of the more expensive probabilistic optimization are performed.

The optimum deterministic design does not use any tuning masses. The dampers are located at nodes 12, direction $\vec{1}_9$ (type 1) and node 11, direction $\vec{1}_8$ (type 3). The safety margin is 2.07 $m/Ns^2$ evaluated with the semi-analytical approximation and 1.67 $m/Ns^2$ evaluated with a full analysis. Table 4.3 contains the nominal peak amplitudes and probabilities of failure, evaluated with the full analysis. The global probability of failure is 4.9%.

**Table 4.3. Deterministic design, nominal amplitudes and probabilities of failure.**

| | Mode 1 | Mode 3 | Total |
|---|---|---|---|
| Nominal peak $[m/s^2N]$ (full analysis) | 3.408 | 4.338 | — |
| Probability of failure [%] (Monte Carlo simulation, 1000 points, full analysis) | 4.4 | 0.5 | 4.9 |

The probabilistic design carries one tuning mass at node number 10. The type 1 damper is attached to node 12, direction $\vec{1}_4$ and the type 3 damper to node 10, direction $\vec{1}_4$. The safety margin for this design is equal to 1.52 from the semi-analytical approximation and 1.54 from the full analysis. Note that the margin is about 8% smaller for this design than for the deterministic

design. However, as shown in Table 4.4 the probability of failure is only 2.2%, which is less than half the probability of failure of the deterministic design. The difference in weight between the two designs is only 16.6 g (1 tuning mass), which is less than 0.4% of the total mass of the truss.

**Table 4.4. Probabilistic design, nominal amplitudes and probabilities of failure.**

| | Mode 1 | Mode 3 | Total |
|---|---|---|---|
| Nominal peak $[m/s^2 N]$ (full analysis) | 2.980 | 4.457 | — |
| Probability of failure [%] (Monte Carlo simulation, 1000 points, full analysis) | 1.4 | 0.8 | 2.2 |

Figure 4.7 contains the computed histograms of the peak accelerations of modes 1 and 3 for the two designs. The failure limit is also represented in the figure. We observe that the deterministic design has a relatively large failure rate in mode 1. The failure rate in the other mode is much smaller. Looking at the probabilistic design, we see that the failure rate in mode 1 has been slightly reduced to the expense of mode 3. However, because there was no margin available between the tail of the mode 3 distribution and the failure limit in the deterministic design, there was not much room for improvement. Note also the very distorted distributions, consequence of the high non-linearities in the response functions.

The difference in probability of failure between the two designs is only 2.7%. Although this is a significant difference, it is not large enough to be measured with a reasonable number of experiments (because the uncertainty in the measured failure rate is large for small samples). In the next chapter, we identify parameters of the design problem itself that can be varied to change this probability difference and increase it. An antioptimization will be performed with a genetic algorithm to identify values for those problem parameters that maximize the probability contrast. Optimum designs corresponding to that "ideal" problem will then be tested for reliability.

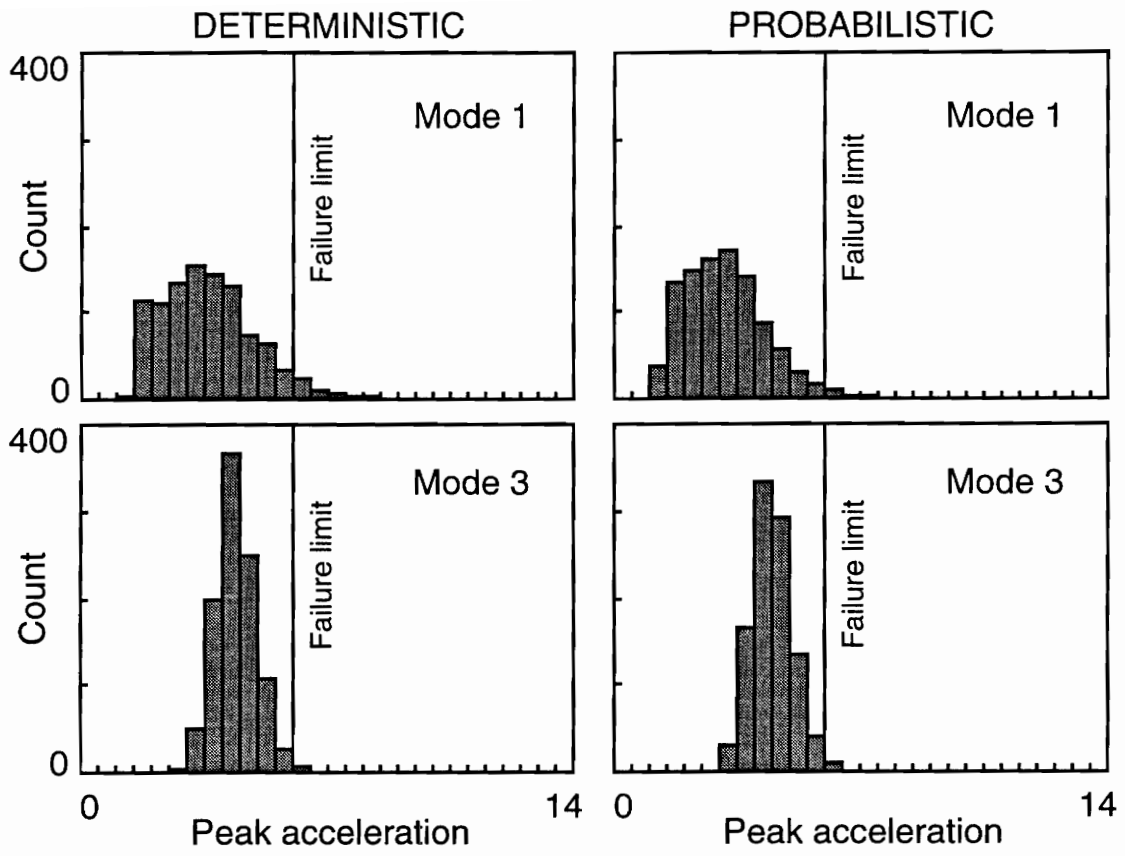


**Figure 4.7. Deterministic and probabilistic designs, distributions of peak amplitudes (Monte Carlo simulations with 1000 points and full-order analysis).**

# Chapter 5

# Experimental Evaluation of Deterministic and Probabilistic Designs

In the previous chapter, we have shown that probabilistic optimization can produce designs that are more reliable than their deterministic counterparts. However, the comparison was based on analytically predicted probabilities of failure. Because of modeling uncertainties not accounted for in the statistical analysis and because of incomplete knowledge of probability distributions, we can only predict a *nominal* probability of failure. This nominal probability can be significantly different from the actual one (see, for example[31]). It is not known if probabilistic optimization based on such nominal probabilities of failure can still yield better designs than deterministic optimization. To answer this question, we need to measure experimentally the performance of a large number of realizations of deterministic and probabilistic designs corresponding to the same design problem.

In this chapter, we evaluate experimentally the actual improvement in reliability that can be achieved through the use of probabilistic design methods. We consider again the design of the 30 bar truss with tuned dampers presented in Chapter 4. The main source of response uncertainty is the variability in the properties of the nominally identical dampers. These uncertainties are quantified by measuring the properties of a large number of dampers. We compare experimentally the probabilities of failure of two alternative designs, one obtained from deterministic optimization and the other from probabilistic optimization. The optimizations are performed with genetic algorithms. The two designs are subject to the same requirements and resource limits. Probabilities of failure are measured by testing the structure with multiple realizations of dampers.

To be able to measure the difference in probability of failure between the two designs with a reasonable number of experiments, we identified a design problem that maximizes the contrast between the two approaches. To achieve this, we used a process known as *antioptimization*[57,58,59] or contrast maximization. The antioptimization was also performed by genetic algorithms.

## 5.1 Designing the Experiment: Contrast Maximization

Our goal is to evaluate the difference in reliability between deterministic and probabilistic designs. Measuring probabilities of failure in the laboratory is time consuming, and measuring very small probabilities or very small differences in probabilities of failure requires a prohibitively large number of experiments. For the designs of chapter 4, for example, the reliabilities achieved with the two approaches differ by only 2.7%. This difference is not large enough to allow experimental verification with reasonable number of measurements (the experimental uncertainties would be of the same order of magnitude as the reliability difference). For this reason, we had to identify a design problem that leads to alternative designs with a large difference in probability of failure. To find such a design problem we carried on a process known as *antioptimization* or *contrast maximization*, which maximizes the *contrast* between the two design approaches.

Antioptimization requires a number of *problem parameters* that can be varied to achieve the increased contrast. For our problem, we selected the following parameters: the mean values of the natural frequencies of the two types of dampers (the amount of mistuning), the failure limit $H_{lim}$ (the stringency of the requirements), and the relative magnitudes of the scatter in the parameters of the two types of dampers.

In a problem with two (or more) failure modes, a probabilistic approach can provide designs that are significantly different from deterministic designs by taking advantage of cost and/or scatter differences between the two failure modes. If the costs of controlling the two failure modes are the same but the scatters are different, the probabilistic optimization will provide a larger safety margin to the large-scatter failure mode. If the scatters are similar but the costs of controlling the different failure modes are different, then the probabilistic optimization will provide a larger safety margin to the cheaper mode. These effects accumulate if the design problem is such that the cheapest mode also has the largest scatter.

Because added masses generally have a greater effect on high frequency modes than low frequency modes, it is easier to control the natural frequency of the third mode of our truss with tuned masses than the first mode (so that the third mode is "cheaper" to control). For the purpose of experimental demonstration, it is therefore desirable to have more scatter in the properties of type-3 dampers than in those of type-1 dampers. Based on preliminary measurements on

prototypes of the dampers, we selected coefficients of variation of 1.5% and 3.5% in the natural frequencies of the type-1 and type-3 dampers, respectively. The standard deviations of all damper parameters were then kept constant in the antioptimization.

To find an appropriate combination of the other problem parameters (mean natural frequencies of the two types of dampers and acceleration limit), we incorporated these variables into a contrast maximization formulation that is solved using genetic algorithms. Since our genetic algorithm (section 4.5) uses integer coding, we first discretized the 3 problem parameters. The mean natural frequencies $f_n^{(1)}$ and $f_n^{(3)}$ were allowed to vary between 90 and 110 Hz in steps of 2 Hz (11 values) and between 182 and 202 Hz in steps of 2 Hz (11 values), respectively (this corresponds to a $\pm 10$ Hz mistuning range). The acceleration limit $H_{lim}$ was varied between 2 and 9 $m/s^2 N$ in steps of 0.5 $m/s^2 N$. Using antioptimization, we can identify values for these three problem parameters that maximize the difference in probability of failure between a deterministic optimum design and a probabilistic optimum design. The antioptimization problem can be formulated as

$$\begin{aligned} \underset{f_n^{(1)}, f_n^{(3)}, H_{lim}}{\textbf{Maximize}} \quad & \Delta P_f = P_f^{det^\star} - P_f^{prob^\star} , \\ \textbf{where} \quad & f_n^{(1)} \in \{90, 92, 94, \ldots, 110\} , \\ & f_n^{(3)} \in \{182, 184, 186, \ldots, 202\} , \\ & H_{lim} \in \{2, 2.5, 3, 3.5, \ldots, 9\} , \end{aligned} \tag{5.1}$$

where $P_f^{det^\star}$ and $P_f^{prob^\star}$ are the probabilities of failure of the deterministic and probabilistic optima corresponding to formulations (4.5) and (4.6) of section 4.4. Conceptually, formulation (5.1) implies embedding complete deterministic and probabilistic optimizations inside a higher level antioptimization to find $P_f^{det^\star}$ and $P_f^{prob^\star}$ for each combination of $f_n^{(1)}$, $f_n^{(3)}$, and $H_{lim}$. The flow chart of this conceptual antioptimization is shown in Fig. 5.1.

Since genetic algorithms are used as optimizers and the probabilities of failure are evaluated with Monte Carlo simulations, we cannot afford such a two-level optimization. With 1000 analyses per Monte Carlo simulation and about 1200 design evaluations for each design optimization, assuming that about 1200 iterations will be needed to reach convergence at the antioptimization level, the flow chart of Fig. 5.1 would represent more than a billion analyses! To avoid this,

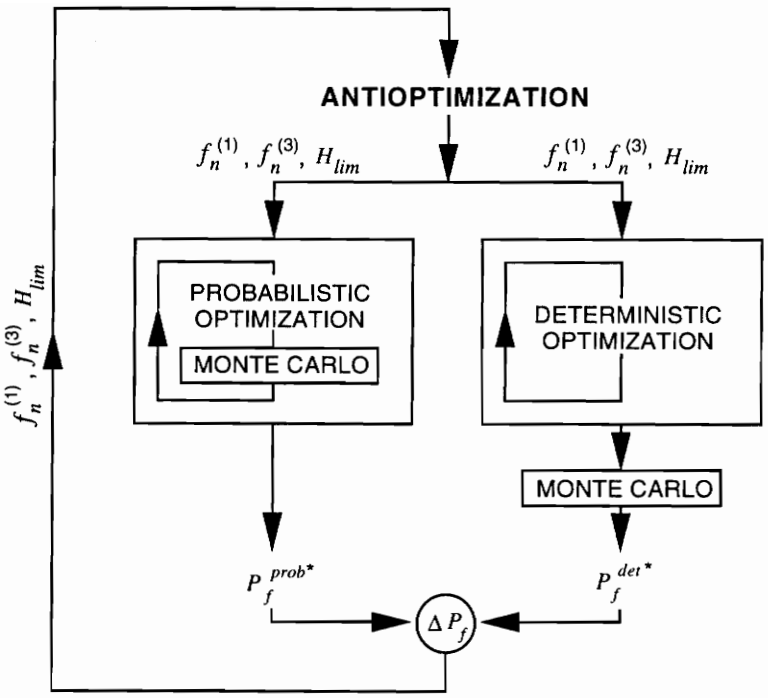


**Figure 5.1. Flow chart of antiopimization.**

we combine the three problem parameters of (5.1) with the design variables of the probabilistic optimization (4.6) so that the inner probabilistic optimization loop is eliminated. The resulting outer optimization loop then **simultaneously** looks for a problem **and** the corresponding probabilistic design that maximize the difference in probability of failure compared to the optimum deterministic design corresponding to the same problem. With this change, (5.1) is reformulated as

$$\begin{aligned} \underset{\substack{f_n^{(1)},f_n^{(3)},H_{lim},\\ a_1,d_1,a_3,d_3,\\ m_1,\ldots,m_{10}}}{\textbf{Maximize}} \quad & \Delta P_f = P_f^{det^\star} - P_f\,, \qquad (5.2) \\ \textbf{where} \quad & f_n^{(1)} \in \{90,92,94,\ldots,110\}\,, \\ & f_n^{(3)} \in \{182,184,186,\ldots,202\}\,, \\ & H_{lim} \in \{2,2.5,3,\ldots,9\}\,, \\ & a_1, a_3 \in \{10,11,12\}\,, \end{aligned}$$

$$d_1, d_3 \in \{1,2,3,4,5,6,7,8,9\},$$

$$m_1, \ldots, m_{10} \in \{0,7,8,9,10,11,12\},$$

where $P_f$ is now the probability of failure of the current problem/ probabilistic design, $a_1$, $d_1$, $a_3$, $d_3$ are the locations and directions of the two dampers and $m_1, \ldots, m_{10}$ the locations of the tuning masses as described in section 4.4. The flow chart of this new formulation is shown in Fig 5.2. Compared to the conceptual formulation of Fig. 5.1, the number of analyses is reduced by 3 orders of magnitude.

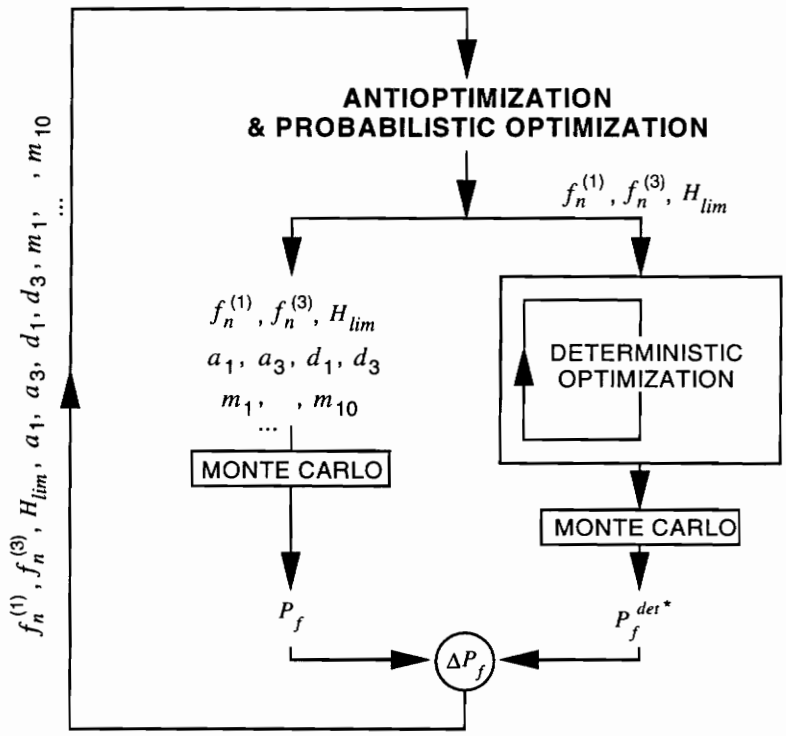


**Figure 5.2. Antiopimization, modified flow chart: the probabilistic loop has been combined with the outer antioptimization loop.**

Notice that we have eliminated the expensive inner probabilistic optimization loop. However, the less expensive deterministic loop is still embedded inside the outer loop. Note that the deterministic optimum is independent of the failure limit (because the same limit is used for both modes) so that the deterministic optimum depends only on the natural frequencies $f_n^{(1)}$ and $f_n^{(3)}$. Since these frequencies can each take 11 different values, there are only $11 \times 11 = 121$ distinct

deterministic design problems in the problem space. Including the deterministic optimization inside the outer optimization loop would imply optimizing the same problem more than once (since the outer loop will require several hundred iterations to converge). To avoid this and reduce computational expenses, we solved all 121 deterministic optimization problems in advance and stored the results in a database for use by the antioptimization.

As mentioned in section 4.5, the result of genetic search is partly random; there is no guarantee of optimality. Occasionally, a single search can lead to a design that is far from optimal. This is not acceptable in the antioptimization: if for one particular combination of problem parameters the deterministic design in the database is far from optimal, its probability of failure will be abnormally high. This will induce the antioptimization to falsely identify that problem as one that maximizes the contrast. This is illustrated in Fig. 5.3 where we plotted the final value of the peak acceleration for 11 of the 121 deterministic design problems.

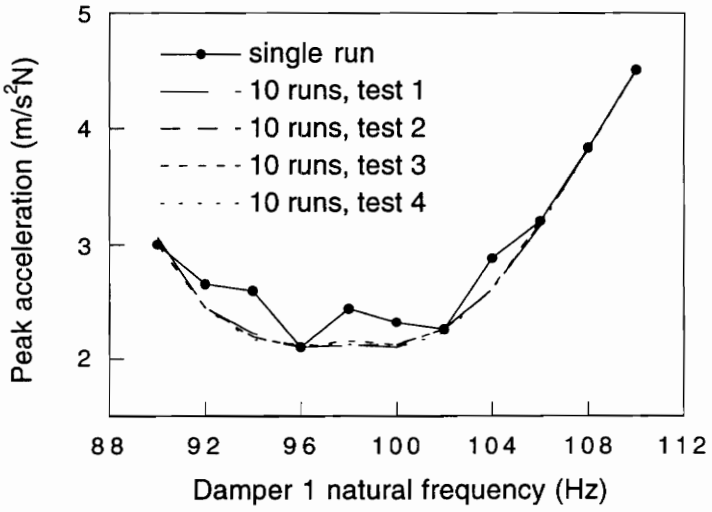


**Figure 5.3. Peak acceleration of optimum deterministic designs for 11 values of the natural frequency of the type-1 damper (type-3 damper tuned at 182 Hz); for each problem the result from a single search is compared for robustness to the best of 10 genetic searches.**

The 11 problems correspond to the 11 candidate values for the natural frequency of the type-1 damper (the natural frequency of the type-3 damper was set to 182 Hz in all 11 problems). The optimizations were performed with the genetic algorithm (GA) described in section 4.5

(population size of 20, 60 generations, 6% mutation, 95% crossover). The solid line with black dots corresponds to designs obtained with a single run of the GA for each problem. The designs plotted on the other 4 lines are obtained as the best result out of 10 GA runs, for each problem. This process was repeated 4 times to evaluate the robustness of the final designs. We see that, although the unique search occasionally finds very good designs (for 90, 96 and 102 Hz for example), it also finds designs that have as much as 20% more peak acceleration than the optimum (for example at 94 and 98 Hz). Using the "best of 10 runs" strategy on the other hand, the designs obtained are consistently within about 2% of the optimum.

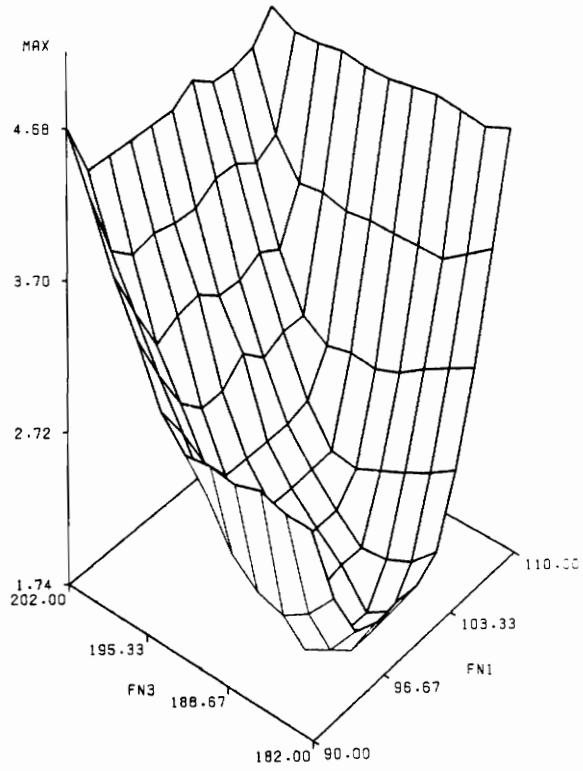


**Figure 5.4. Peak acceleration of optimum deterministic designs for 121 problems; for each problem the "optimum" was obtained as the best of 10 genetic searches.**

All 121 problems were optimized using this scheme and the resulting designs were stored in a database. The 3-dimensional graph of Fig. 5.4 represents the peak amplitude of the 121 deterministic optima as a function of the two problem parameters $f_n^{(1)}$ and $f_n^{(3)}$. The relative

smoothness of the surface is again an indication of the high optimization reliability achieved by performing 10 searches for each problem. The few kinks are the result of the limited resource (10 masses maximum) and the discrete nature of the tuning corrections that can be achieved (plus or minus one mass). Monte Carlo simulations with 1000 replications were performed on those 121 optimum deterministic designs and the probabilities of failure were evaluated for all candidate values of the failure limit $(2, 2.5, 3, 3.5, \ldots, 9)$ and also stored in the database.

With this last improvement, the antioptimization is reduced to a single loop that combines the contrast maximization and the probabilistic optimization. The deterministic optimization has been eliminated and replaced by a simple table lookup. Figure 5.5 shows the corresponding flow chart. The only significant computational effort left inside the loop consists of a 1000 point Monte Carlo simulation to evaluate the probability of failure of the current design. The semi-analytical approximation of section 3.3.2 is consistently used throughout the antioptimization and the preparation of the database.

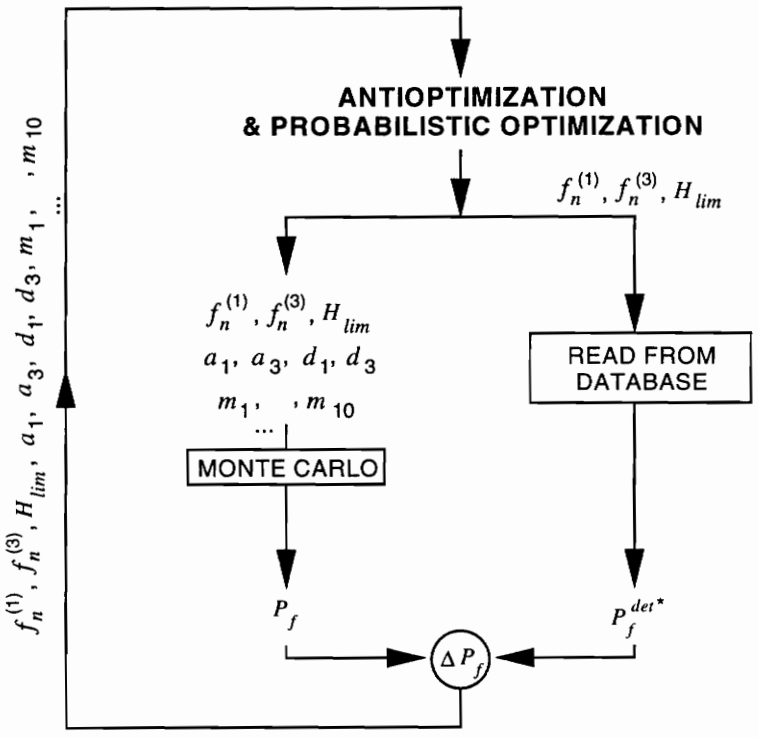


**Figure 5.5. Antioptimization, final flow chart: the deterministic optimization has been removed from inside the antioptimization loop and replaced by a table lookup.**

The genetic algorithm used for antioptimization is identical to the one used for the deterministic and probabilistic optimizations (section 4.5). Since the number of design and problem variables is 17 instead of 14, the size of the population is increased from 20 to 30 and the number of generations in the search is increased from 60 to 120. The probabilities of mutation and crossover are left to 6% and 95%, respectively.

In initial runs of the antioptimization, the algorithm converged almost systematically to a design problem where the failure limit was as low as allowed ($H_{lim} = 2$) and the probabilities of failure of the deterministic and probabilistic designs were both 100%. This is easily explained as follows: since the initial population of the search is random, all problems and corresponding probabilistic designs in that population are likely to be very poor. Their probability of failure is likely to be close to 100%. The deterministic designs corresponding to the same problems on the other hand, have been optimized in advance (and stored in the database) and so have better reliability so that the probability contrast $\Delta P_f$ in (5.2) is negative! There are two ways for the antioptimization to improve that contrast (at least make it non-negative). One is to improve the current probabilistic design (14 design variables) and the other is to lower the failure limit so that the deterministic design also fails with 100% probability (1 problem variable). Clearly, the second option is much more likely to occur because it only requires modifying a single variable. Once that happens, both designs have 100% probability of failure ($\Delta P_f = 0$) and the search has very little chance of escaping that strong local maximum.

To remedy this problem, we once again reformulated (5.2) as

$$\underset{\substack{f_n^{(1)},f_n^{(3)},H_{lim},\\ a_1,d_1,a_3,d_3,\\ m_1,\ldots,m_{10}}}{\textbf{Maximize}} \quad \begin{cases} 50 - P_f, & \text{if } P_f \geq 50\% \\ P_f^{det^\star} - P_f, & \text{if } P_f < 50\% \end{cases}, \tag{5.3}$$

$$\begin{aligned} \textbf{where} \quad & f_n^{(1)} \in \{90, 92, 94, \ldots, 110\}, \\ & f_n^{(3)} \in \{182, 184, 186, \ldots, 202\}, \\ & H_{lim} \in \{2, 2.5, 3, \ldots, 9\}, \\ & a_1, a_3 \in \{10, 11, 12\}, \\ & d_1, d_3 \in \{1, 2, 3, 4, 5, 6, 7, 8, 9\}, \\ & m_1, \ldots, m_{10} \in \{0, 7, 8, 9, 10, 11, 12\}. \end{aligned}$$

With this new formulation, the probability of failure $P_f$ of the current problem/design is minimized ($50 - P_f$ is maximized) if it is larger than 50%. This forces the failure limit to stay at reasonable levels, giving the algorithm a chance to improve the current design before trying to maximize the contrast with the deterministic design. The transition from one objective to the other is of course gradual, since it depends on the performance of each particular problem/design in the population: in the first few generations, most designs are evaluated using $50 - P_f$ while in later generations, the probability contrast is used for most designs.

The contrast maximization procedure identified the following problem as an ideal example: the dampers of type 1 would have an average natural frequency of 110 Hz (about 10 Hz overtuned), type-3 would have a mean natural frequency of about 182 Hz (about 11 Hz undertuned), and the failure limit $H_{lim}$ would be equal to 6.5 $m/s^2N$. For this problem, the deterministic design has a probability of failure of 18.6% compared to only 2.5% for the probabilistic design. This corresponds to a difference of 16.1% between the probabilities of failure. The design problem corresponds to a situation where one type of damper is overtuned and the other undertuned. The optimum deterministic and probabilistic designs represent different compromises between improving the behavior of one mode and degrading the other (since adding masses can only reduce the natural frequencies of the truss).

In this contrast maximization, we have assumed that we could control the mean values and deviations of the parameters of the two types of dampers. The 29 dampers tested in section 4.6 do not have the desired statistical characteristics identified by the antioptimization. The first step in the experimental validation is to create samples of dampers that match the desired properties as close as possible. The new samples are then remeasured and experimental statistics of the damper parameters are obtained. The deterministic and probabilistic designs are then reoptimized, using the experimental data. Finally, section 5.3 describes tests of several realizations of those 2 designs to evaluate the actual probabilities of failure and compare them to predictions.

## *5.2 Optimization of Deterministic and Probabilistic Designs*

### 5.2.1 Creating Samples of Dampers

The measured statistical distributions of damper parameters listed in section 4.6 do not

exhibit the mean values and standard deviations identified by the contrast maximization. As seen in section 3.4, the natural frequencies are the most important parameters affecting the performance of the dampers. If we want to approximate the ideal test scenario identified by the antioptimization, we should at least realize the desired distribution of natural frequencies. This can be achieved by readjusting the tuning screws of the 29 dampers of each type. The readjustment applied to each damper is calculated to create "ideal" samples with the desired mean and standard deviation.

The classical technique to experimentally evaluate probabilities of failure is to pick a random sample of $n$ realizations, test them, and count the number of failures. There are two sources of uncertainties in the estimated probabilities when using this approach. The first one is a resolution error that is only due to the limited size of the sample. The other is related to the randomness of the sample (but also depends on the sample size). If the probability of failure $P_f$ is estimated from a **random** sample of size $n$, the standard error $\sigma_{P_f}$ on $P_f$ is[60]

$$\sigma_{P_f} = \sqrt{\frac{P_f(1-P_f)}{n}}. \tag{5.4}$$

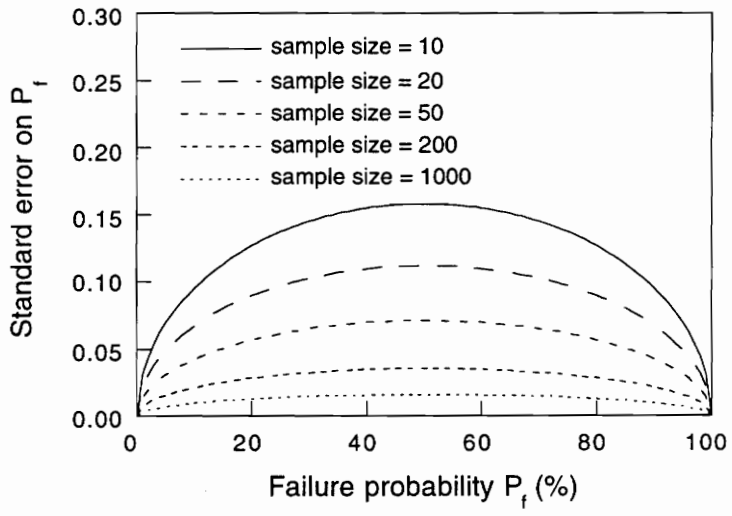


**Figure 5.6. Uncertainty on a probability measure based on limited samples.**

Figure 5.6 represents this standard error as a function of the probability of failure for various

sample sizes. With a sample size of 29*, this standard error is so large that it would obscure the probability contrast we want to measure. It is also clear from the figure that the uncertainty on the estimated $P_f$ decreases very slowly as the sample size goes up (it is an inverse square root dependence as shown in Eq. (5.4)). Getting the uncertainty on $P_f$ small enough to allow meaningful measurements of the probability difference between the two designs would require prohibitively large samples.

However, this uncertainty can be eliminated if we use a non-random sample. Since we will create the samples of dampers by readjusting their tuning screws, we have the opportunity to tailor these samples in a way that minimizes the resulting uncertainty in the measured probabilities. This can be achieved by distributing the natural frequencies of the dampers uniformly along the probability axis of a normal sample. This process is illustrated in the cumulative probability plot of Fig. 5.7.

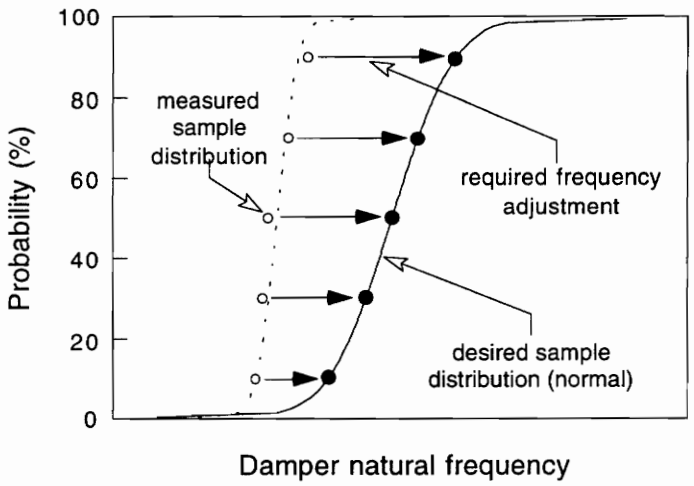


**Figure 5.7. Creation of an "ideal" sample of 5 dampers.**

The natural frequencies of the dampers are given on the horizontal axis and the probability of occurrence in the sample is given on the vertical axis. The solid line in the figure represents a

* There is very little interaction between the two modes of the structure; a damper of type 1 has no measurable effect on the response of mode 3 and vice versa. Because of this, we cannot create more than 29 independant combinations of a type 1 and a type 3 damper, from the 29 dampers of each type.

normal distribution of the natural frequencies with the desired mean and standard deviation. We first distributed the 29 dampers of the sample uniformly along the probability axis. Using the ideal distribution, we then inferred the desired natural frequency for each damper. Comparing those values with the measured natural frequencies of the 29 dampers, we obtained a desired change in natural frequency for each damper. Using measured sensitivity derivatives of the natural frequency with respect to the number of turns on the tuning screws, these changes in natural frequency were approximately translated into readjustments of the tip screws.

**Table 5.1. Type 1 dampers, statistics of parameters (sample of 29).**

| Parameter: | $m$ | $f_n$ | $\eta$ | $m_T$ |
|---|---|---|---|---|
| Mean | 7.075 g | 109.97 Hz | 0.12604 | 10.811 |
| St. dev. | 0.0788 g | 1.7487 Hz | 0.006772 | — |
| C.O.V. | 1.11% | 1.59% | 5.37% | — |
| Correlation coefficients | | | | |
| $m$ | 1.000 | | | |
| $f_n$ | 0.693 | 1.000 | | |
| $\eta$ | 0.689 | 0.375 | 1.000 | |

**Table 5.2. Type 3 dampers, statistics of parameters (sample of 29).**

| Parameter: | $m$ | $f_n$ | $\eta$ | $m_T$ |
|---|---|---|---|---|
| Mean | 7.340 g | 180.16 Hz | 0.15811 | 11.528 |
| St. dev. | 0.0944 g | 5.5609 Hz | 0.009987 | — |
| C.O.V. | 1.29% | 3.09% | 6.32% | — |
| Correlation coefficients | | | | |
| $m$ | 1.000 | | | |
| $f_n$ | 0.697 | 1.000 | | |
| $\eta$ | 0.511 | 0.016 | 1.000 | |

We carried out this sample tailoring procedure on both types of dampers. The dampers were then adjusted and remeasured. The resulting samples of dampers are not random; rather, they are discretized representations of the desired distributions of natural frequencies.

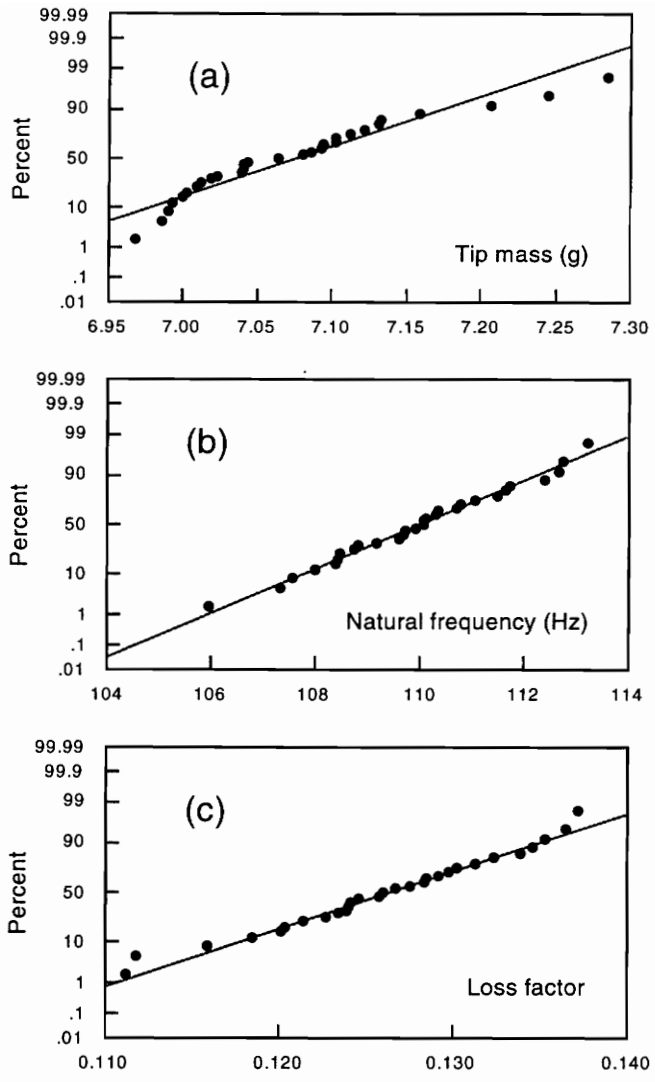


**Figure 5.8. Type 1 dampers, distribution of measured parameters.**

Each damper was measured 3 times and the parameters were averaged through the 3 measurements. The resulting samples of parameters were used to evaluate the means, standard deviations, coefficients of variation and correlation coefficients between parameters for both types of dampers. Tables 5.1 and 5.2 list these values for types 1 and 3, respectively. Figures 5.8 a, b, and c show normal probability plots of the measured distributions of the natural frequencies, tip masses, and loss factors of the 29 dampers of type 1. The same plots are given in Fig. 5.9 a, b and c for 29 dampers of type 3. The scale used on the probability axes of these plots is such that

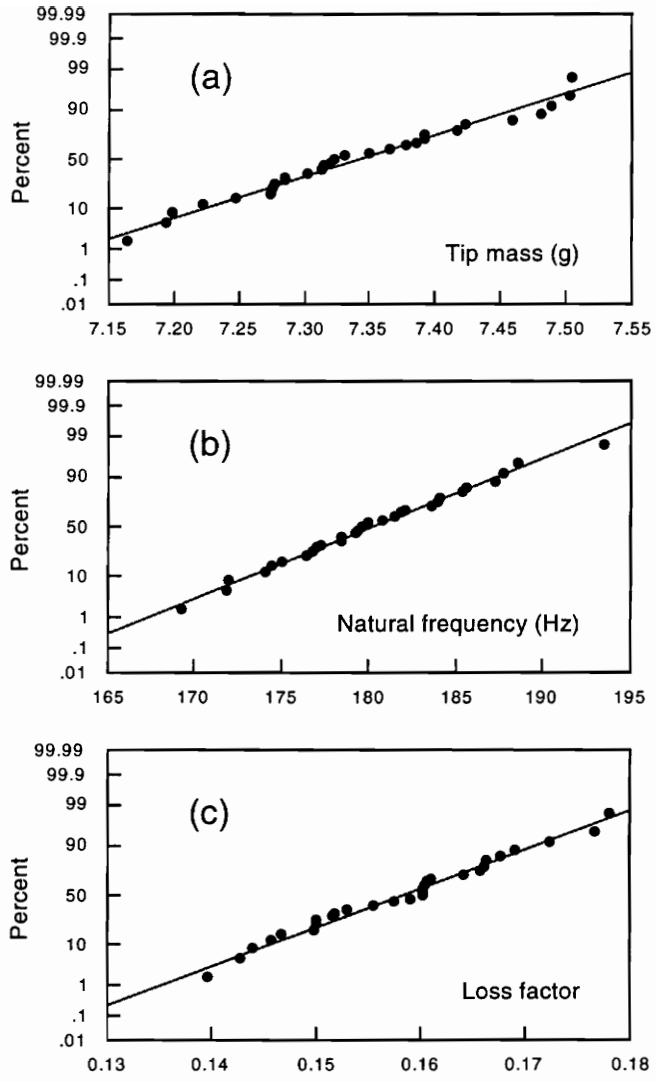


**Figure 5.9. Type 3 dampers, distribution of measured parameters.**

a perfectly normally distributed sample would lie on a straight line. Obviously, the distributions of the other damper parameters were also altered by the adjustment of the tip screws. However, as mentioned earlier, the natural frequency is the most important damper parameter. Note also that the distributions of the other parameters are not far from ideal even though they have not been explicitly tailored. The figures show that the normality assumption used in the statistical analysis is justified. With these tailored samples, the uncertainty of Eq. (5.4) is eliminated. The only uncertainty left is due to the small sample size; it consists of a resolution error on $P_f$ of

3.3% (100% divided by $n + 1$ with $n = 29$).

## 5.2.2 Validation and Calibration of Analytical Models

### *5.2.2.1 Truss Model Refinement*

As mentioned before, the truss is considered deterministic. Its model is adjusted based on measured natural frequencies and damping ratios. The stiffnesses and loss factors of the support springs contained in the finite element model as well as the loss factor of the truss members (assumed to be the same for all members) are identified by fitting the analytical natural frequencies and damping ratios of the first 3 modes of the original truss (without tuning masses or dampers) to measured values. The procedure is described in detail in Appendix C. The resulting model predicts exactly the first and third natural frequencies and damping ratios.

### *5.2.2.2 Measurement of Peak Accelerations*

The excitation (refer to chapter 2, Fig. 2.5) is provided by an electromagnetic shaker (Ling Dynamics 102) attached to the steel base plate and connected to node #6 of the truss through a stinger orthogonal to the wall. A piezoelectric load cell (PCB 208B) measures the excitation force. The shaker is driven by the signal generator of the Tektronix 2630 FFT analyser through a power amplifier (KEPCO BOP 50-2M). The response accelerations are measured at node 11, direction $\vec{1}_8$ (see Eq. 2.1) for mode 3 and node 12, direction $\vec{1}_4$ for mode 1. We use subminiature piezoelectric accelerometers (PCB 353B17) attached to the nodes with wax. A sine dwell technique is used to measure the transfer functions in frequency windows around modes #1 and #3 (refer to Chapter 4, Fig. 4.3). The postprocessing of the measurements is automated with MATLAB. The peaks of the measured transfer functions are smoothed by polynomial fitting and the experimental values are obtained from the fitted polynomials.

### *5.2.2.3 Calibration of Analytical Peak Accelerations*

We performed two series of tests on a few dampers of each type, chosen among the 29 available to cover the whole range of the parameter distributions. The parameters of each damper were measured 3 times and averaged to reduce experimental errors and temperature effects. The resulting sets of parameters were used to predict analytically the peak of the frequency response

curve of the original truss (no tuning masses) with a damper at the location and in the direction corresponding to the largest amplitude in its target mode. The peak amplitudes were then measured 3 times and averaged.

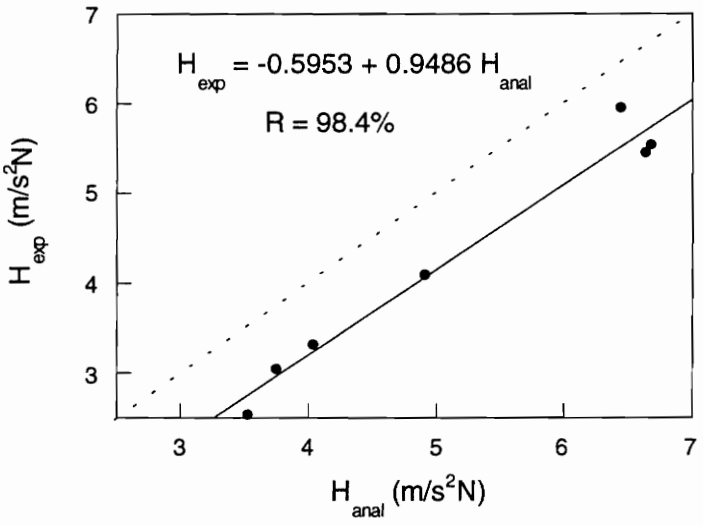


**Figure 5.10. Mode 1, analytical-experimental correlation and model calibration (Full analysis).**

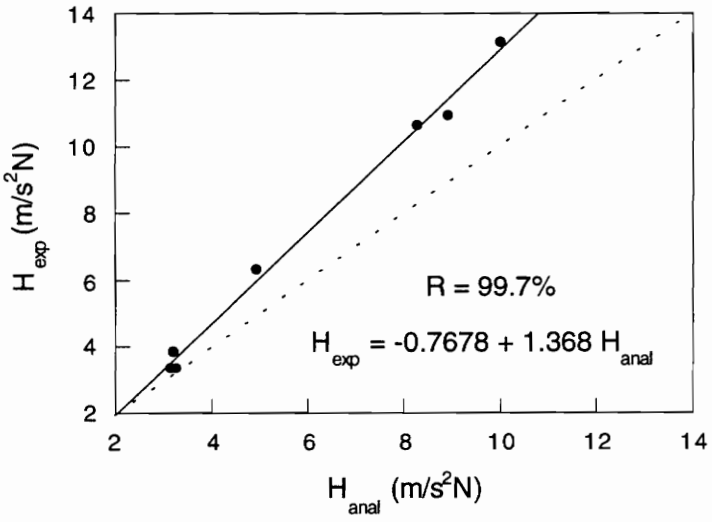


**Figure 5.11. Mode 3, analytical-experimental correlation and model calibration (Full analysis).**

These experimental results are plotted versus the corresponding analytical predictions in Fig. 5.10 and 5.11. The analytical values in the figure were obtained using the full analysis. The coefficient of correlation between analysis and experiment is equal to 98.4% for type 1 and 99.7% for type 3. This indicates the good quality of the measurements.

Straight lines have been fitted to the data in each plot. These lines indicate a mismatch between the experiment and the analytical results (the dotted lines in the figures represent ideal one to one correspondence between analysis and experiment). The equations of these fitted lines are shown in the figures and were incorporated into the full analysis to correct the mismatch. The same procedure was repeated to evaluate corrections for the results of the semi-analytical approximation used in the optimizations.

### 5.2.3 Optimization Results

During the optimizations, all analyses are performed using the semi-analytical approximation. The final designs are then reanalysed with the full order analysis.

The deterministic optimum was obtained with nominal values for the damper parameters. The nominal values were taken equal to the mean damper parameters shown in Tables 5.1 and 5.2. The optimization was repeated 10 times to improve the reliability of the genetic search.

The convergence history of the best of these ten runs is shown in Fig. 5.12. The figure shows the peak amplitudes of the transfer function of modes 1 and 3 of the best design in the current population of the genetic search as a function of the generation number, and the total number of objective function evaluations.

Because we minimize the largest of these amplitudes and we do not penalize for the number of tuning masses used in the design, the amplitudes of the two modes tend to equalize in the optimum design. The final value of the safety margin (using semi-analytical approximation and with $H_{lim} = 6.5m/Ns^2$) was 2.062 $m/Ns^2$. Reevaluated with the full analysis, the margin is 2.105 $m/Ns^2$. The difference between the two analyses is only about 2% in this case, which justifies a posteriori the use of the semi-analytical approximation in the optimization.

The deterministic design uses a total of 7 masses. Six masses are attached to node 7 and one to node 10. The type-1 and type-3 dampers are attached to nodes 12, direction $\vec{1}_4$ and 11,

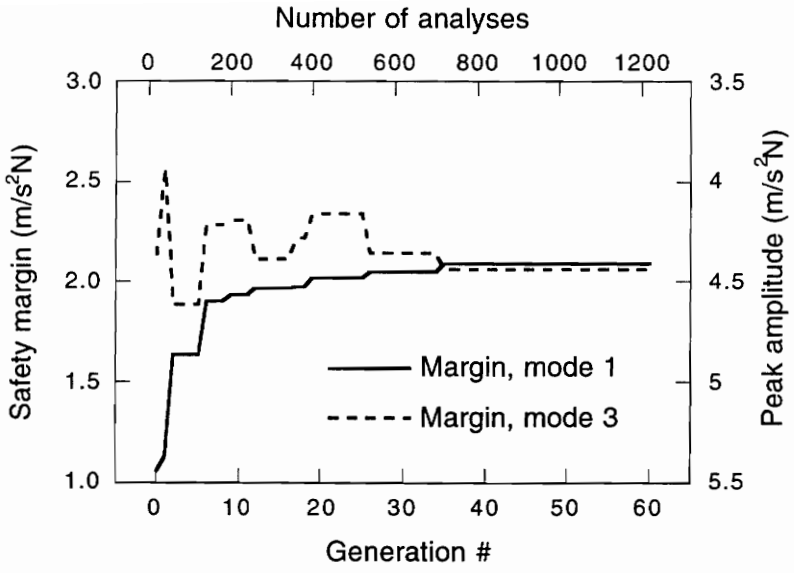


**Figure 5.12. Best of ten deterministic optimizations, convergence of safety margins of modes 1 and 3.**

direction $\vec{1}_8$ respectively. The nominal amplitudes and the probabilities of failure were evaluated with the full analysis. They are listed in Table 5.3. Note the large difference in probabilities of failure in each failure mode. This is because although the deterministic optimization uses a uniform safety margin for both failure modes the magnitudes of the scatter in the two modes are different.

**Table 5.3. Deterministic design, nominal amplitudes and probabilities of failure.**

| | Mode 1 | Mode 3 | Total |
|---|---|---|---|
| Nominal peak $[m/s^2N]$ (full analysis) | 4.395 | 4.172 | — |
| Probability of failure [%] (Monte Carlo simulation, 1000 points, full analysis) | 0.0 | 15.3 | 15.3 |

Using the data of Table 5.1 and 5.2 for the statistics of the parameters, we performed the probabilistic optimization. Because of its much larger computational cost, this optimization was repeated only 3 times. The convergence curve of the best of these 3 runs is shown in Fig. 5.13.

The curves in the figure show the probabilities of failure of the best design in the population as a function of the generation number (for mode 1, mode 3, and the whole system, from the semi-analytical approximation).

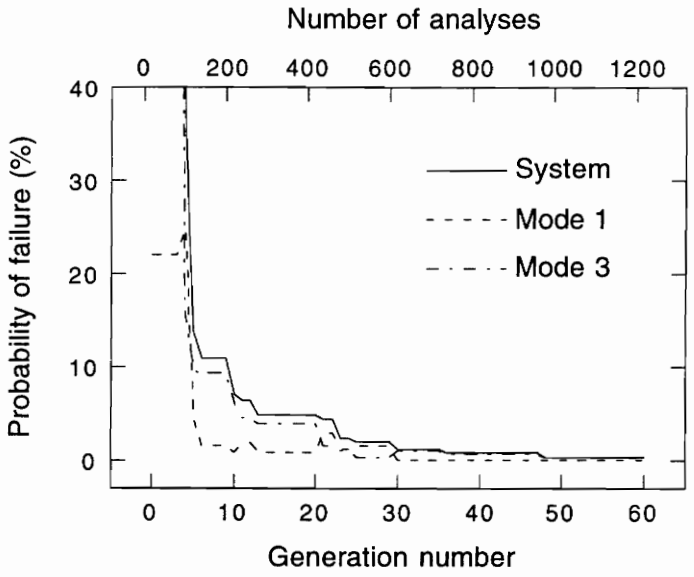


**Figure 5.13. Best of three probabilistic optimizations, convergence of probabilities of failure.**

Since we do not penalize for the number of added masses, the probabilities of failure of the two failure modes tend to equalize in the final design. The final system probability of failure was equal to 0.4% as evaluated with the semi-analytical approximation. The same design, reanalysed with the full analysis gives a probability of failure of 0.6%. Again, the difference is small enough to justify the use of the approximation in the optimization.

The probabilistic optimum design uses all 10 tuning masses. One of those masses is attached to node 7 and nine to node 10. The damper locations and directions are the same as in the deterministic design. The nominal peak amplitudes and probabilities of failure, evaluated with the full analysis, are listed in Table 5.4.

Note that the probabilities of failure of the deterministic and probabilistic designs (15.3% and 0.6%, respectively) are not exactly equal to the values predicted in the antioptimization (18.6%

**Table 5.4. Probabilistic design, nominal amplitudes and probabilities of failure.**

| | Mode 1 | Mode 3 | Total |
|---|---|---|---|
| Nominal peak $[m/s^2N]$ (full analysis) | 4.999 | 2.366 | — |
| Probability of failure [%] (Monte Carlo simulation, 1000 points, full analysis) | 0.1 | 0.5 | 0.6 |

and 2.5%, see section 5.1). This is because the statistics of the damper parameters used in the antioptimization were educated guesses, not actual measured values. In contrast, the two designs presented in this section are based on the *measured* statistics of the samples of dampers which differ slightly from those guesses. However, the contrast in probability of failure between the two designs is equal to 14.7%, which is very close to the value of 16.1% found in the antioptimization.

Figure 5.14 shows a graphical comparison of those two alternative designs. The figure contains the histograms of the peak amplitudes of the two failure modes (from the full analysis) for each design. The dashed vertical line in each histogram represents the failure limit ($H_{lim} = 6.5m/Ns^2$). For the deterministic design, all failures occur in the third mode, due to the large scatter in the response of that mode. The first mode, on the other hand, has been given too wide a safety margin; the tail of the distribution is away from the failure limit.

The probabilistic design represents another compromise for the same design problem: the safety margin has been tailored to the magnitude of the scatter in each mode. Compared to the deterministic design, the tuning masses have been moved to locations that are more effective on mode 3 and a few more masses have been used. This has considerably reduced the nominal peak amplitude of the third mode while slightly degrading the response of the first mode. Notice also that the scatter in mode 3 has been reduced.

The probabilistic design uses only 3 more tuning masses than the deterministic one, which represent less than 0.8% increase in the total mass of the structure compared to the deterministic design. The predicted reliability of the system has increased from 84.7% to 99.4%.

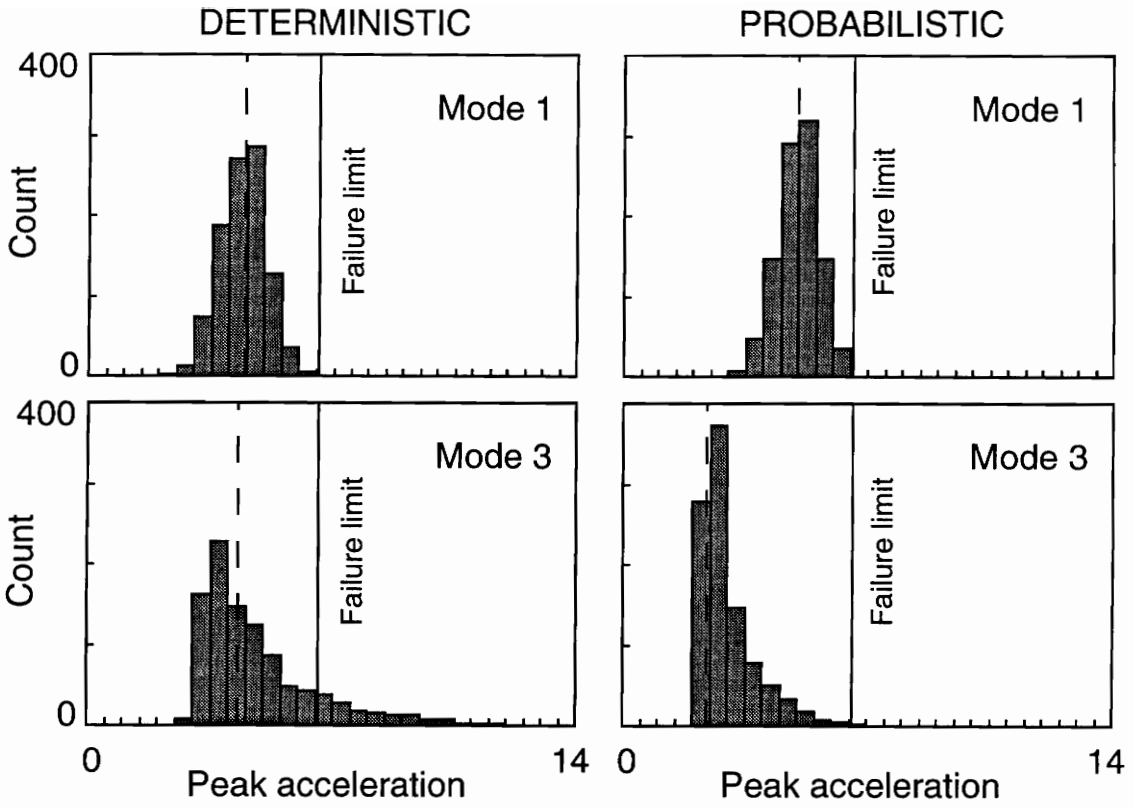


**Figure 5.14. Deterministic and probabilistic designs, distributions of peak amplitudes (Monte Carlo simulations with 1000 points and full order analysis).**

## *5.3 Experimental Comparison of Deterministic and Probabilistic Designs*

We prepared 29 sets of two absorbers by pairing randomly the 29 dampers of each type (all dampers were used and none was used twice). These 29 sets are used to create 29 realizations of each design. The same truss was used for all realizations and its model was adjusted to predict the natural frequencies and damping ratios exactly (without tuning masses or dampers). Each realization was tested 3 times in the laboratory and the measured peak amplitudes were averaged through the 3 measurements (this averaging is intended to reduce the effect of measurement errors and temperature changes). The probabilities of failure were evaluated for each design by counting the number of realizations that violate the requirement on the peak amplitudes. With a sample of 29 measurements, the resolution of the probability measurement is about 3.3%. Since the

difference in reliability between the two designs is 14.7%, this resolution is sufficient to measure the difference experimentally.

The results of the experiments are listed in Table 5.5. The experimental probabilities of failure of the two designs are compared to predicted values from Monte Carlo simulations using 1000 points and the full-order analysis. We observe that the experimental probabilities are within resolution error from the analytical predictions.

**Table 5.5. Deterministic and probabilistic designs, comparison of experimental (sample of 29) and analytical results (Monte Carlo, sample of 1000, full analysis).**

| | **Deterministic Design** | | **Probabilistic Design** | |
|---|---|---|---|---|
| | Analytical | Experimental | Analytical | Experimental |
| Mode 1 [%] | 0.0 | 0.0 | 0.1 | 3.5 |
| Mode 3 [%] | 15.3 | 17.2 | 0.5 | 0.00 |
| Total [%] | **15.3** | **17.2** | **0.6** | **3.5** |

Figures 5.15 and 5.16 show the cumulative probability curves for the two failure modes of the deterministic and probabilistic designs, respectively. The good agreement between experimental results and analytical predictions is clear. The experimental results confirm the higher reliability obtained with the probabilistic approach.

It is important to note that, although the measured reliability of the probabilistic design is much higher than that of the deterministic design, this result could have been reversed if more important modeling errors had been present. For example, let us evaluate the reliabilities of the two designs of Fig. 5.15 and 5.16 for a reduced value of the failure limit $H_{lim} = 6.0\, m/Ns^2$ (which is equivalent to a situation where the modeling error is larger). Analytical predictions give $P_f = 20.0\%$ for the deterministic design and 4.7% for the probabilistic design. The experimental results give 6 failures out of 29 designs (i.e. $P_f = 20.7\%$) for both designs!

This can be explained based on the following observation. In the deterministic design, failures only occur in mode 3. Because that mode has a large scatter (Fig. 5.14), the distribution of peak amplitudes is wide and therefore modeling errors are not likely to create very large errors

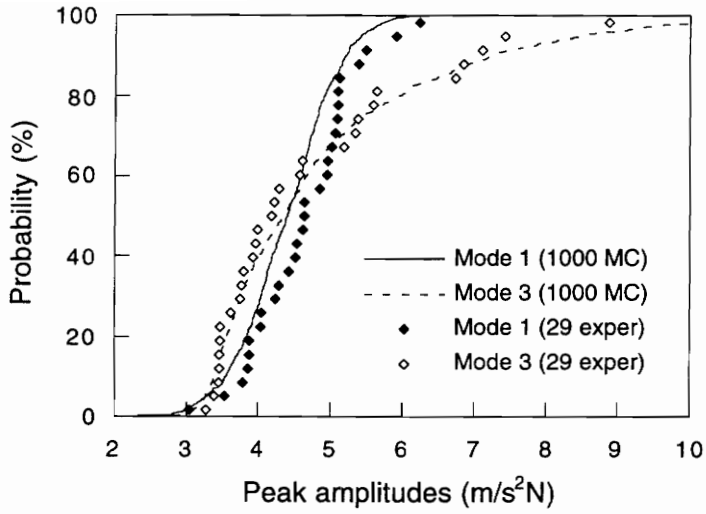


**Figure 5.15. Deterministic design, cumulative probability distributions from experiment and analytical Monte Carlo simulations.**

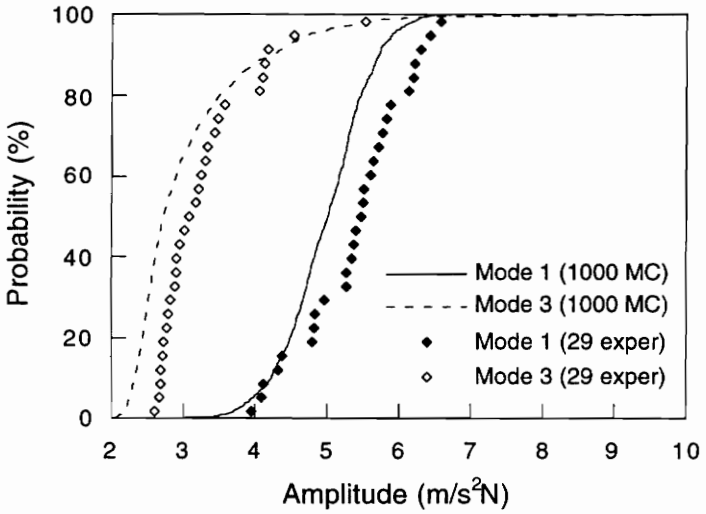


**Figure 5.16. Probabilistic design, cumulative probability distributions from experiment and analytical Monte Carlo simulations.**

in probability of failure. In the probabilistic design on the other hand, both modes are on the verge of causing failures. Because the distribution of peak amplitudes of the first mode is very sharp, a small shift in the distribution (caused, for example, by modeling errors) can cause a very large change in failure rate. For the example presented here, the failure limit is high enough that

we are working in the tails of the distributions. The density in the tail being small, the modeling error observed in Fig. 5.16 did not lead to a large – unpredicted – increase in probability of failure. For smaller values of the failure limit, however, the probabilities of failure in each mode are larger and the sensitivity to modelling errors is also larger because we are then working in denser areas of the distributions. This is especially true if the distribution is sharp, as in the case of the first mode in the probabilistic design.

To avoid this danger, modeling errors have to be accounted for in the formulation of the probabilistic optimization. This would prevent the optimizer from pushing the sharp distribution of mode 1 too close to the failure limit, thereby creating a small margin to absorb the modeling errors. Unfortunately, the magnitude and direction of the modeling errors are usually very difficult to predict. Very little data is usually available to support any particular description of those errors. In the deterministic formulation, the safety factors can absorb the modeling error if they were correctly chosen. This is not the case in probabilistic design where the uncertainties are assumed to be included in the model. It should never be forgotten that, however large the amount of information about parametric uncertainties in the system and however refined the analytical model used, there always are unmodeled effects or biases left in the system. Even though the probabilistic analysis uses (and needs) much more information about a system than deterministic analysis, this information is much more difficult to obtain and relies on assumptions that are difficult to justify (for example the shape of the tails of the distributions of uncertainties). Because of this, the result of the statistical analysis is itself subject to uncertainty and care should be taken to account for that uncertainty in the design process.

A few options exist to compensate the uncertainty in the predicted probabilities of failure. If the designer can somehow evaluate bounds on the effect of unmodeled uncertainties, then the design requirements could be padded by amounts equal to those upper limits before applying probabilistic optimization. In other words, the uncertainties that can be modeled and characterized statistically would be accounted for by the probabilistic optimization while protection from modeling errors and other unmodeled effects would be provided by safety margins (but these margins would be much smaller than those used in a deterministic design because they are intended for protection from part of the uncertainties only).

Another approach consists of assuming that the modeling errors can be represented with random variables and include them directly in the probabilistic formulation. One way to do this is

to apply a random multiplier (or bias) to the results of the analyses. This would "blur" the response distributions calculated in the probabilistic optimization and prevent the sharp distributions from being to close to the failure limits. However, the effect on the optimal probabilistic design is likely to depend on the assumed distribution of the error for which very limited amounts of data – if any at all – are typically available. This approach is currently under investigation. Statistics of the modeling errors will be estimated from measurements of analytical-experimental mismatch for different distributions of tuning masses (the added masses are thought to be responsible for the modeling errors observed in Fig. 5.15 and 5.16). They will then be included as random multipliers or shifts in the analysis and new optimal designs will be obtained and tested.

A third option could consist of blurring the definition of the failure limit instead of the predicted output distributions. The effect should be very similar to that of the previous approach. The preference function concept used in fuzzy set theory can to some extent be related to this last approach. In that theory, the strict, abrupt failure limit is replaced by a more gradual transition from a design being completely unacceptable to perfectly satisfactory. In the transition region, designs are given a preference that gradually decreases as their performance decreases. The effect is to some extent equivalent to blurring the definition of failure.

# Chapter 6
# Conclusions

The primary objective of this work was to obtain a realistic picture of the potential of probabilistic optimization in an actual design situation. To this end, we provided experimental results that accomplished the following goals:

1. **They confirmed the feasibility of obtaining accurate predictions of the transmitted scatter in response quantities of a structure from data about parametric uncertainties.** A truss structure was used as the example because of its relatively simple analysis and the fact that it is assembled from discrete components. This allowed to attribute the uncertainties to variations in the properties of those components. In addition, it allowed us to assemble several copies of the same truss one after the other at low cost by picking components randomly from a stock (the "tinker-toy" approach). The statistics of the uncertainties were evaluated from measurements on samples of components and used to predict output scatter in natural frequencies with a first order method. Although this scatter was extremely small and difficult to measure, the experimental results were in good agreement with predictions.

2. **They validated the process of probabilistic optimization for a practical design problem.** A truss equipped with tuned vibration absorbers was used as the example. The tuned absorbers were designed specifically for this study and proved very efficient. Tuning masses were used as design variables to refine the tuning of the truss to the dampers. Upper limits were set on the peak dynamic response at given points on the truss and violations of these limits were called failures. The damped truss was designed for maximum safety with a limit on total weight. A deterministic and a probabilistic approach were used to obtain optimal designs. In the deterministic design, safety is provided by margins with respect to the requirements while in the probabilistic approach, the probability of failure is minimized. Antioptimization was successfully used to identify an "ideal" design problem that maximizes the contrast between the optimal designs obtained with the two approaches. For that "ideal" problem, two designs were obtained using probabilistic and deterministic optimization. The difference in probability of failure between these two designs was more than 14%. Several

realizations of these designs were then tested for failure in the laboratory. The use of tuned dampers allowed us to generate cheaply and rapidly the large number of realizations needed by simply using different dampers on a single structure. The measured rates of failure were in excellent agreement with the predicted values and confirmed the much higher reliability of the probabilistic design.

Although for the maximum contrast problem used in the experimental comparison, the improved reliability of the probabilistic design was confirmed, our results show that probabilistic designs can be very sensitive to unmodeled effects. We have shown that, if modeling uncertainties are not accounted for in the probabilistic formulation, the reliability of the resulting design can be much lower than predicted. In some cases, the probabilistic design could even be less reliable than a deterministic design.

If an estimate of the amplitude of the residual unmodeled effects is available, it can be included in the formulation for example by applying a random scaling factor to the response quantities. This should reduce the sensitivity of the probabilistic design to unmodeled uncertainties. Unfortunately, it is very difficult to estimate the characteristics (amplitude, distribution, ...) of unmodeled effects and very little data is usually available to help the designer in this estimation. However, we speculate that even very rough estimates of the modeling errors can be used to achieve the desired goal. Additional tests are planned to investigate this last point.

Further research will investigate the application of fuzzy sets theory to this problem. Designs obtained with that approach will be compared to deterministic and probabilistic designs. Designs obtained from the application of the popular Taguchi methods will also be evaluated.

Finally, let us restate that our results have shown that probabilistic optimization has a definite potential for providing more reliable designs. However, this potential will be realized only under the following conditions:

1. Large amounts of data must be accumulated about the input uncertainties to arrive at an accurate description of their statistics.

2. The fact that probabilistic optimization accounts for uncertainties should not lead to overconfidence as there are always unmodeled effects that should be conservatively accounted for. Our results show that if modeling uncertainties are not accounted for, the probabilistic design can be very sensitive to them and could be much less reliable than predicted.

# References


[1] C. Mischke, "A Method for Relating Factor of Safety and Reliability," *Journal of Engineering for Industry*, Vol. 92, No. 3, August, 1970, pp. 537–542.

[2] F. Moses and D. E. Kinser, "Optimum Structural Design with Failure Probability Constraints," *AIAA Journal*, Vol. 5, No. 6, June, 1967, pp. 1152–1158.

[3] F. Moses, "Structural System Reliability and Optimization," *Computers & Structures*, Vol. 7, 1977, pp. 283–290.

[4] J. M. T. Thompson and G. W. Hunt, "Dangers of Structural Optimization," *Engineering Optimization*, Vol. 1, 1974, pp. 99–110.

[5] B. H. Aubert, J. F. Abel, J. Lu, and J. S. Thorp, "Effects of Structural Imperfections on Constant-Feedback-Gain Control of a Spatial Structure," *Computing Systems in Engineering*, Vol. 1, Nos. 2–4, 1990, pp. 601–606.

[6] R. T. Haftka, Z. N. Martinovic, W. L. Hallauer Jr., and G. Schamel, "An Analytical and Experimental Study of the Sensitivity of a Control System to Structural Modifications," *AIAA Journal*, Vol. 25, No. 2, 1987, pp. 310–315.

[7] E. Ponslet, R. T. Haftka, W. L. Hallauer Jr., and H. H. Cudney, "Desensitizing Structural-Control Design," *Journal of Guidance, Control and Dynamics*, Vol. 17, No. 1, January–February, 1994, pp. 175–180.

[8] J. A. Bennett and R. V. Lust, "Conservative Methods for Structural Optimization," *AIAA Journal*, Vol. 28, No. 8, August, 1989, pp. 1491–1496.

[9] A. Parkinson, C. Sorensen, J. Free, and B. Canfield, "Tolerances and Robustness in Engineering Design Optimization," *Advances in Design Automation*, DE-Vol. 23-1, edited by B. Ravani, ASME, New York, NY, 1990, pp. 121–128.

[10] A. Charnes and W. W. Cooper, "Chance Constrained Programming," *Management Sciences*, Vol. 6, 1958, pp. 73–79.

[11] A. M. Hasofer and N. C. Lind, "Exact and Invariant Code Format," *Journal of Engineering Mechanics Division*, Vol. 100, No. EM1 1974, pp. 111–121.

[12] F. Moses and J. D. Stevenson, "Reliability-based Structural Design," *Journal of the Structural Division*, February, 1970, pp. 221–244.

[13] J. W. Davidson, L. P. Felton, and G. C. Hart, "Optimum Design of Structures with Random Parameters," *Computers & Structures*, Vol. 7, 1977, pp. 481–486.

[14] J. W. Davidson, L. P. Felton, and G. C. Hart, "Reliability-based Optimization for Dynamic Loads," *Journal of the Structural Division*, Vol. 103, No. ST10, October, 1977, pp. 2021–2035.

[15] S. R. Parimi and M. Z. Cohn, "Optimal Solutions in Probabilistic Structural Design - Part I: Theory," *Journal de Mécanique Appliquée*, Vol. 2, No. 1, 1978, pp. 47–72.

[16] S. R. Parimi and M. Z. Cohn, "Optimal Solutions in Probabilistic Structural Design - Part II: Applications," *Journal de Mécanique Appliquée*, Vol. 2, No. 1, 1978, pp. 73–92.

[17] D. Frangopol, "A Reliability-based Optimization Technique for Automatic Plastic Designs," *Computer Methods in Applied Mechanics and Engineering*, Vol. 44, 1983, pp. 105–117.

[18] D. Frangopol, "Interactive Reliability-based Structural Optimization," *Computers & Structures*, Vol. 19, No. 4, 1984, pp. 559–563.

[19] D. Frangopol, "Structural Optimization using Reliability Concepts," *Journal of Structural Engineering*, Vol. 111, No. 11, November, 1985, pp. 2288–2301.

[20] D. Frangopol, "Computer-automated Sensitivity Analysis in Reliability-based Plastic Design," *Computers & Structures*, Vol. 22, No. 1, 1986, pp. 63–75.

[21] Y. S. Feng and F. Moses, "A Method of Structural Optimization based on Structural System Reliability," *Computers & Structures*, Vol. 14, No. 4, 1986, pp. 437–453.

[22] Y. S. Feng and F. Moses, "Optimum Design, Redudancy and Reliability of Structural Systems," *Computers & Structures*, Vol. 24, No. 2, 1986, pp. 239–251.

[23] J. D. Sørensen and P. Thoft-Christensen, "Integrated Reliability-based Optimal Design of Structures," in *Reliability and Optimization of Structural Systems*, edited by P. Thoft-Christensen, Proceedings of the First IFIP WG 7.5 Working Conference, (Aalborg, Denmark, May 6–8, 1987), *Lectures Notes in Engineering*, Vol. 33, Springer-Verlag, New York, NY, pp. 385–398.

[24] M. J. Baker and A. C. W. M. Vrouwenvelder, "Reliability Methods for the Design and Operation of Offshore Structures," *Proceedings of the 11th International Conference on Offshore Mechanics and Arctic Engineering* (Calgary, Alberta, Canada, June 7–12, 1992), Vol. 2, ASME, New York, NY, pp. 123–132.

[25] S. S. Rao, "Structural Optimization by Chance Constrained Programming Techniques," *Computers & Structures*, Vol. 12, 1980, pp. 777–781.

[26] S. S. Rao, "Reliability-based Optimization under Random Vibration Environment," *Computers & Structures*, Vol. 14, Nos. 5–6, 1981, pp. 345–355.

[27] E. P. Fox, "The Pratt & Whitney Probabilistic Design System," *Proceedings of the AIAA/ ASME/ ASCE/ AHS/ ASC 35th Structures, Structural Dynamics, and Materials Conference*,

(Hilton Head, SC, April 18–20, 1994), Vol. 2, AIAA, Washington, DC, 1994, pp. 1075–1085 (AIAA Paper 94–1442).

[28] J. D. Adamson, "The Probabilistic Design System Development Experience," *Proceedings of the AIAA/ ASME/ ASCE/ AHS/ ASC 35th Structures, Structural Dynamics, and Materials Conference*, (Hilton Head, SC, April 18–20, 1994), Vol. 2, AIAA, Washington, DC, 1994, pp. 1086–1094 (AIAA Paper 94–1444).

[29] M. R. Khalessi, H.-Z. Lin, and M. S. Alvarez "Reliability Analysis of the Orbiter Docking System External Airlock Frame Structure," *Proceedings of the AIAA/ ASME/ ASCE/ AHS/ ASC 35th Structures, Structural Dynamics, and Materials Conference*, (Hilton Head, SC, April 18–20, 1994), Vol. 2, AIAA, Washington, DC, 1994, pp. 655–664 (AIAA Paper 94–1387).

[30] E. P. Fox, "Methods of Integrating Design within an Organization's Design System Using Box-Behnken Matrices," *Proceedings of the AIAA/ ASME/ ASCE/ AHS/ ASC 34th Structures, Structural Dynamics, and Materials Conference*, (La Jolla, CA, April 19–22, 1993), Vol. 2, AIAA, Washington, DC, 1993, pp. 714–723 (AIAA Paper 93–1380).

[31] Y. Ben-Haim and I. Elishakoff, *Convex Models of Uncertainty in Applied Mechanics*, Elsevier Science Publishing Company, New York, NY, 1990.

[32] E. P. Fox and F. Safie, "Statistical Characterization of Life Drivers for a Probabilisitic Design Analysis," *AIAA/ SAE/ ASME/ ASEE 28th Joint Propulsion Conference and Exhibit*, (Nashville, TN, USA), July 6–8, 1992, (AIAA Paper 92–3414).

[33] D. Frangopol, "Sensitivity of Reliability-based Optimum Design," *Journal of Structural Engineering*, Vol. 111, No. 8, August, 1985, pp. 1703–1721.

[34] T. Y. Torng and R. J. Yang, "A Reliability-based Design Optimization Procedure for Minimal Variations," *Proceedings of the AIAA/ ASME/ ASCE/ AHS/ ASC 35th Structures, Structural Dynamics, and Materials Conference*, (Hilton Head, SC, April 18–20, 1994), Vol. 2, AIAA, Washington, DC, 1994, pp. 842–852 (AIAA Paper 94-1415).

[35] E. Nikolaidis and R. Burdisso, "Reliability Based Optimization: a Safety Index Approach," *Computers & Structures*, Vol. 28, No. 6, 1988, pp. 781–788.

[36] M. V. Reddy, R. V. Grandhi, and D. A. Hopkins, "Reliability Based Structural Optimization: a Simplified Safety Index Approach," *Proceedings of the AIAA/ ASME/ ASCE/ AHS/ ASC 34th Structures, Structural Dynamics, and Materials Conference*, (La Jolla, CA, April 19–22, 1993), Vol. 2, AIAA, Washington, DC, 1993, pp. 990–999 (AIAA Paper 93-1418).

[37] T. K. Hasselman and J. D. Chrostowski, "Statistical Analysis of Modeling Error in Structural Dynamic Systems," *Proceedings of the AIAA/ ASME/ ASCE/ AHS/ ASC 31st Structures, Structural Dynamics, and Materials Conference*, (Long Beach, CA, April 2–4, 1990), Vol. 4, AIAA, Washington, DC, 1990, pp. 1945–1951 (AIAA Paper 90–1041).

[38] T. K. Hasselman and J. D. Chrostowski, "Interval Prediction in Structural Dynamic Analysis," *Proceedings of the AIAA/ ASME/ ASCE/ AHS/ ASC 33rd Structures, Structural Dynamics, and Materials Conference*, (Dallas, TX, April 13–15, 1992), Vol. 3, AIAA, Washington, DC, 1992, pp. 1272–1284 (AIAA Paper 92–2215).

[39] R. S. Ryan and J. S. Townsend, "Application of Probabilistic Analysis/ Design Methods in Space Programs: The Approaches, The Status, and The Needs," presented at the AIAA/ ASME/ ASCE/ AHS/ ASC 34th Structures, Structural Dynamics, and Materials Conference (La Jolla, CA, April 19–22,1993), not included in the proceedings, (AIAA Paper 93–1381).

[40] B. Ellingwood and M. K. Ravindra, "Issues in the Validation of Probabilisitc Methods," in *Structural Design, Analysis and Testing*, edited by A. H-S. Ang, ASCE, New York, NY, Proceedings of Structures Congress '89, (San Fransisco, CA, May 1–5, 1989), pp. 319–324.

[41] J. R. Benjamin, "The Validation Problem - Historical Developments," in *Structural Design, Analysis and Testing*, edited by A. H-S. Ang, ASCE, New York, NY, (Partial Proceedings of Structures Congress '89, San Fransisco, CA, May 1–5), pp. 311–318.

[42] H. M. Adelman, "Experimental Validation of Structural Optimization Methods," NASA–TM 104203, January, 1992.

[43] P. G. Maghami, S. Gupta, S. M. Joshi, and J. E. Walz, "Experimental Validation of Optimization-based Integrated Controls-structures Design Methodology for Flexible Space Structures," *Proceedings of the 2nd IEEE Conference on Control Applications* (Vancouver, British Columbia, Canada, September 13–16, 1993), Vol. 1, IEEE, Piscataway, NJ, pp. 7–14.

[44] E. H. Cramer and P. Friss-Hansen, "Reliability Based Optimization of Multi-component Welded Structures," *Proceedings of the 11th International Conference on Offshore Mechanics and Arctic Engineering* (Calgary, Alberta, Canada, June 7–12, 1992), Vol. 2, ASME, New York, NY, pp. 265–271.

[45] A. Surahman and K. B. Rojiani, "Reliability Based Design of Concrete Frames," *Journal of Structural Enfineering*, Vol. 109, No. 3, March, 1983, pp. 741–757.

[46] D. Frangopol and J. Rondal, "Optimum Probability-based Design of Plastic Structures," *Engineering Optimization*, Vol. 3, 1977, pp. 17–25.

[47] T. W. Lee and B. M. Kwak, "A Reliability-based Optimal Design using Advanced First Order Second Moment Method," *Mechanics of Structures and Machines* , Vol. 15, No. 4, 1987–1988, pp. 523–534.

[48] E. Nikolaidis and W. J. Stroud, "Reliability-based Optimization: a Proposed Analytical-experimental Study," *Proceedings of the AIAA/ ASME/ ASCE/ AHS/ ASC 35th Structures,*

*Structural Dynamics, and Materials Conference*, (Hilton Head, SC, April 18–20, 1994), Vol. 2, AIAA, Washington, DC, 1994, pp. 1105–1114 (AIAA Paper 94–1446).

[49] W. K. Belvin, A. Bruner, J. Sulla, and J. Bailey, "The LaRC CSI Phase-0 Evolutionary Model Testbed: Design and Experimental Results," presented at the 4th Annual NASA/ DOD Conference on Control/ Structures Interaction Technology, Orlando, FL, November 5–7, 1990.

[50] R. T. Haftka, Z. Gürdal, and M. P. Kamat, *Elements of Structural Optimization*, 2nd edition, Kluwer Academic Publishers, Dordrecht, The Netherlands, 1990.

[51] G. C. Canavos, *Applied Probability and Statistical Methods*, Little, Brown & Company, Boston, MA, 1984.

[52] M. L. Parin, A. D. Nashif, and T. M. Lewis, "PACOSS Damping Material Measurement," *Proceedings of "Damping 86", Vibration Damping Workshop II*, (Las Vegas, NV, USA), March 5–7, 1986, pp. AE-1 – AE-56.

[53] *MATLAB User's Guide*, The MathWorks, Inc., Natick, MA, 1992.

[54] R. R. Craig Jr., *Structural Dynamics; an Introduction to Computer Methods*, John Wiley & Sons, New York, NY, 1981.

[55] T. K. Hasselman and J. D. Ross, "Propagation of Modeling Uncertainty through Structural Dynamic Models," *Proceedings of the AIAA/ ASME/ ASCE/ AHS/ ASC 35th Structures, Structural Dynamics, and Materials Conference*, (Hilton Head, SC, April 18–20, 1994), Vol. 1, AIAA, Washington, DC, 1994, pp. 72–83 (AIAA Paper 94-1316).

[56] J. H. Holland, *Adaptation in Natural and Artificial Systems*, University of Michigan Press, Ann Arbor, MI, 1975.

[57] R. T. Haftka and P. J. Kao, "The Use of Optimization for Sharpening Differences between Models," presented at the *ASME Winter Annual Meeting*, (Dallas, TX, USA), November 25–30, 1990.

[58] S. N. Gangadharan, E. Nikolaidis, and R. T. Haftka, "The Use of Antioptimization to Compare Alternative Structural Models," *Proceedings of the AIAA/ ASME/ ASCE/ AHS/ ASC 34th Structures, Structural Dynamics, and Materials Conference*, (La Jolla, CA, April 19–22, 1993), Vol. 1, AIAA, Washington, DC, 1993, pp. 534–543 (AIAA Paper 93–1355).

[59] A. van Wamelen, E. R. Johnson, and R. T. Haftka, "Optimal Design of Laminated Specimens to Evaluate Competing Composite Failure Criteria," presented at the *American Society for Composites 8th Technical Conference on Composite Materials*, Cleveland, OH, October 19–21, 1993

[60] J. L. Devore, *Probability and Statistic for Engineering and the Sciences*, 2nd edition, Brooks/Cole, Monterey, CA, 1987.

[61] P. A. Ioannou and J. Sun, "The Theory and Design of Robust Direct and Indirect Adaptive Control Schemes," *International Journal of Control*, Vol. 47, No. 3, 1988, pp. 775-813.

[62] J. Doyle and K. Glover, "State Space Formulae for all Stabilizing Controllers that Satisfy an $H_\infty$-Norm Bound and Relations to Risk Sensitivity," *System Control Letters*, Vol. 11, 1988, pp. 167-172.

[63] P. P. Khargonekar, I. R. Petersen, and K. Zhou, "Robust Stabilization of Uncertain Systems: Quadratic Stabilizability and $H_\infty$ Control Theory," *IEEE Transactions on Automatic Control*, Vol. 35, No. 3, 1990, pp. 356-361.

[64] M. Athans, "A Tutorial on the LQG/LTR Method," *Proceedings of the American Control Conference*, June, 1986, pp. 1289-1296.

[65] R. K. Cavin and S. P. Bhattacharyya, "Robust and Well-Conditioned Eigenstructure Assignment via Sylvester's Equations," *Optimal Control Applications and Methods*, Vol. 4, No. 3, 1983, pp. 205–212.

[66] J. Kautsky, N. K. Nichols, and P. Van Dooren, "Robust Pole Assignment in Linear State Feedback," *International Journal of Control*, Vol. 41, No. 5, 1985, pp. 1129–1155.

[67] J.-N. Juang and P. G. Maghami, "Robust Eigensystem Assignment for Second-Order Dynamic Systems," in *Mechanics and Control of Large Flexible Structures*, edited by J. L. Junkins, AIAA, Washington, DC, 1990, pp. 373–387.

[68] Z. N. Martinovic, G. C. Schamel II, R. T. Haftka, and W. L. Hallauer Jr., "Analytical and Experimental Investigation of Output Feedback vs Linear Quadratic Regulator," *Journal of Guidance, Control, and Dynamics*, Vol. 13, No. 1, 1990, pp. 160–167.

[69] H. Benaroya and H. J. Fleisher, "Probabilistic Aircraft Structural Dynamics Models," *Proceedings of the AIAA/ ASME/ ASCE/ AHS/ ASC 32nd Structures, Structural Dynamics, and Materials Conference*, (Baltimore, MD, April 8–10, 1991), Vol. 2, AIAA, Washington, DC, 1991, pp. 1254–1260 (AIAA Paper 91-0921).

[70] R. V Grandhi, I. Haq, and N. S. Khot, "Enhanced Robustness in Integrated Structural/ Control Systems Design," *Proceedings of the AIAA/ ASME/ ASCE/ AHS/ ASC 31st Structures, Structural Dynamics, and Materials Conference*, (Long Beach, CA, April 2–4, 1990), Vol. 1, AIAA, Washington, DC, 1990, pp. 268–276.

[71] Y. Juang, T. Kuo, and C. Hsu, "New Approach to Time-Domain Stability Robustness of Dynamic Systems," *International Journal of Systems Science*, Vol. 18, No. 7, 1987, pp. 1363–1376.

[72] J. L. Junkins and D. W. Rew, "Unified Optimization of Structures and Controllers," in *Large Space Structures: Dynamics and Control*, edited by S.N. Atluri and A.K. Amos, Springer-Verlag, New York, NY, 1987.

[73] K. B. Lim and J. L. Junkins, "Robust Optimization of Structural and Controller Parameters," *Journal of Guidance, Control and Dynamics*, Vol. 12, No. 1, 1989, pp. 89–96.

[74] H. Thomas and L. A. Schmit, "Synthesis of Structural/Control Systems Robust with Respect to Design Variable Tolerances," *Proceedings of the AIAA/ ASME/ ASCE/ AHS/ ASC 32nd Structures, Structural Dynamics, and Materials Conference*, (Baltimore, MD, April 8–10, 1991), Vol. 1, AIAA, Washington, DC, 1991, pp. 506–516.

[75] E. A. Czajkowski, A. Preumont, and R. T. Haftka, "Spillover Stabilization of Large Space Structures," *Journal of Guidance, Control, and Dynamics*, Vol. 13, No. 6, 1990, pp. 1000–1007.

[76] G. Kreisselmeier and R. Steinhauser, "Systematic Control Design by Optimizing a Vector Performance Index," *Proceedings of IFAC Symposium on Computer Aided Design of Control Systems*, Zurich, Switzerland, 1979, pp.113-117.

[77] J.-F. M. Barthelemy and M. F. Riley, "An Improved Multilevel Optimization Approach for the Design of Complex Engineering Systems," *AIAA Journal*, Vol. 26, 1988, pp. 353–360.

[78] A. Preumont, J.-P. Dufour, and C. Malekian, "Active Damping by a Local Force Feedback with Piezoelectric Actuators," *Proceedings of the AIAA/ ASME/ ASCE/ AHS/ ASC 32nd Structures, Structural Dynamics, and Materials Conference*, (Baltimore, MD, April 8–10, 1991), Vol. 3, AIAA, Washington, DC, 1991, pp. 1879–1887.

[79] A. Preumont, M. Sparavier, and J.-P. Dufour, "Application of Piezoelectric Actuators to the Active Damping of a Truss Structure," *Proceedings of the AIAA/ ASME/ ASCE/ AHS/ ASC 31st Structures, Structural Dynamics, and Materials Conference*, (Long Beach, CA, April 2–4, 1990), Vol. 3, AIAA, Washington, DC, 1990, pp. 1907–1913 (AIAA paper 90-0950).

[80] E. Ponslet, R. T. Haftka, and H. H. Cudney, "Improved Procedure for Eigenvalue Approximation and Sensitivities to Modeling Uncertainties for Active Structures," *Proceedings of the AIAA/Air Force/NASA/OAI 4th Symposium on Multidisciplinary Analysis and Optimization* (Cleveland, OH, September 21–23, 1992), Vol. 1, 1992, pp. 26–32.

[81] C. A. Sandridge and R. T. Haftka, "Accuracy of Eigenvalue Derivatives from Reduced-order Structural Models," *Journal of Guidance, Control and Dynamics*, Vol. 12, No. 6, 1989, pp. 822–829.

[82] R. V. Grandhi, R. Thareja, and R. T. Haftka, "NEWSUMT-A: a General Purpose Program for Constrained Optimization using Constraint Approximations," *Journal of Mechanisms, Transmission and Automation in Design*, Vol. 107, No. 1, ASME, New York, NY, March, 1985, pp. 94–99.

[83] P. G. Maghami and S. M. Joshi, "Sensor-Actuator Placement for Flexible Structures with Actuator Dynamics," *Proceedings of the AIAA Guidance, Navigation, and Control Conference*, (New Orleans, LA, Aug. 12-14, 1991), Vol. 1, pp. 46–54.

[73] K. B. Lim and J. L. Junkins, "Robust Optimization of Structural and Controller Parameters," *Journal of Guidance, Control and Dynamics*, Vol. 12, No. 1, 1989, pp. 89–96.

[74] H. Thomas and L. A. Schmit, "Synthesis of Structural/Control Systems Robust with Respect to Design Variable Tolerances," *Proceedings of the AIAA/ ASME/ ASCE/ AHS/ ASC 32nd Structures, Structural Dynamics, and Materials Conference*, (Baltimore, MD, April 8–10, 1991), Vol. 1, AIAA, Washington, DC, 1991, pp. 506–516.

[75] E. A. Czajkowski, A. Preumont, and R. T. Haftka, "Spillover Stabilization of Large Space Structures," *Journal of Guidance, Control, and Dynamics*, Vol. 13, No. 6, 1990, pp. 1000–1007.

[76] G. Kreisselmeier and R. Steinhauser, "Systematic Control Design by Optimizing a Vector Performance Index," *Proceedings of IFAC Symposium on Computer Aided Design of Control Systems*, Zurich, Switzerland, 1979, pp.113-117.

[77] J.-F. M. Barthelemy and M. F. Riley, "An Improved Multilevel Optimization Approach for the Design of Complex Engineering Systems," *AIAA Journal*, Vol. 26, 1988, pp. 353–360.

[78] A. Preumont, J.-P. Dufour, and C. Malekian, "Active Damping by a Local Force Feedback with Piezoelectric Actuators," *Proceedings of the AIAA/ ASME/ ASCE/ AHS/ ASC 32nd Structures, Structural Dynamics, and Materials Conference*, (Baltimore, MD, April 8–10, 1991), Vol. 3, AIAA, Washington, DC, 1991, pp. 1879–1887.

[79] A. Preumont, M. Sparavier, and J.-P. Dufour, "Application of Piezoelectric Actuators to the Active Damping of a Truss Structure," *Proceedings of the AIAA/ ASME/ ASCE/ AHS/ ASC 31st Structures, Structural Dynamics, and Materials Conference*, (Long Beach, CA, April 2–4, 1990), Vol. 3, AIAA, Washington, DC, 1990, pp. 1907–1913 (AIAA paper 90-0950).

[80] E. Ponslet, R. T. Haftka, and H. H. Cudney, "Improved Procedure for Eigenvalue Approximation and Sensitivities to Modeling Uncertainties for Active Structures," *Proceedings of the AIAA/Air Force/NASA/OAI 4th Symposium on Multidisciplinary Analysis and Optimization* (Cleveland, OH, September 21–23, 1992), Vol. 1, 1992, pp. 26–32.

[81] C. A. Sandridge and R. T. Haftka, "Accuracy of Eigenvalue Derivatives from Reduced-order Structural Models," *Journal of Guidance, Control and Dynamics*, Vol. 12, No. 6, 1989, pp. 822–829.

[82] R. V. Grandhi, R. Thareja, and R. T. Haftka, "NEWSUMT-A: a General Purpose Program for Constrained Optimization using Constraint Approximations," Journal of Mechanisms, Transmission and Automation in Design, Vol. 107, No. 1, ASME, New York, NY, March, 1985, pp. 94–99.

[83] P. G. Maghami and S. M. Joshi, "Sensor-Actuator Placement for Flexible Structures with Actuator Dynamics," *Proceedings of the AIAA Guidance, Navigation, and Control Conference*, (New Orleans, LA, Aug. 12-14, 1991), Vol. 1, pp. 46–54.

[84] R. A. Burdisso and R. T. Haftka, "Statistical Analysis of Static Shape Control in Space Structures," *AIAA Journal*, Vol. 28, No. 8, 1990, pp.1504–1508.

[85] R. E. Skelton and M. L. DeLorenzo, "Selection of Noisy Actuators and Sensors in Linear Stochastic Systems," *Journal of Large Scale Systems, Theory and Applications*, Vol. 4, 1983, pp.109–136.

[86] Haftka, R.T., and Adelman, H.M., "Selection of Actuator Locations for Static Shape Control of Large Space Structures by Heuristic Integer Programming," *Computers and Structures*, Vol. 20, No. 1–3, 1985, pp. 575–582.

[87] R. T. Haftka, "Limits on Static Shape Control for Space Structures," *AIAA Journal*, Vol. 29, No. 11, 1991, pp. 1945–1950.

[88] E. Ponslet, R. T. Haftka, W. L. Hallauer and H. H. Cudney, "Desensitizing Structural Control Design," *Proceedings of the 8th VPI & SU Symposium on Dynamics and Control of Large Space Structures* (Blacksburg, VA, May 6–8, 1991), pp. 149–158.

[89] S. L. Padula and C. A. Sandridge, "Active Strut Placement Using Integer Programming for the CSI Evolutionary Model," *Proceedings of the 4th AIAA/ USAF/ NASA/ OAI Symposium on Multidisciplinary Analysis and Optimization*, (Cleveland, OH, September 21–23, 1992), pp. 784–793.

[90] N. Metropolis, A. W. Rosenbluth, M. N. Rosenbluth, A. H. Teller, and E. Teller, "Equation of State Calculations by Fast Computing Machines," *Journal of Chemistry and Physics*, Vol. 21, No. 6, 1953, pp. 1087–1092.

[91] G.-S. Chen, R. J. Bruno, and M. Salama, "Optimal Placement of Active/Passive Members in Structures Using Simulated Annealing," *AIAA Journal*, Vol. 29, No. 8, 1991, pp. 1327–1334.

[92] S. S. Rao, T.-S. Pan, and V. B. Venkayya, "Optimal Placement of Actuators in Actively Controlled Structures Using Genetic Algorithms," *AIAA Journal*, Vol. 29, No. 6, 1991, pp. 942–943.

[93] J. Onoda, and Y. Hanawa, "Optimal Locations of Actuators for Statistical Shape control of Large Space Structure: A Comparison of Approaches," AIAA Paper 92–2558.

[94] L. Schrage, *User's Manual for LINDO*, 4th edition, The Scientific Press, Redwood City, CA, 1989.

[95] J. D. Greenfield, *Practical Digital Design Using ICs*, 2nd edition, John Wiley & Sons, 1983, pp 393–397.

# Appendix A

# Targeted Robustness Design of Actively Controlled Trusses

In this appendix, a method for targeted robustness optimization is presented. This method allows the analyst to target the most critical performance parameter for enhanced protection from uncertainties in the model. To create this protection, the method uses statistical data about the uncertainties in the parameters of the model to predict – and minimize – the scatter in the most critical design requirement(s).

## *A.1 Introduction*

There are several approaches to developing active control systems based on inaccurate models. One solution is to use adaptive control techniques (e.g., [61]). With this approach the model is being identified while the structure is being controlled, and the control gains are adjusted according to this identified model. Another solution is to design robust control systems that do not depend on accurate structural models for adequate performance. Examples of these techniques include H-infinity designs (e.g., [62,63]), restoring robustness to the well known linear-quadratic Gaussian (LQG) control (e.g., using loop-transfer recovery[64]), optimizing various measures of system robustness while satisfying limits on the eigenvalues or assigning them to desired locations (e.g., [65,66,67]), or using very simple and inherently robust control designs such as collocated direct-rate feedback control (e.g., [68]).

The above techniques provide blanket robustness, or robustness to unstructured uncertainties. That is, there is no attempt to capitalize on knowledge of the nature of the uncertainties for each parameter, such as statistical properties, or on knowledge of the particular vulnerabilities of the system to be designed (such as knowledge that a certain mode of vibration is likely to be the most difficult to control). In the past few years there has been growing interest in robustness

techniques that capitalize on such knowledge—techniques that are called here targeted robustness methods. Robustness can be targeted by tailoring the design to known statistical properties of the uncertainties in the system or by focusing on shielding selected (target) response quantities from the effect of these uncertainties. This targeted robustness approach can benefit from recent interest in statistically based structural dynamics models (e.g., Benaroya and Fleisher[69]).

Targeted robustness methods allow the choice of structural parameters as well as control system gains to enhance robustness. Also, targeted robustness approaches can make use of knowledge of uncertainties in the structural model. Grandhi, Haq and Khot[70] considered optimizing structural and control parameters to improve a robustness measure due to Juang *et al.*[71]. One attractive feature of that robustness measure is that it allows the structural analyst to assign different levels of uncertainty to the different elements of the structural matrices used in the control design, reflecting the differing levels of uncertainties in different physical parameters. Junkins and coworkers (e.g., Refs.[72,73]) designed structural and control parameters to minimize the sensitivity of the eigenvalues of the closed loop system to critical parameters. This approach allows the targeting of the most critical eigenvalue for protection from uncertainties. Thomas and Schmit[74] optimized structural parameters to shield the most critical constraints from the worst combination of uncertainties in the values of the design variables of the structure and control system. Here, we develop a method of targeted robustness that shields the most critical response quantities from the cumulative effect of uncertainties in some parameters of the system.

In the rest of this appendix, the targeted robustness method will be derived. In section A.2 we first show how the robustness can be targeted on the most critical response quantity, and define the KS function used to express it mathematically. In section A.3, we then focus on the special case of the control of truss structures using active members. The targeted robustness design procedure will be applied to the special case of protecting the most critical damping ratio of a controlled truss. Results from two numerical examples which demonstrate the power of this method are described in section A.4.

## *A.2 Targeted Robustness Formulation*

### A.2.1 Minimization of the Most Critical Standard Deviation

The first premise of targeted robustness formulations is that the analyst can obtain some

statistics of the uncertainties associated with various parameters of the structure and control system, such as geometrical dimensions, stiffness values, mass properties and control system gains. The present state of the art is such that detailed statistical properties of these parameters are usually not available, but it is expected that both the nominal values of these parameters and some rough estimates of their standard deviations should be available to the designer. While the technique described here is more general in nature, the following derivations assume that the statistical behavior of the parameters can be reasonably approximated by the normal distribution.

Consider a response quantity $r(p)$, a function of vector $p$ of problem parameters, which have a nominal value of $p_0$ and some known statistical distribution, with $r_0 = r(p_0)$. We can find the statistical properties of $p$ by Monte Carlo simulation. However, some statistical measures of $r$ can be easily estimated directly. To do this, approximate $r$ by a first-order Taylor series as

$$r(p) = r_0 + \nabla r^T \Delta p \,, \tag{A.1}$$

where $\nabla r$ denotes the gradient of $r$ and

$$\Delta p = p - p_0 \,, \tag{A.2}$$

An approximation $V(r)$ to the variance of $r$ (square of the standard deviation) is

$$V(r) = E\left[(r - r_0)^2\right] = \nabla r^T E(\Delta p \Delta p^T) \nabla r \,, \tag{A.3}$$

where $E$ denotes the expected value operator, and $E(\Delta p \Delta p^T)$ is the covariance matrix of the uncertainties. The diagonal terms of this covariance matrix are the squares of the standard deviations of the components of $p$, which we assume can be estimated. The off-diagonal entries in the covariance matrix measure the strength of the correlation between the uncertainties in the components. If no information is available about these correlations, the off-diagonal terms are typically assumed equal to zero.

The targeted robustness procedure designs the structure and control system to satisfy performance requirements while minimizing the scatter in the most critical performance requirement. In the design procedure we have the freedom to change some of the system parameters, while others stay fixed. Denoting $p_d$ as the subset of $p$ which consists of design variables, the design problem can be formulated as

$$\begin{aligned} &\underset{p_d}{\textbf{Maximize}} \quad V(c_m) \\ &\textbf{such that} \quad c_j(p) \leq 0 \,, \qquad j = 1, \ldots, n_c \,, \end{aligned} \tag{A.4}$$

where $c_j$ represent $n_c$ performance constraints such as limits on damping ratios, or design limits such as upper bounds on gains, and $c_m$ is the most critical (most positive) constraint. There are some computational problems associated with the solution of such an optimization problem because the identity of the most critical constraint changes as we search the design space. Also, if there are several constraints that are all as critical or nearly as critical, then we would want to minimize the variation $V$ for all of them. These problems are solved through the use of an envelope function, discussed in the next section, that replaces the individual constraints.

The design obtained by the solution of (A.4) satisfies both aspects of targeted robustness. First, it takes advantage of any knowledge about the uncertainties available to the designer. Such knowledge need not be complete. As long as there is some information about the statistics of important sources of uncertainties, the solution of (A.4) will endow the design with robustness with respect to these uncertainties. The solution will not affect robustness with respect to other uncertainties, and for this reason it is desirable to use design techniques that help with unstructured uncertainties. Also, protection against the effect of inaccuracies associated with model reduction or nonlinearities is not addressed by the targeted robustness approach. Thus, targeted robustness is not intended as a replacement for techniques such as $H_\infty$ design or spillover alleviation methods (e.g., Ref. [75]), but as a supplemental procedure.

The design obtained by the solution of (A.4) also satisfies the second aspect of targeted robustness — the most critical response quantities are targeted for extra protection.

## A.2.2 The KS Envelope Function

The Kresselmeier-Steinhauser (KS) function[76,77] was developed to collapse a number of constraints into a single (envelope) constraint. Consider a vector of design parameters (such as structural dimensions and control gains) $p$, and a set of $n_c$ constraints written as

$$c_j(p) \leq 0, \qquad j = 1, \ldots, n_c \,. \tag{A.5}$$

In active structural control problems, a typical constraint is

$$c_j = 1 - \frac{\zeta_j}{\zeta_{Rj}} \leq 0 \,, \tag{A.6}$$

where $\zeta_j$ is the damping ratio associated with the $j$th mode, and $\zeta_{Rj}$ is the required damping ratio. The KS function replaces these constraints with a single constraint

$$KS(c_j) = (1/\rho) \ln \left[ \sum_{j=1}^{n_c} e^{\rho c_j} \right] \leq 0 . \tag{A.7}$$

Because of the exponential sum in the KS function, for large values of $\rho$ the function $\mathrm{KS}(c_j)$ is virtually equal to the most critical (most positive) constraint. Since the identity of the most positive constraint changes with changes in the design $x$, the most critical constraint is not a smooth function of the design. The KS function is a smooth envelope of the $c_j$'s, but for large values of $\rho$ it can have very large curvatures. For this reason, we usually work with moderate values of $\rho$, for which the envelope function is slightly more stringent than the constraints. We can use the standard deviation of the KS function as an approximation to the standard deviation of the most critical constraint. When that constraint is a limit on the damping ratio, such as Eq. (A.6), this is equal to the standard deviation of the most critical damping ratio. Thus, by minimizing the standard deviation of the KS function we can minimize the standard deviation of the most critical damping ratio without knowing a priori the identity of this damping ratio.

In many cases we would be interested in minimizing not only the standard deviation of the most critical damping ratio, but also the standard deviations of all near critical damping ratios. This can also be accommodated by using a moderate value of $\rho$. As $\rho$ is reduced the distinction between critical and near critical constraints becomes more blurred, and the standard deviation of the KS function reflects contributions from all constraints that are within a certain band of the most critical one.

The following equation relates the largest allowable distance $\beta$ between the KS envelope and the constraint boundaries, the value of $\rho$ and the number of constraints $n_c$:

$$\rho = \frac{\ln n_c}{\beta} . \tag{A.8}$$

It can be used as a guideline to choose an appropriate value of $\rho$ for practical problems.

## *A.3 Application: Control of a Truss Structures with Active Members*

We now consider the targeted robustness design of a truss with a number of active members, using decentralized control. The objective in this class of problems will be to satisfy minimum

requirements on the damping ratios of selected modes and to minimize the sensitivity of the most critical of these requirements by adjusting a selection of structural and control parameters. Since we are dealing with trusses controlled with active members, it is clear that the locations of these active members influence both the performance and the robustness of the design. Ideally, they would be included as design variables in the targeted robustness optimization. However, actuator locations in a truss being discrete variables in nature, they are not handled easily with conventional gradient based optimization algorithms. For that reason, and because our purpose is merely to establish the feasibility of the targeted robustness approach, we consider the locations of the active members as given and tune the structure and the control gains to improve robustness. Two techniques for finding optimal locations for the active members (linear programming and genetic algorithms) are presented in appendix D.

## A.3.1 Active Member

Each active member $i$ consists of a piezoelectric stack to provide actuation, and a force transducer to provide sensing. The actuator responds to an applied voltage $V_i$ by a change $\delta_i$ in its natural length

$$\delta_i = g_{a_i} V_i \,, \tag{A.9}$$

where $g_{a_i}$ is the actuator gain. The force sensor produces a voltage signal $v_i$ given as

$$v_i = g_{s_i} p_{e_i} = g_{s_i} k_{a_i} (\Delta_i - \delta_i) \,, \tag{A.10}$$

where $g_{s_i}$ is a sensor gain, $p_{e_i}$ is the force in the member, $k_{a_i}$ is the element spring constant, $\Delta_i$ is the total elongation of the element, and $\delta_i$ is the elongation due to any applied voltage.

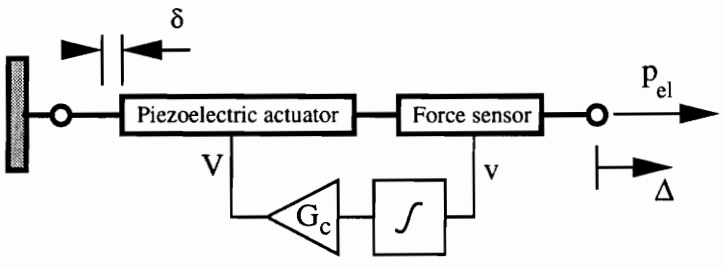


**Figure A.1. Active member with integral force feedback.**

The control law[78,79] relates the applied voltage to the force sensor voltage as

$$V_i = \int g_{c_i} v_i(t) dt \,, \tag{A.11}$$

where $g_{c_i}$ is an adjustable control gain. The closed-loop description of the active member (see Fig. A.1) is therefore

$$\delta_i = \int g_i k_{a_i} (\Delta_i - \delta_i) \, dt \,, \qquad g_i = g_{s_i} g_{a_i} g_{c_i} \,. \tag{A.12}$$

## A.3.2 Analysis and Approximations

For a truss with $\ell$ degrees of freedom, $m$ active members, a mass matrix $M(\ell \times \ell)$ and a stiffness matrix $K(\ell \times \ell)$, the equations of motion (neglecting inherent damping) are written as

$$M\ddot{x} + Kx = f + Bf_a = f + BK_a\delta \,, \tag{A.13}$$

where a dot denotes differentiation with respect to time, $x(\ell \times 1)$ is the nodal displacement vector, $f(\ell \times 1)$ is an applied force vector, $B(\ell \times m)$ is an influence matrix containing directional cosines of the active members, $f_a(m \times 1)$ is a vector of active member forces, $K_a(m \times m)$ is a diagonal matrix containing the spring constants $k_a$ of the active members, and $\delta(m \times 1)$ is a vector of applied elongations $\delta_i$ in the active members. Differentiating Eq. (A.12) with respect to time and writing it for all active members we obtain

$$\dot{\delta} = GK_a(B^T x - \delta) \,, \tag{A.14}$$

where $G(m \times m)$ is a diagonal matrix containing the gains $g_i$ of the $m$ active members. We now assume that there are no applied forces, and write Eqs. (A.13) and (A.14) in state-space form as

$$\dot{z} = Az \,, \tag{A.15}$$

where

$$z = \begin{Bmatrix} x \\ \dot{x} \\ \delta \end{Bmatrix}, \qquad A = \begin{bmatrix} 0 & I & 0 \\ -M^{-1}K & 0 & M^{-1}BK_a \\ GK_aB^T & 0 & -GK_a \end{bmatrix} . \tag{A.16}$$

In the optimization, the computation of the constraints and objective function requires the repetitive solution of the eigenvalue problem for $A$. For structures with a large number of degrees of freedom, this can entail a massive computational effort, and therefore we employ an approximation for estimating the eigenvalues of the matrix $A$. We found that the usual modal reduction technique used in structural analysis can be very inaccurate in predicting the damping ratios of structures with active members. The explanation lies in the local character of the actuation. In reference [80] we show that with the use of Ritz vectors for the static response to actuation forces in addition to mode shapes in the reduced basis, the accuracy of the approximation is improved by up to three orders of magnitude (also see [81]).

For the calculation of the standard deviations of the damping ratios, we need the derivatives of the eigenvalues with respect to uncertainty parameters. Furthermore, for the optimization of the most critical standard deviation we need derivatives of the standard deviation, which amounts to a need for second derivatives of the eigenvalues. This creates the need for a very efficient procedure for evaluating these derivatives. Reference [80] shows how an efficient analytical expression can be derived for the sensitivity derivatives by taking advantage of symmetries in the eigensystem. The Ritz model mentioned above is used to evaluate approximate eigenvectors to be used in that expression.

### A.3.3 Minimization of Scatter in Most Critical Damping Ratio

The standard deviation of the most critical constraint is optimized by varying control gains $g$ and structural parameters $s$. The problem can be restated, rewriting formulation (A.4) with the $KS$ function (Eq. A.7) and the parameters relevant to a truss,

$$\begin{aligned} &\underset{g,s}{\textbf{Minimize}} \quad V[KS(c_k)] \\ &\textbf{such that} \quad c_k(g,s,\epsilon) = 1 - \frac{\zeta_k}{\zeta_k^R} \leq 0\,, \qquad k = 1,\ldots,n_{modes}\,, \end{aligned} \tag{A.17}$$

where $g$, $s$, and $\epsilon$ respectively stand for the gains of the active members, the structural design variables and the uncertainties in the model, $n_{modes}$ is the number of modes to be controlled and $V[KS]$ is the variance of the $KS$ function. As explained before, the $KS$ function is a close approximation to the most critical constraint(s).

The optimization was performed with the NEWSUMT-A program[82] which is based on an extended interior penalty function with approximate second derivatives and Newton's method for unconstrained minimization.

## *A.4 Numerical Examples*

To demonstrate the targeted robustness approach, the standard deviation of the most critical damping ratio was minimized for two truss examples. Minimum values for the damping ratios of the first few modes were selected, and constraints in the form of Eq. (A.6) were imposed. The locations of the active members were assumed given and kept unchanged while control gains as well as structural parameters were tuned to minimize the standard deviation of the most critical constraint.

### A.4.1 Active Control of a Ten-Bar Truss.

The ten bar truss shown in Fig. A.2 is composed of two square bays, each 9 meter wide. Four non-structural masses of 10 kg each are attached at the 4 free nodes. The aluminum members have a Young's modulus of $70 \times 10^9$ N/m$^2$ and a specific mass of 3000 kg/m$^3$. All have the same cross-sectional area with a nominal value of $70 \times 10^{-6}$ m$^2$. The undamped natural frequencies of the first four modes are 7.3 Hz, 22.0 Hz, 23.6 Hz, and 42.0 Hz. Two integral force feedback active members (see section A.3.1) are to be included in the truss to provide each of the first 4 modes with at least 3% relative damping. The active members are assumed to have the same mass and stiffness as the bars they replaced.

The locations for the active members were found using the linear programming approach of appendix D. Those locations are shown in Fig. A.2; they will be considered given and will not be changed in the optimization.

The gains of the two active members $(g_1, g_2)$ and the cross-sectional area of the bars $(A)$ (all bars are assumed to have the same cross-sectional area) were adjusted to minimize the sensitivity of the most critical damping ratio to parametric uncertainties. The uncertainties were confined to the magnitudes $m_i$ of the four added masses, which were assumed to be uncorrelated normal

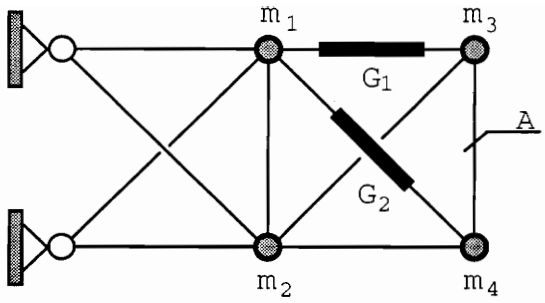


**Figure A.2. Ten-Bar Truss Example.**

random variables with a coefficient of variation (C.O.V., equal to the standard deviation divided by the mean value) of 1%. Additional constraints were placed on the maximum values of the gains and on the maximum cross-sectional area ($A_{max}$). The formulation of Eq. (A.17) can be rewritten for this particular problem as

$$\begin{aligned} \underset{g_1,g_2,A}{\textbf{Minimize}} \quad & V[KS(c_k)] \\ \textbf{such that} \quad & c_k = 1 - \frac{\zeta_k}{0.03} \leq 0\,, \qquad k = 1,\ldots,4\,, \\ & 0 \leq g_1, g_2 \leq 5. \times 10^{-4} \text{ m/Ns}\,, \\ & 0 \leq A \leq A_{max} \\ \textbf{with} \quad & \sigma(m_i) = 0.1 \text{ kg} \end{aligned} \tag{A.18}$$

The value of $\rho$ in the $KS$ function (Eq. A.7) was set to 27.7 (this value corresponds to a maximum error on the constraints due to smoothing of about 5%, see Eq. A.8). Since in this example the finite element model is of very small size, a full order analysis was used during the optimization to evaluate the damping ratios and their derivatives.

Two optimal structure-control designs were obtained by changing the upper limit $A_{max}$ on the cross sectional area of the bars. Both optimal designs were reanalyzed and the standard deviations of the damping ratios were evaluated from Monte Carlo simulations (50 points). Table A.1 lists – for both designs – the value of the upper limit on the cross section $A_{max}$, the optimal values of the gains and cross section, and the mean values, standard deviations and C.O.V.'s of the damping ratios of the first four modes. For the low-weight design the damping ratio of the fourth mode was critical (at the 3% limit), while for the high-weight design the second mode's damping ratio was critical. Notice that the standard deviations of the damping ratios vary widely between

the two designs, and that the critical damping ratio has, indeed, the lowest standard deviation in both designs. The standard deviation of the damping ratio of the second mode is an indication of the power of the method. The mean damping ratio of that mode is similar for both designs, but the standard deviation is one-tenth as large when this mode is the critical one: for the low-weight design the coefficient of variation in that mode is about 4%, while for the high-weight design it is about 0.4%. The results indicate that it is indeed possible to confer selective robustness to the most critical measure of the response.

**Table A.1. Ten bar truss, optimal designs.**

| | **Low-Weight** ($A_{max} = 190. \times 10^{-6}$) $g_1 = 1.036 \times 10^{-4}$ $g_2 = 0.484 \times 10^{-4}$ $A = 131.6 \times 10^{-6}$ | | | **High-Weight** ($A_{max} = 670. \times 10^{-6}$) $g_1 = 0.961 \times 10^{-4}$ $g_2 = 0.467 \times 10^{-4}$ $A = 667.2 \times 10^{-6}$ | | |
|---|---|---|---|---|---|---|
| mode | $\bar{\zeta}$ | $\sigma(\zeta)$ | C.O.V.(%) | $\bar{\zeta}$ | $\sigma(\zeta)$ | C.O.V.(%) |
| 1 | 0.0413 | 0.00018 | 0.44 | 0.1200 | 0.00026 | 0.22 |
| 2 | 0.0335 | 0.00136 | 4.06 | **0.0300*** | **0.00013** | 0.43 |
| 3 | 0.0360 | 0.00106 | 2.94 | 0.1960 | 0.00082 | 0.42 |
| 4 | **0.0300*** | **0.00016** | 0.53 | 0.0833 | 0.00038 | 0.46 |

* critical constraint

## A.4.2 Active Control of a Space Truss

The space truss shown in Fig. A.3 has 207 members and 71 nodes. It is a large H-shaped beam-truss assembled from a repeated "building block". The building block is a pyramidal bay with a square base. All bars have the same length (0.500 meter), except for the diagonals of the square bases which are $\sqrt{2}$ times longer (0.707 meter). These bars were modeled as rod members (using translations only as degrees of freedom) with uniform properties from node center to node center. These properties are the same for all members in the truss: the cross sectional area $A = 66.00 \times 10^{-6}$ m$^2$, the specific mass $\rho = 6000.$ kg/m$^3$, and Young's modulus $E = 81.82 \times 10^9$ N/m$^2$. The nodes are modeled as infinitely stiff point masses of 0.2285 kg. The truss is free floating and its model contains a total of 213 degrees of freedom.

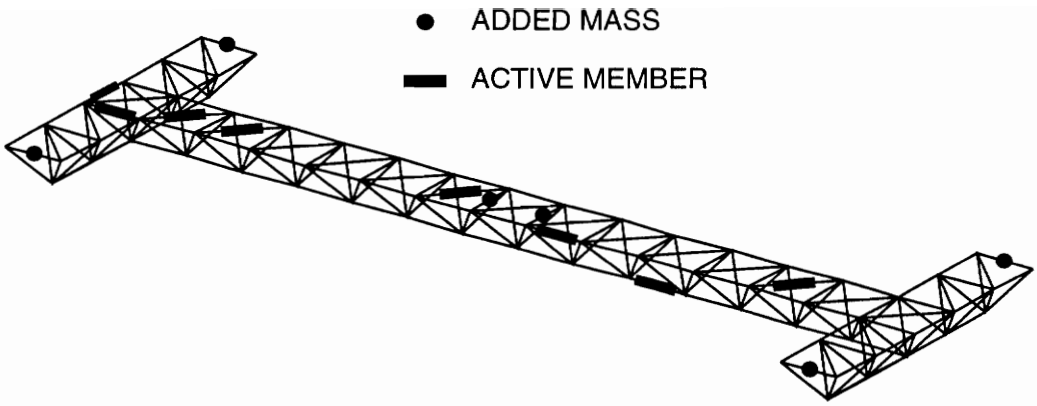


**Figure A.3. 3D truss, active member and mass locations.**

Six masses (representing about 40% of the total mass of the structure) have been added to the truss to create closely spaced frequencies. The locations of these masses are fixed and shown in Fig. A.3. Each mass consists of a 0.55 meter by 0.05 meter rectangular steel plate attached in parallel with a 0.5 meter member. The thickness of the plate will be used as a design variable so that the total mass $M$ of each plate can be adjusted. The presence of the steel bar also increases the stiffness of the member. The change in mass and stiffness is modeled by modifying the values of $\rho$, $A$, and $E$ for the particular member and adding a concentrated mass $m_c$ to each end node. The values of $\rho$, $A$, $E$ and $m_c$ are defined in terms of the total mass $M$ of the bar according to the following relations

$$\begin{aligned} \rho &= 7830.0 \text{ kg/m}^3 , \\ E &= 210.0 \times 10^9 \text{ N/m}^2 , \\ A &= \frac{M}{0.55\rho} \text{ m}^2 , \\ m_c &= 0.04545M . \end{aligned} \qquad \text{(A.19)}$$

The nominal value of $M$ was set to 6.640 kg. With all 6 masses at their nominal mass, the natural frequencies of the first 11 modes of the undamped structure are as listed in table A.2.

**Table A.2. Space truss, undamped natural frequencies.**

| mode | 1 | 2 | 3 | 4 | 5 | 6 | 7 | 8 | 9 | 10 | 11 |
|---|---|---|---|---|---|---|---|---|---|---|---|
| $f_n$ (Hz) | 4.7 | 8.7 | 9.3 | 17.5 | 24.9 | 32.0 | 36.4 | 37.9 | 53.1 | 55.2 | 57.1 |

Eight integral feedback active members were included at locations shown in Fig. A.3. The active members are assumed to have the same mass and stiffness as the member they replaced. The locations of the active members are not part of the robustness optimization; they have been obtained using the linear programming technique of appendix D and will be kept unchanged.

The design variables of the targeted robustness optimization include the magnitudes of the 6 masses and the gains of the 8 active members. The uncertainties are limited to the magnitudes of the 6 masses and the gains of the 8 active members. All are assumed to be uncorrelated normal random variables with fixed coefficients of variation (standard deviations divided by mean values) of 10% for the gains and 5% for the masses.

The objective is to achieve minimum values for the damping ratios of the first 11 natural vibration modes of the truss. The requirements on the damping ratios correspond to a uniform decay rate of 1.2 $\text{sec}^{-1}$ on all but the second mode (the decay rate is equal to the product of the damping ratio by the undamped natural frequency). We have chosen a uniform value for the decay rate instead of the damping ratios because of the wide range of natural frequencies in this example. Uniform damping ratios would give very fast decay to high frequency modes and much slower decay to low frequency modes. The requirement on the second mode was increased to 4% relative damping (see table A.3) to make it a critical mode.

The magnitudes of the 6 masses ($M_1, \ldots, M_6$) are constrained between 70% and 130% of their nominal value of 6.460 kg. The gains $g_1, \ldots, g_8$ of the active members are allowed to vary between 0 and 10 times a nominal value of $1 \times 10^{-6}$ m/Ns. We can rewrite the formulation of Eq. (A.17) for this particular problem as

$$
\begin{aligned}
\underset{g_1,\ldots,g_8,M_1,\ldots,M_6}{\textbf{Minimize}} \quad & V[KS(c_k)]\,, \\
\textbf{such that} \quad & c_k = 1 - \frac{\zeta_k}{\zeta_k^R} \leq 0\,, \qquad k = 1,\ldots,11\,, \\
& 0 \leq g_1,\ldots,g_8 \leq 1 \times 10^{-5}\ \text{m/Ns}\,, \\
& 4.522\,kg \leq M_1,\ldots,M_6 \leq 8.398\ \text{kg}\,, \\
\textbf{with} \quad & \sigma(g_i) = 0.10\,\bar{g}_i, \quad i = 1,\ldots,8\,, \\
\textbf{and} \quad & \sigma(M_i) = 0.05\,\bar{M}_i, \quad i = 1,\ldots,6\,.
\end{aligned}
\tag{A.20}
$$

where $\bar{g}_i$ and $\bar{M}_i$ denote the mean values of the gains and masses.

The optimum design obtained with this formulation will be referred to as the *minimum sensitivity design*. The Ritz technique and the analytical expression for the sensitivity derivatives mentioned before was used to evaluate the damping ratios and their derivatives.

For comparison, we generated a baseline *minimum gain design* subject to the same requirements. For this, we modified the objective function of formulation (A.20) to minimize the sum of the squares of the gains of the 8 active members, i.e.

$$\underset{g_1,\ldots,g_8,M_1,\ldots,M_6}{\textbf{Minimize}} \quad \sum_{i=1}^{8} {g_i}^2 \ , \tag{A.21}$$

The design variables, limits and constraints are identical to those in formulation (A.20).

The optimum designs obtained from those two formulations are as follows:

**Minimum Gain Design:**

$$g_1,\ldots,g_8 = 1.0 \times 10^{-6}\,\text{m/Ns} \times (3.63, 2.22, 2.73, 2.67, 2.27, 6.45, 1.87, 2.69)$$

$$M_1,\ldots,M_6 = 6.460\,\text{kg} \times (1.30, 1.29, 1.29, 0.90, 1.27, 1.30)$$

**Minimum Sensitivity Design:**

$$g_1,\ldots,g_8 = 1.0 \times 10^{-6}\,\text{m/Ns} \times (8.97, 2.24, 8.80, 9.65, 9.69, 9.59, 8.31, 9.86)$$

$$M_1,\ldots,M_6 = 6.460\,\text{kg} \times (0.89, 0.82, 0.72, 1.08, 1.08, 1.12)$$

Table A.3 lists the performance requirements, nominal values $\bar{\zeta}$ and standard deviations $\sigma(\zeta)$ of the damping ratios of the first 11 modes for the minimum sensitivity design and the minimum gain design. The nominal values and standard deviations in the table were obtained using the first order technique of section A.2.1.

We observe that the minimum gain design has all modes close to critical, and 5 modes are critical to 3 significant figures (modes 2 and 4). The minimum sensitivity design, on the other hand has only 2 modes almost critical, and only one of them is critical to 3 significant digits (mode number 2). All other constraints are satisfied with comfortable margins. We also observe that the standard deviation of the damping ratio of the critical mode (number 2) has been reduced by a factor of more than 2.3 in the minimum sensitivity design, while the corresponding mean value is the same in both designs. This shows that the robustness has again been targeted onto the most critical response quantity.

Table A.3. Space truss, minimum gain and minimum sensitivity designs.

| | | Minimum Gain Design | | Minimum Sensitivity Design | |
|---|---|---|---|---|---|
| mode | $\zeta^R$ (%) | $\bar{\zeta}$ (%) | $\sigma(\zeta)$ (%) | $\bar{\zeta}$ (%) | $\sigma(\zeta)$ (%) |
| 1 | 4.09 | 4.09* | 0.19 | 12.29 | 0.60 |
| 2 | 4.00 | 4.00* | 0.40 | 4.03* | 0.17 |
| 3 | 2.05 | 2.38 | 0.15 | 8.38 | 0.74 |
| 4 | 1.09 | 1.09* | 0.08 | 1.13 | 0.08 |
| 5 | 0.77 | 0.96 | 0.05 | 2.15 | 0.09 |
| 6 | 0.59 | 0.61 | 0.03 | 1.58 | 0.07 |
| 7 | 0.53 | 0.53* | 0.17 | 1.51 | 0.08 |
| 8 | 0.51 | 0.51* | 0.16 | 1.10 | 0.09 |
| 9 | 0.36 | 0.40 | 0.04 | 0.99 | 0.10 |
| 10 | 0.35 | 0.43 | 0.03 | 1.04 | 0.08 |
| 11 | 0.33 | 0.41 | 0.02 | 0.74 | 0.04 |

* Critical constraint.

Figure A.4 compares graphically the performance of the two designs. The horizontal axis shows the mode number, and the vertical axis gives the damping ratio of each mode, normalized by the corresponding required value. The horizontal line at $\zeta_k/\zeta_k^R = 1$ represents the required levels of damping. The bars represent the range of damping ratios corresponding to the nominal value plus and minus 3 standard deviations. The damping ratio of each mode of an actual structure has a 99.7% probability of falling inside these boxes.

As seen in Fig. A.4, the baseline design is unacceptably sensitive to the uncertainties. This is the result of two factors: first, almost all modes are critical or close to critical, so that any deviation from the nominal structure is likely to pull the damping ratios below the required values; and second, the sensitivities of some critical damping ratios (modes 2, 4, 7, and 8 in particular) are large so that uncertainties are likely to create large violations of the requirements.

The minimum sensitivity design on the other hand, is far better protected from the effects of uncertainties. The optimizer has made most modes non-critical by increasing the nominal values of their damping ratios (modes 7 and 8 in particular). Mode 2 has remained critical but has been made less sensitive to uncertainties as can be seen from the reduced value of its standard deviation. This protection has in effect been targeted on the critical mode in the final design (i.e.,

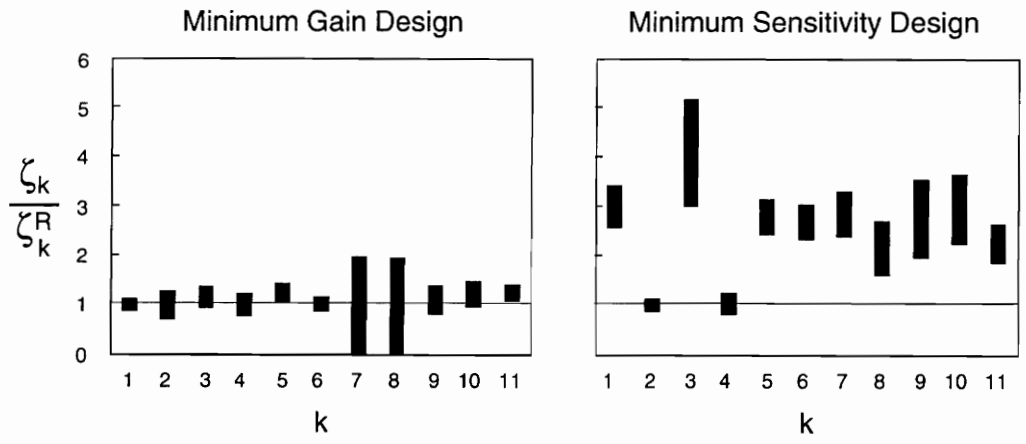


**Figure A.4. $\pm 3$ standard deviation intervals for minimum gain and minimum sensitivity designs.**

mode number 2). The design has been tailored in a way that favors critical modes at the expense of less critical ones. The sensitivities of the damping ratios of modes 1 and 3, for example, have increased, but their average value has been pushed away from the constraint limit so that the increased scatter is not likely to produce constraint violations. The net result of the optimization is a reduced probability for the design to violate performance requirements because of uncertainties in physical properties of the actual structure.

# Appendix B
# Non-Uniform Rod Element

In this appendix, we derive the mass matrix of a 3-dimensional, non-uniform, straight rod element, symmetric about its middle point. The element (see Fig. B.1) is defined by two nodes (1 and 2) with 3 translation degrees of freedom each (no bending allowed, this is a pinned-pinned rod element). The mass per unit length of the rod varies along the length of the member and will be denoted $m(s)$, where $s$ is a local coordinate defining a point along the axis of the rod. The length of the member is denoted $L$.

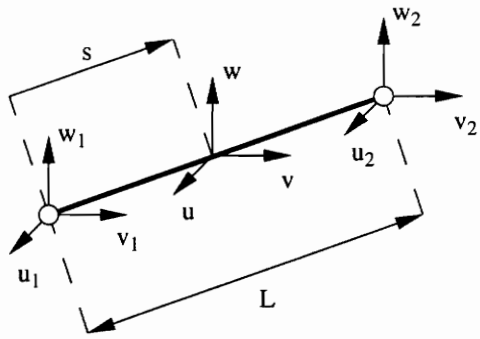


**Figure B.1. Non-uniform rod element.**

The components of displacement $\{u, v, w\}^T$ of any point along the rod axis, at a distance $s$ from node 1 are

$$\begin{Bmatrix} u \\ v \\ w \end{Bmatrix} = [N] \begin{Bmatrix} u_1 \\ v_1 \\ w_1 \\ u_2 \\ v_2 \\ w_2 \end{Bmatrix}, \tag{B.1}$$

where $\{u_1, v_1, w_1\}^T$ and $\{u_2, v_2, w_2\}^T$ are the degrees of freedom of nodes 1 and 2, respectively. The $3 \times 6$ matrix $[N]$ contains the interpolation functions

$$[N] = [\, \tfrac{L-s}{L} I_3 \quad \tfrac{s}{L} I_3 \,], \tag{B.2}$$

where $I_3$ stands for the $3 \times 3$ identity matrix.

The consistent mass matrix $[m]$ of the element is, by definition

$$[m] = \int_0^L m(s)[N]^T[N]\,ds\,. \tag{B.3}$$

Using Eq. B.2 for $[N]$ we find

$$\begin{aligned}[m] &= \begin{bmatrix} I_3 \frac{1}{L^2}\int_0^L m(s)(L-s)^2 ds & I_3 \frac{1}{L^2}\int_0^L m(s)s(L-s)ds \\ I_3 \frac{1}{L^2}\int_0^L m(s)s(L-s)ds & I_3 \frac{1}{L^2}\int_0^L m(s)s^2 ds \end{bmatrix} \\ &= \begin{bmatrix} I_3(\frac{M}{4} + \frac{J_0}{L^2}) & I_3(\frac{M}{4} - \frac{J_0}{L^2}) \\ I_3(\frac{M}{4} - \frac{J_0}{L^2}) & I_3(\frac{M}{4} + \frac{J_0}{L^2}) \end{bmatrix}, \end{aligned} \tag{B.4}$$

where $M = \int_0^L m(s)ds$ is the total mass of the member and $J_0 = 2\int_{L/2}^L m(s)(s - L/2)^2 ds$ is the moment of inertia of the member about its middle point (which is also the center of mass since the member is assumed symmetric). This expression of the mass matrix has the advantage to be based on directly measurable physical characteristics of the member. Note that for a rod with uniform mass distribution, Eq. (B.4) reduces to the usual expression

$$[m] = \frac{M}{6}\begin{bmatrix} 2I_3 & I_3 \\ I_3 & 2I_3 \end{bmatrix}. \tag{B.5}$$

Written in terms of the axial mechanical stiffness $K$ of the member, the stiffness matrix $[k]$ of this element is identical to that of a uniform rod element, i.e.

$$[k] = K\begin{bmatrix} [\kappa] & -[\kappa] \\ -[\kappa] & [\kappa] \end{bmatrix}, \tag{B.6}$$

where $[\kappa]$ is a function of the directional cosines $(cos\,\alpha, cos\,\beta, cos\,\gamma)$ of the rod axis with respect to the global axis system

$$[\kappa] = \begin{bmatrix} (cos\,\alpha)^2 & cos\,\alpha cos\,\beta & cos\,\alpha cos\,\gamma \\ cos\,\alpha cos\,\beta & (cos\,\beta)^2 & cos\,\beta cos\,\gamma \\ cos\,\alpha cos\,\gamma & cos\,\beta cos\,\gamma & (cos\,\gamma)^2 \end{bmatrix}. \tag{B.7}$$

# Appendix C
# Truss Model Refinement

The finite element model of the truss includes 9 complex stiffness springs that account for the flexibility of the support plates and the wall (Fig. C.1). Also, the internal damping of the truss members is modeled with a uniform structural loss factor. The stiffnesses and loss factors of the support springs and the uniform structural loss factor were not measured directly. Rather, they were adjusted to match experimental values of the first 3 natural frequencies $f_i^{exp}, i = 1, \ldots, 3$ and damping ratios $\zeta_i^{exp}, i = 1, \ldots, 3$ of the structure.

This model tuning is performed automatically. The tuning problem is formulated as a least square error minimization, using the following assumptions:

(1) All 3 support springs aligned in the $x$ direction (1, 4 and 7) have stiffnesses equal to $k_x$. The springs in the $y$ direction (2, 5 and 8) have stiffnesses equal to $k_y$ and those in the $z$ direction (3, 6, and 9) have stiffnesses equal to $k_z$.

(2) All 9 support springs have the same loss factor, equal to $\eta_w$.

(3) The loss factor of all truss members is equal to $\eta_s$.

These 5 parameters $k_x$, $k_y$, $k_z$, $\eta_w$, and $\eta_s$ constitute the 5 design variables of the error minimization problem. The objective is to minimize a compound error function $E$ defined as

$$E = \sum_{i=1}^{3} W_{f_i} \left( f_i^{exp} - f_i^{anal} \right)^2 + \sum_{i=1}^{3} W_{\zeta_i} \left( \zeta_i^{exp} - \zeta_i^{anal} \right)^2 , \qquad \text{(C.1)}$$

where $f_i^{anal}$ and $\zeta_i^{anal}$ are the natural frequencies and the damping ratios predicted by the model being adjusted. The weights $W_{f_i}$ and $W_{\zeta_i}$ are used to adjust the relative importance of the different components of the error.

The second mode of the structure proved troublesome in the experiment. Its measured damping ratio is about 10 times larger than in the other 2 modes. This is believed to be due to

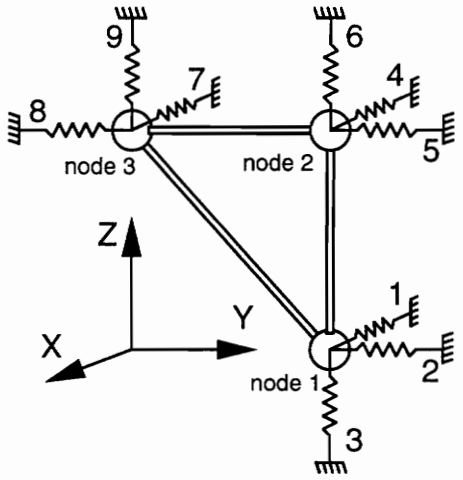


**Figure C.1. Support springs included in the FEM model.**

coupling with the dynamics of the wall. If we tried to adjust the predicted damping of that mode to the measured value, we would be artificially boosting the loss factors of the support springs and structure. For that reason, we chose to ignore the value of the damping ratio of the second mode in the fit. This is achieved by setting the weight $W_{\zeta_2}$ to zero.

With $W_{\zeta_2} = 0$, we are minimizing the errors in 3 natural frequencies and 2 damping ratios. Note that 3 of our 5 design variables ($k_x$, $k_y$, and $k_z$) give us direct control on frequencies and the remaining 2 ($\eta_w$ and $\eta_s$) control the amount of damping. This makes the error minimization problem very well conditioned and provides in most cases a unique solution, with zero residual error.

Using this procedure, we obtain an adjusted model that predicts all 3 natural frequencies and the damping ratios of the first and third mode with zero error.

# Appendix D

# Optimum Locations of Discrete Devices on Truss Structures

This appendix describes methods for finding optimal locations for discrete devices such as sensors, actuators or tuning masses on truss structures. Such problems are discrete in nature because these peripherals have to be attached to truss members or nodes. The problem of finding their optimal locations is a combinatorial optimization problem.

Combinatorial optimization problems are difficult to solve, and so various techniques have been developed for taking advantage of special features in particular applications to alleviate the computational burden. Standard methods available for combinatorial optimization have also been used in spite of the high computational cost. The first part of this appendix presents a survey of some of the methods that have been used, focusing on methods, rather than on surveying all the scores of papers that have been published. Then, we present applications of two methods we have used for solving such problems: integer programming and genetic algorithms.

## *D.1 Review of Available Methods*

**Continuous approximation** One approach consists of replacing the discrete problem with a continuous one by letting the peripherals move over an entire domain, and then find a nearby discrete solution. This approach was taken, for example, by Maghami and Joshi[83] for placing actuators along a beam truss, and by Burdisso and Haftka[84] for placing actuators on an antenna backup structure to minimize geometric shape distortions due to manufacturing errors in the truss members. For this last problem, Fig. D.1 shows an example of the position of the actuators obtained by continuous optimization, the nearby discrete solution, and one of the optima obtained by solving directly the combinatorial problem. The performance index $g$, given for each design, measures the reduction in average shape error. It is seen that it is not easy to translate the

continuous optimum into a discrete selection, and that this discrete selection is not necessarily optimal. The loss in performance associated with using a continuous optimization was found to be small. However, the computational advantage of the continuous optimization method was not substantial either.

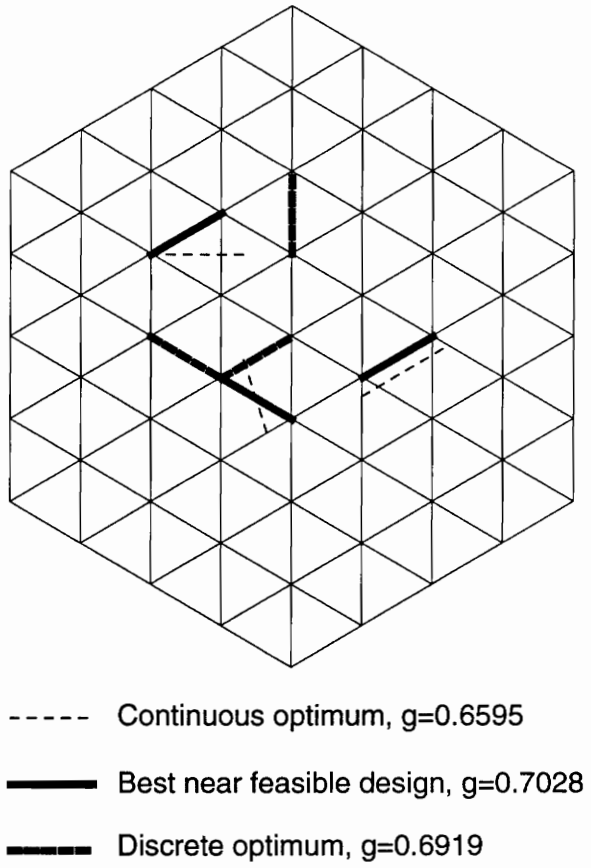


**Figure D.1. Optimum actuator locations for static shape control of antenna structure.**

**Specialized sub-optimal methods** Another type of approach for dealing with the combinatorial problem at a reduced cost is to use ad-hoc methods that do not require large computational cost. For example, Skelton and DeLorenzo[85] studied the optimal placement of actuators in a truss; they suggested starting with a configuration with an actuator at every available location, and then removing one by one the least effective actuators. This method is inexpensive, but can lead to designs that are far from optimal. Haftka and Adelman[86] suggested another ad-hoc method called ESPS that gave near optimal designs for actuator placement for static shape control. The

ESPS approach was coupled with an efficient reanalysis procedure that took advantage of the fact that the method changes the position of a single actuator at a time. However, these ad-hoc methods have one great disadvantage in that one always wonders about the quality of the results they produce.

**Preselection** Another way of taking advantage of the idiosyncrasies of the problems at hand is to develop effectiveness indices for the possible peripheral locations. Consider, for example, the problem of selecting locations of active members or damping treatments for increasing the damping in a selected number of vibration modes. It can be easily shown (e.g., Preumont *et al.*.[78]) that a truss member is a good site for an active member or damping treatment if it contributes substantially to the elastic energy associated with the vibration modes of interest. Thus, a logical strategy for reducing the size of the combinatorial problem is to consider only members that contribute more than a chosen threshold to the elastic energy of at least one mode. For static shape control a similar approach has been used to develop member effectiveness indices (Haftka[87]).

**Linear programming** When the effect of each device is small the total effect provided by several devices is approximately additive. The problem then reduces to finding locations that maximize the sum of the individual contributions. This is a linear integer programming problem, and can be solved by standard software. This type of approach has been used by Ponslet *et al.*.[88] and Padula *et al.*[89] for placing active members. It is detailed in section D.2.1.

All the above methods attempt to simplify the combinatorial optimization problem. The risk in using any of these methods is that the solution may not be optimal. Random search techniques try to solve the combinatorial problem directly, possibly at great computational cost. Several random search techniques are available for solution of combinatorial problems. Here we discuss two that simulate physical processes - simulated annealing and genetic algorithms.

**Simulated annealing** Simulated annealing mimics the process of solidification of metals, where a number of solid states with different internal atomic or crystalline structure that correspond to different energy levels can be achieved, depending on the rate of cooling. If the system is cooled rapidly, it is likely that atoms will reach an energy state which is only locally minimal. In order to reach a more stable, globally minimum energy state, the process of annealing is used, in which the metal is reheated to a high temperature and cooled slowly, allowing the atoms enough time to

find positions that minimize the potential energy. At a given temperature the system may use the thermal energy to jump temporarily to a higher energy state before finding a lower energy state. It is this characteristic of the annealing process which makes it possible to achieve near global minimum energy states.

A computational algorithm that simulates the annealing process was proposed by Metropolis *et al.*[90]. At a given temperature, $T$, the algorithm perturbs the position of an atom randomly and computes the resulting change in the energy of the system, $\Delta E$. If the new energy state is lower than the initial state, then the new configuration of the atoms is accepted. If, on the other hand $\Delta E \geq 0$, the perturbed state causes an increase in the energy, the new state might be accepted or rejected based on a random probabilistic decision. The probability of acceptance, $\mathcal{P}(\Delta E)$, of a higher energy state is computed as

$$\mathcal{P}(\Delta E) = e^{\left(\frac{-\Delta E}{k_B T}\right)}, \tag{D.1}$$

where $k_B$ is Boltzmann's constant. If the temperature of the system is high, then the probability of acceptance of a higher energy state is close to one. If, on the other hand, the temperature is close to zero, then the probability of acceptance becomes very small.

The analogy between the simulated annealing and the optimization of functions with many variables was established recently by several authors. By replacing the energy state with an objective function $f$, and using variables $x$ for the configurations of the particles, we can apply the algorithm to optimization problems. The method requires only function values. The moves in the design space from one point to another cause a change in the objective function, $\Delta f$. The temperature $T$ now becomes a control parameter that regulates the convergence of the process. Important elements that affect the performance of the algorithm are the selection of the initial value of the "temperature", $T_0$, and its update schedule. In addition, the number of iterations (or combinations of design variables) needed to achieve "thermal equilibrium" must be decided before the $T$ can be reduced. These parameters are collectively referred to as the "cooling schedule". Once the temperature is set, a number of moves in the variable space is performed by perturbing the design. The number of moves at a given temperature must be large enough to allow the solution to escape from a local minimum.

The application of simulated annealing to optimal placement problems is quite straight forward. The only requirement is to select a reasonable procedure for perturbing the design by

moving an actuator from one location to another. For example, Chen *et al.*[91] applied simulated annealing to the placement of active and passive members. They selected at random one of the locations occupied by an active/passive member, and moved it at random to one of the unoccupied locations.

**Genetic algorithms** Genetic algorithms mimic the principle of Darwin's theory of survival of the fittest. When a population of biological creatures evolves over generations, individual characteristics that are useful for survival tend to be passed on to future generations, because individuals carrying them get more chances to breed. Those individual characteristics in biological populations are stored in chromosomal strings. The mechanics of natural genetics is based on operations that result in structured yet randomized exchange of genetic information (i.e., useful traits) between the chromosomal strings of the reproducing parents, and consists of *reproduction*, *crossover*, and occasional *mutation* of the chromosomal strings.

Genetic algorithms, developed by Holland[56], simulate the mechanics of natural genetics for artificial systems based on operations which are the counterparts of the natural ones (and are even called by the same names). Application of the operators of the genetic algorithm to a search problem first requires the representation of the possible combinations of the variables in terms of strings that are counterparts of the chromosomes. Naturally, the measure of goodness of a specific combination of genes is represented in an artificial system by the objective function of the search problem.

Because of the string representation of the variables, genetic algorithms are ideally suited for problems where the variables are required to take discrete or integer values. Often we can represent the design by several forms of coding. For the problem of placing peripherals at $n$ possible locations we can have a string of $n$ bits with ones representing occupied locations and zeroes representing unoccupied locations. If we have $m$ peripherals to place, another possible representation is a string of $m$ numbers each varying from 1 to $n$ that indicate at which locations peripherals are placed. These $n$ numbers can be coded either in a decimal form or in a binary form and assembled into a string of integers or a longer string of binary bits. The choice of a particular coding can have a large influence on the performance of the search. We compare three different codings in the last section of this paper.

Unlike most search algorithms which move from one point to another in the design variable space, genetic algorithms work with a population of candidate designs (strings). The population

evolves from generation to generation and the fitness of its individuals improves gradually. This aspect of the genetic algorithms is responsible for capturing near global solutions, by keeping many solution points that may have the potential of being close to minima (local or global) in the pool during the search process rather than singling out a point early in the process and running the risk of getting stuck at a local minimum. Also, the outcome of a genetic search is a population of good designs rather than a single design. Thus the designer can obtain several designs to compare in terms of criteria which were not formulated as part of the optimization problem. This aspect can be very useful to the designer because often criteria and constraints are left out of an optimization formulation because of their complexity, because of uncertainties about their effect on performance or because the designer did not think about them.

Initially the size of the population is chosen and a population of designs is generated randomly. The next important step in the process is *reproduction*, in which individual designs with good objective function values are selected as parents for a new generation of designs. The bias towards designs with better performance is achieved by increasing the probability of their selection in relation to the rest of the population. This is often done by creating a biased roulette wheel where individual strings occupy areas proportional to their objective function values (for a maximization) or to their rank in the population.

Next, the parents selected are paired off for *crossover*. The mating of the pair also involves a random process. Typically, a random integer $k$ between 1 and $L-1$, where $L$ is the string length, is selected and two new strings are generated by exchanging the numbers that come after the $k$th location in the first parent with the corresponding locations of the second parent. For example, with the two binary strings of length $L = 9$

**parent 1** : *0 1 1 0 1* || *0 1 1 1*

**parent 2** : 0 1 0 0 1 || 0 0 0 1

mated with a crossover point of $k = 5$, the offsprings have the following composition,

**offspring 1** : *0 1 1 0 1* 0 0 0 1

**offspring 2** : 0 1 0 0 1 *0 1 1 1*

There exist several other variants of crossover operators, but all try to implement the idea of exchanging features between successful designs in the hope of generating even better designs that combine "good" features of both parents.

*Mutation* serves an important task of preventing premature loss of important genetic traits by occasionally introducing random alterations in designs. The reproduction process tends to favor the design characteristics of the best individuals in the original population. Good characteristics of the poorer designs can be lost. For example, if a particular location which corresponds to an optimum design was present in the original population only in a design that was otherwise poor, this location can be lost if this design never gets selected as a parent. If no mutation is used in a genetic search, the population tends to become uniform at an early stage to the point where all individuals in the population are identical. Any further reproduction results in offsprings that are perfect clones of their parent designs. Mutation prevents this difficulty by introducing new genetic information, and is implemented by randomly changing some genes in the design string.

Rao et al.[92] applied a genetic algorithm to the problem of selecting three active member locations in a ten bar truss, using zero/one coding for occupied/unoccupied locations. Onoda and Hanawa[93] described a simulated annealing algorithm with some features of a genetic algorithm and applied it to the selection of actuator locations on a 234-member truss structure. In section D.2.2, we describe an application of genetic algorithms to placing tuning masses on a laboratory structure for the purpose of driving the lowest two frequencies to be as close together as possible.

# *D.2 Examples of Applications*

## D.2.1 Optimal Locations of Active Members in a Truss by Linear Programming

The space truss shown in Fig. D.2 has 207 members and 71 nodes. It is a large H-shaped beam-truss assembled from a repeated pyramidal bay. All bars have the same length (0.500 meter), except for the diagonals of the square bases which are $\sqrt{2}$ times longer (0.707 meter). The truss was modeled with 207 rod elements. It is free floating and its model contains a total of 213 degrees of freedom.

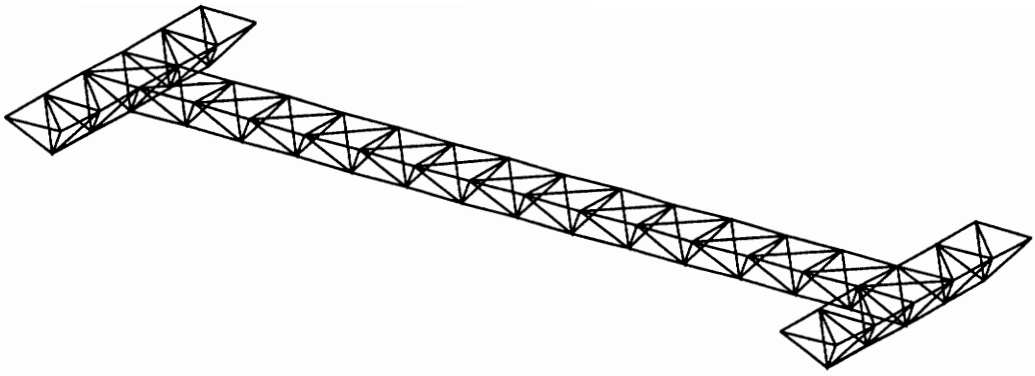

**Figure D.2. Space truss.**

**Table D.1. Space truss, undamped natural frequencies.**

| mode | 1 | 2 | 3 | 4 | 5 | 6 | 7 | 8 | 9 | 10 | 11 |
|---|---|---|---|---|---|---|---|---|---|---|---|
| $f_n$ (Hz) | 4.7 | 8.7 | 9.3 | 17.5 | 24.9 | 32.0 | 36.4 | 37.9 | 53.1 | 55.2 | 57.1 |

The natural frequencies of the first 11 modes of the undamped structure are as listed in table D.1.

Eight integral feedback active members[78,79] are to be included in the truss to provide damping. The active members consist of collocated piezoelectric actuators and force sensors with a local feedback. The voltage applied to the actuator is proportional to the integral with respect to time of the measured axial force in the member. The actuator responds to the applied voltage with a change in its natural length. The $90^o$ phase shift (due to the integration) between the mechanical load in the member and the change in length of the actuator produces damping in the structure.

Considering the controlled structure as a small perturbation from the uncontrolled structure and using a linear expansion of the eigenvalues, it can be shown[79] that the damping ratio $\zeta_m$ of the $m$th mode of the structure equipped with 8 active members is approximately equal to

$$\zeta_m \approx \frac{1}{2\omega_m} \sum_{i=1}^{8} g_i \nu_{im} k_i \,, \tag{D.2}$$

where $\omega_m$ is the natural frequency of the $m$th mode, $g_i$ is the gain of the $i$th active member, $k_i$ is the mechanical stiffness of that active member, and $\nu_{im}$ is the fraction of modal strain energy

in the $i$th member of the truss deformed under the $m$th mode shape. Note that $\omega_m$ and $\nu_{im}$ are evaluated in the original truss, without active members; they can be computed in advance for use in the optimization. The accuracy of the approximation D.2 is excellent for relatively small values of the damping ratios; it will be demonstrated in Tables D.2 and D.3 for the optimal configurations.

Expression D.2 is linear in the gains $g_i$. If we consider all 207 members of the truss as candidate locations for active members, we can define 207 *decision variables* $e_j$ that decide whether any of the truss members is active. The variables $e_j$ can only be equal to 0 or 1. A value of 1 identifies member #$j$ as an active member while a value of 0 corresponds to a regular member. With these variables and assuming a uniform value $g$ for the gains of all active members, Eq. D.2 can be rewritten

$$\zeta_m \approx \frac{g}{2\omega_m} \sum_{j=1}^{207} \nu_{jm} k_j e_j \,, \tag{D.3}$$

where the sum now extends to all members of the truss. This last expression is linear in the decision variables $e_j$.

**Design for maximum damping ratio** We first consider the problem of maximizing the damping ratio in the first 11 natural modes of the truss. Using expression D.3 for the damping ratios, this problem can be formulated as a standard linear integer programming problem

$$\begin{aligned}
\textbf{Find} \quad & e_j,\ j = 1,\ldots,207 \quad \text{and} \quad \zeta \\
\textbf{to maximize} \quad & \zeta \\
\textbf{such that} \quad & \zeta_m = \frac{g}{2\omega_m} \sum_{j=1}^{207} \nu_{jm} k_j e_j \geq \zeta, \quad m = 1,\ldots,11 \\
\textbf{and} \quad & \sum_{j=1}^{207} e_j = 8 \,.
\end{aligned} \tag{D.4}$$

The calculation of the damping ratios at every iteration consists of a simple matrix multiplication, using the precomputed values of the strain energies. The value of the gain $g$ of the active members was set to $5 \times 10^{-6}$ m/Ns (note, however, that the optimal configuration does not depend on that value). The problem was solved using LINDO[94] (branch and bound algorithm). Because of the very large design space, the search was limited to 4000 branches and 50000 pivots so that the final design is not guaranteed to be optimal.

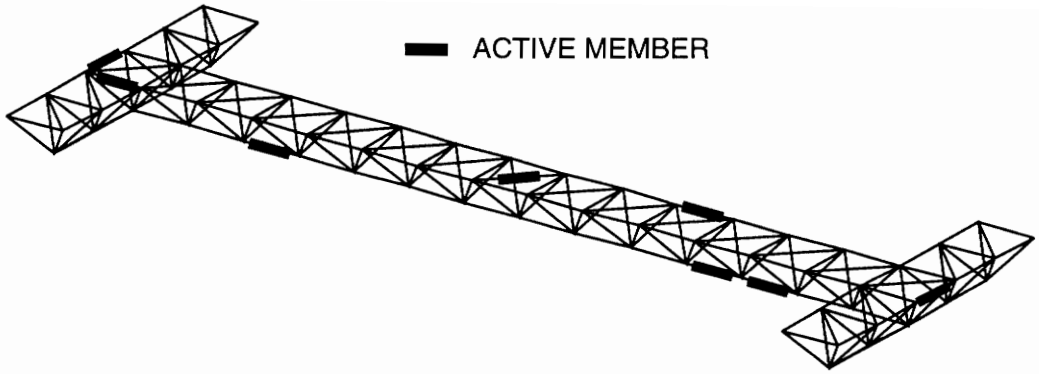


**Figure D.3. Optimal locations for maximum damping ratio.**

**Table D.2. Space truss, design for maximum damping ratio.**

| | **Damping ratio** (%) | | **Decay rate** ($sec^{-1}$) | |
|---|---|---|---|---|
| mode | approx. | exact | approx | exact |
| 1 | 2.20 | 2.20 | - | 0.64 |
| 2 | 2.64 | 2.61 | - | 1.42 |
| 3 | 4.35 | 4.39 | - | 2.57 |
| 4 | 2.09 | 2.09 | - | 2.29 |
| 5 | 1.12 | 1.12 | - | 1.75 |
| 6 | 1.52 | 1.52 | - | 3.06 |
| 7 | 1.36 | 1.36 | - | 3.11 |
| 8 | 1.18 | 1.28 | - | 3.05 |
| 9 | 1.16 | 1.16 | - | 3.87 |
| 10 | 1.21 | 1.21 | - | 4.21 |
| 11 | 1.12 | 1.12 | - | 4.00 |
| 12 | - | 0.10 | - | 0.46 |
| 13 | - | 0.11 | - | 0.49 |
| 14 | - | 0.09 | - | 0.40 |
| 15 | - | 0.04 | - | 0.19 |

The optimization resulted in the locations shown in Fig. D.3. The damping ratios obtained with that configuration are listed in table D.2. The table lists the damping ratios of the first 15 modes of the truss, as obtained from the approximation formula (Eq. D.3) and from a full analysis. The decay rates are also listed in the table. We can see that all 11 first modes have at least 1.12% relative damping. Note that modes 12 to 15 (which were not optimized) have only

about 0.1% damping. Comparing the approximate damping to the "exact" values, we see that the largest error is only about 0.03% out of 2.61% in the damping ratio of mode 2. This corresponds to less than 1.2% relative error and demonstrates the accuracy of the approximation.

**Design for maximum decay rate** From table D.2, it is clear that, because of the wide range of natural frequencies of the first 11 modes of the truss, the decay rate is fairly non-uniform. In reaction to a disturbance, the amplitudes of vibration of the different modes of the structure would then decrease exponentially at very different rates so that the high frequency modes would damp out much faster than lower frequency modes. In view of this, we might want to uniformize the decay rate of the different modes. This can be achieved by modifying the formulation of Eq. D.4 to maximize the smallest decay rate. The decay rate $d_m$ of a natural mode $m$ is equal to the product of the damping ratio $\zeta_m$ of that mode by the undamped natural frequency $\omega_m$, i.e.

$$d_m = \omega_m \zeta_m \,. \tag{D.5}$$

Using again the first order approximation of Eq. D.3, we formulate the optimal location problem for 8 active members as a linear integer programming problem

$$\begin{aligned} \textbf{Find} \quad & e_j,\ j = 1,\ldots,207 \quad \text{and} \quad d \\ \textbf{to maximize} \quad & d \\ \textbf{such that} \quad & d_m = \frac{g}{2} \sum_{j=1}^{207} \nu_{jm} k_j e_j \geq d, \quad m = 1,\ldots,11 \\ \textbf{and} \quad & \sum_{j=1}^{207} e_j = 8 \,. \end{aligned} \tag{D.6}$$

This problem was solved with LINDO and provided the configuration of Fig. D.4. Table D.3 lists the damping ratios and decay rates of the first 15 modes of the structure. Note that the decay rates are now much more uniform, with a minimum value of 1.74 $\text{sec}^{-1}$. Again, modes 12 to 15 have not been included in the formulation and their decay rates are much smaller (less than 0.42 $\text{sec}^{-1}$). Finally, the quality of the approximation is again demonstrated by the excellent aggreement between the approximate and "exact" decay rates.

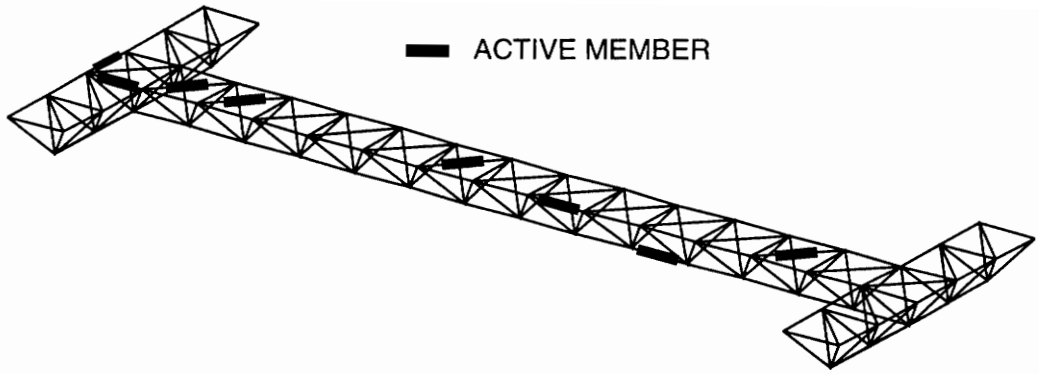


**Figure D.4. Optimal locations for maximum decay rate.**

**Table D.3. Space truss, design for maximum decay rate.**

| | **Damping ratio** (%) | | **Decay rate** ($sec^{-1}$) | |
|---|---|---|---|---|
| mode | approx. | exact | approx | exact |
| 1 | - | 6.95 | 2.04 | 2.04 |
| 2 | - | 3.18 | 1.76 | 1.74 |
| 3 | - | 4.03 | 2.33 | 2.35 |
| 4 | - | 1.64 | 1.80 | 1.80 |
| 5 | - | 1.73 | 2.71 | 2.71 |
| 6 | - | 0.98 | 1.98 | 1.98 |
| 7 | - | 0.89 | 2.03 | 2.02 |
| 8 | - | 0.76 | 1.82 | 1.81 |
| 9 | - | 0.63 | 2.10 | 2.10 |
| 10 | - | 0.55 | 1.93 | 1.92 |
| 11 | - | 0.55 | 1.98 | 1.98 |
| 12 | - | 0.06 | - | 0.25 |
| 13 | - | 0.09 | - | 0.42 |
| 14 | - | 0.03 | - | 0.15 |
| 15 | - | 0.05 | - | 0.23 |

## D.2.2 Optimal Locations of Tuning Masses in a Truss Using a Genetic Algorithm

The laboratory truss shown in Fig. D.5 was designed for experimental research on large space structures. To simulate closely spaced frequencies characteristic of large space structures,

the first two natural frequencies were brought together by adding tuning masses at proper locations on the structure. The masses are steel bars with a specific mass, and the positions are in parallel to the truss elements, so that the problem of finding optimal locations is of combinatorial nature, and is solved using a genetic algorithm.

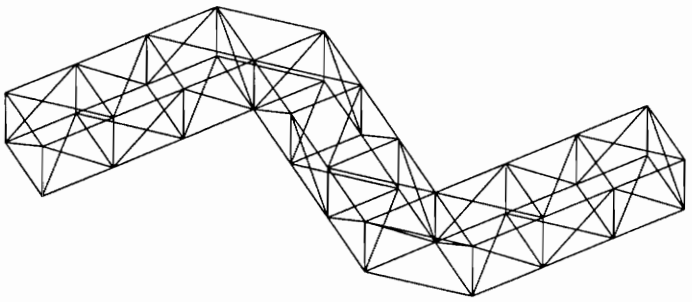

**Figure D.5. Laboratory truss.**

The structure (Fig. D.5) is a Z-shaped space truss made of 128 tubular aluminum members and 44 spherical nodes. A 0.254 meter (10 in.) cubical bay is used as a building block. The total mass of the structure is 18.8 kg (41.4 lbs). The structure is in a free-free condition. A finite element model predicted the natural frequencies listed in Table D.4.

**Table D.4. Natural frequencies of structure without tuning masses.**

| mode | frequency (Hz) |
|---|---|
| 1 | 66.06 |
| 2 | 86.98 |
| 3 | 110.88 |

The separation between mode 1 and mode 2 is more than 20 Hz; the objective of this optimization is to minimize the frequency separation by adding extra masses to the structure. Each mass has a magnitude of 2.63 Kg (5.8 lbs) and is modelled by increasing the mass per unit length of an existing member.

The frequencies of any configuration of added masses are evaluated by solving the eigenvalue problem using a subspace iteration technique. Because the structure is free in space,

calculating the elastic modes requires also the use of the rigid body modes. The starting vectors of the subspace iteration are the mode shapes of the last analysed configuration. Since these are rough approximations to the solution, the convergence of the method is relatively fast. The calculation of the lowest 3 natural frequencies requires about 380 CPU milliseconds on an IBM 3090.

**Optimum locations of 8 masses** As a first step in this study we decided to determine optimum locations for 8 masses in our laboratory truss. The masses can be joined to any truss member for a total of 128 possible locations. The size of the feasible design space is $C_{128}^{8} = 1.43 \times 10^{12}$ (where $C_j^i$ denotes the number of combinations of $i$ elements in a set of $j$ elements). The objective function is defined as

$$f = 100. - (f_2 - f_1), \tag{D.7}$$

where $f_1$ and $f_2$ are the first and second natural frequencies in Hz and 100 is added to make $f$ strictly positive for convenience. Maximizing $f$ is equivalent to minimizing the frequency separation from mode 1 to mode 2.

To implement the genetic algorithm, we first need to define a string representation for the location of the masses. In this first step the position of each mass in the truss is coded as a 7 bit binary number, with 8 such substrings put together to form a $7 \times 8 = 56$ bit chromosome that completely defines the locations of the 8 added masses. For example, a configuration with 3 masses added at locations number 12, 72 and 128 is coded as: 0001011 1000111 1111111 (1 is first substracted from the location number to obtain a number between 0 and 127 which is then coded in binary form).

With the coding described above, it is possible for the genetic operators to generate designs where more than one mass is assigned to a unique location. These infeasible designs were discarded. We use a 2-point crossover where two cutting points are randomly selected and the substring between these points is exchanged between the parents. The selection uses a ranking strategy by which the area attributed to each design on the roulette wheel (and therefore its probability of selection) is proportional to its rank in the population. Also, we used an elitist strategy where the best design of every generation is always directly copied into the next generation. No

1. Create initial population of $n_d$ random designs.
2. Rank the individuals according to the value of the fitness function.
3. Copy the best design into the next generation.
4. Apply a linear roulette wheel selection rule to pick two parents: the probability of selection of an individual for breeding is proportional to its rank in the population.
5. Create one offspring by applying a two-point crossover to the parents (two cut points are selected at random and the substrings between these cuts are exchanged between parents).
6. Perform random mutations in the offspring chromosome (the probability for any given gene in the chromosome to mutate is denoted as $p_m$)
7. If the resulting design is infeasible (more than one mass at one location), discard it and return to step 5.
8. Repeat steps 4–7 until $n_d$ feasible designs have been generated for the new generation.
9. If generation number is less than $n_{gen}$ go to step 2.
10. Select the best design in the current population and stop.

**Figure D.6. Genetic algorithm for locating tuning masses.**

convergence check is used and the search is simply stopped after a specified number of generations ($n_{gen}$). The probability of mutation was set to $p_m$ =1%, the population size to $n_d = 50$ and the number of generations to $n_{gen} = 50$. The genetic algorithm is summarized in Fig. D.6.

The results and convergence histories of one search are presented in Figure D.7. The frequency separation has been reduced to 0.1 Hz. Only 2,500 analyses were performed to achieve this result. This means that less than $2 \times 10^{-7}$% of the $1.43 \times 10^{12}$ feasible designs have been evaluated.

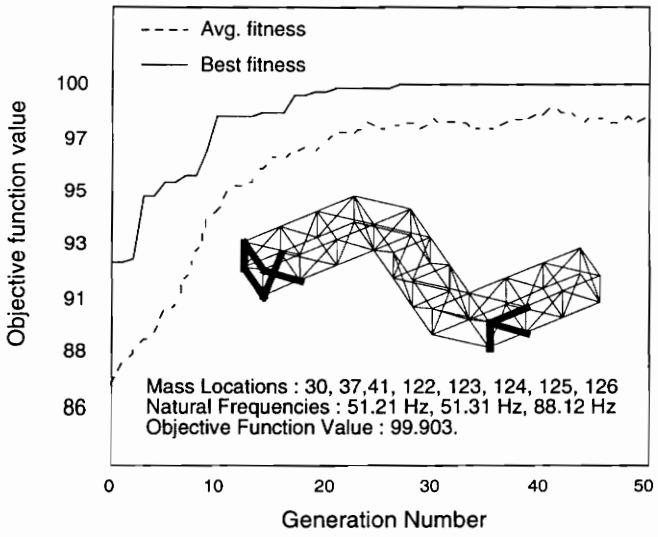


**Figure D.7. Location of 8 tuning masses, convergence history and optimal design.**

**Optimum locations of a minimum number of masses** Since the optimum designs with eight masses gave us frequency separations as small as 0.1 Hz, we checked whether the number of masses cannot be reduced. We modified the algorithm to decide on the number of masses needed by minimizing both the number of masses added in the structure and the frequency separation. This was done by adding one logical bit to each 7 bit substring of our chromosome. The value of that additional bit indicates the presence (1) or absence (0) of a mass at the location coded in the remaining 7 bits. By doing this, we increase the size of our chromosome to $8 \times 8 = 64$ bits. The size of the feasible design space has also increased to $\sum_{i=0}^{8} C_{128}^{i} = 1.5 \times 10^{12}$, since we are now searching for designs with any number of masses between 0 and 8.

Since we now allow for a variable number of masses, it might seem more natural to use a string of 128 zero/one variables for the absence/presence of an added mass at each member location. However, using such a representation not only doubles the length of the chromosome but also increases the size of the design space by more than 26 orders of magnitude ($\sum_{i=0}^{128} C_{128}^{i} = 3.4 \times 10^{38}$ instead of $1.5 \times 10^{12}$) because it allows for any number of masses between 0 and 128. As expected, when we tried using the 0/1 coding in the same algorithm we observed much slower convergence than with the adopted coding.

The objective function was modified to

$$f = 100. - (f_2 - f_1) - \alpha\, n, \tag{D.8}$$

where $n$ is the number of masses added in the structure and $\alpha$ (Hz) is a penalty parameter. The value of $\alpha$ (chosen as 0.5) specifies how much we are willing to lose in frequency closeness for each mass we save. After some tuning, the parameters of the algorithm were set to $n_d = 100$, $n_{gen} = 100$ and $p_m = 2\%$. This implies that no more than $10,000$ designs will be tested during the search which represents less than $6.5\ 10^{-7}$ % of the feasible design space.

A specific *local mutation* was used in the last 30 generations instead of the random mutation described before, to improve the final convergence rate of the algorithm. It was found that after about 50 generations, the population was quite uniform and that further improvement was very slow. The effect of the random mutation is to displace one or more masses from its current location to any other location in the structure. Since it is assumed that the algorithm has found the vicinity of an optimum, such drastic change is not likely to improve the design. Clearly, what is needed at this stage is fine tuning the position of the masses around their current locations. This fine tuning is provided by the *local mutation operator.* It randomly changes the locations of the masses within a limited range around their current locations. In the example studied here, the range was set to $\pm 12$. This allows the masses to move approximately one bay away on either side of their current location. This operator was found to help final convergence.

With these changes the algorithm reduced the number of masses from 8 to 7 in most cases. Table D.5 gives a set of results obtained from repeated runs of the algorithm. The designs listed in the table are the best design in the final population of each run. Note that each final population contains many other designs that perform almost as well and can be useful in practical situations. Figure D.8 shows the mass locations for some of the best designs of table D.5. A genetic algorithm being a random search, the results should not be expected to be strictly optimum. Rather, a pool of near-optimum designs is generated. Some designs have 8 masses and others have only 7, although their objective function values are almost the same. This allows the designer to choose whichever design is the most appropriate when other considerations are taken into account.

**Comparison with other codings** As mentioned earlier, several options are available to code a given design into a string of numbers to be used as the chromosome of a genetic search. Also, it

Table D.5. Optimum designs with variable number of masses.

| run | n | $f_1$ | $f_2$ | $f_3$ | $\Delta f_{21}$ | obj.fct. |
|---|---|---|---|---|---|---|
| 1 | 7 | 52.95 | 53.41 | 90.79 | 0.465 | 96.035 |
| 2 | 8 | 51.21 | 51.28 | 89.79 | 0.072 | 95.928 |
| 3 | 7 | 53.64 | 53.73 | 92.14 | 0.092 | 96.408 |
| 4 | 7 | 53.39 | 53.44 | 91.81 | 0.048 | 96.452 |
| 5 | 7 | 53.11 | 53.38 | 90.25 | 0.264 | 96.236 |

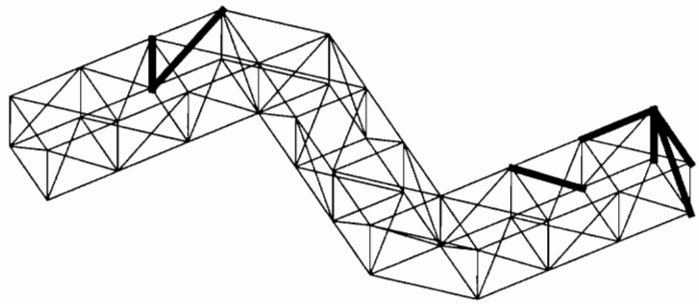

**Design 4** : freq. separation = 0.048 Hz
7 Masses at locations : 1, 2, 3, 7, 23, 97, 101.

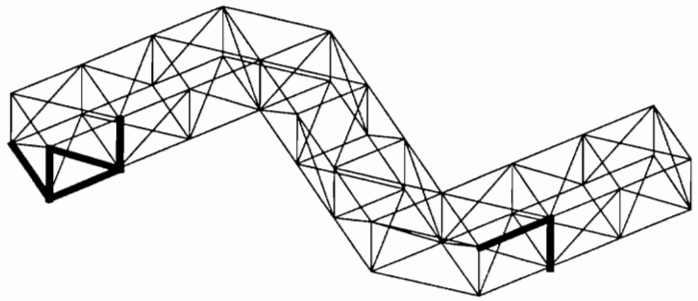

**Design 3** : freq. separation = 0.092 Hz
7 Masses at locations : 29, 30, 115, 118, 123, 126, 127.

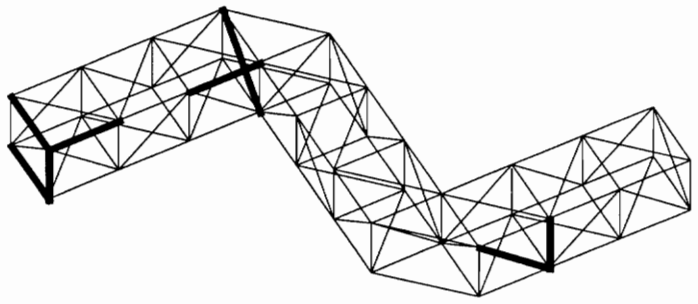

**Design 2** : freq. separation = 0.072 Hz
8 Masses at locations : 29, 37, 87, 92, 116, 124, 126, 127.

Figure D.8. Three designs with variable number of masses.

is clear that the choice of a particular coding is a determining factor in the efficiency of the search. Although the binary coding used for the previous results was found to perform satisfactorily, we wanted to evaluate the performance of two alternative codings: the *Gray Code* and the *integer coding*. A fourth option has been used for similar but smaller problems (Rao et al.[92]) and consists of a string of $n$ logical 0/1 variables that define the absence/presence of a mass at each of $n$ candidate locations. This technique is not readily applicable to problems with a large number of candidate locations and a fixed number of peripherals, because the crossover operation would almost always generate designs with a number of peripherals different from the required number. For that reason, we do not include the 0/1 formulation in this comparison.

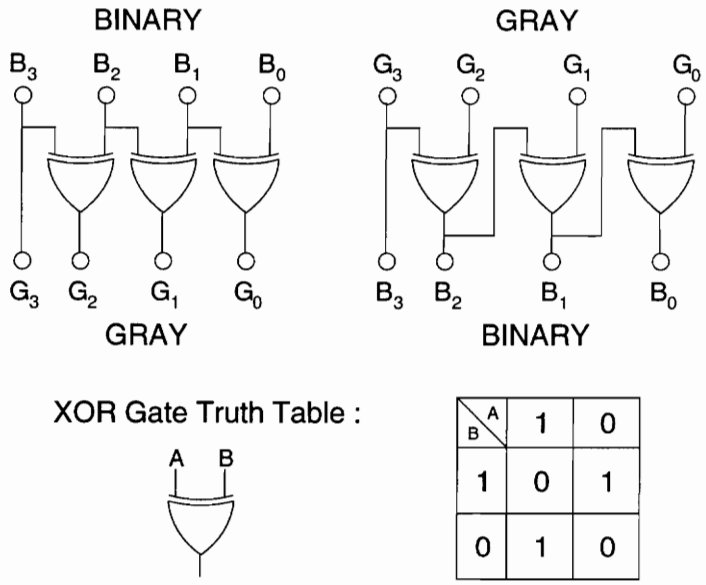


**Figure D.9. Binary to Gray and Gray to binary conversions.**

The Gray code is another form of binary representation commonly used for electronic applications (see for example Greenfield[95]). We use this unusual coding because of an unfavorable characteristic of the base-2 representation: when going from one decimal number to the next, the base-2 string often switches from mostly ones to mostly zeros. On the contrary, in the Gray code an increment or decrement of one always corresponds to changing the value of only one bit (note that for the same reason the Gray code is used in digital counters, where the base-2 binary coding would create ambiguity because of non-simultaneous switching of the different

bits). For example, going from 63 to 64 decimal value implies going from 0111111 to 1000000 in a 7 bit, base-2 coding. The corresponding representations in the Gray code are: 0100000 and 1100000. This characteristic of the base-2 binary representation is thought to be detrimental to the performance of a genetic algorithm, because the operators of the reproduction process are very unlikely to generate such radical changes in the chromosome. The search then tends to leave "unexplored areas" in the design space. Decimal to Gray and Gray to decimal conversions are easily performed by using the base-2 code as an intermediate step. The transformations between base-2 binary and Gray code are performed by an array of simulated exclusive OR gates (XOR) as shown in Fig. D.9.

The use of binary codings creates the need for repetitive conversions to and from the decimal counterpart and increases the complexity of the algorithm. A more natural representation for placement problems is to use a string of integer numbers in decimal form as described earlier. One possible difficulty when using a decimal string is the lack of diversity in the initial random population: if the size of the population is much smaller than the number of candidate locations, the initial pool of designs will only sample a subset of the possible locations. If the crossover is performed by simply exchanging substrings between parents then the mutation is the only source of new genetic information and the search will tend to remain limited to the initial subset. This does not happen with the binary coding because the crossover is allowed to cut into any of the 7 bit substrings, thereby introducing new locations in the population. This difficulty with the integer coding can be alleviated by defining a special *averaging crossover* operator. In this new operator, one gene location is selected at random. The substrings on either side of but not including that location are then exchanged between parents as in the regular crossover. The value of the remaining gene of the offspring is generated as a weighted average of the parent genes. This process is illustrated in the following example. Suppose two parents have been selected for reproduction

**parent 1** : *2 58 3 102 74 82 1 7*

**parent 2** : 6 18 99 26 128 7 9 21

A random *real* number $r$ is generated, say $r = 3.7$. The truncated value of $r$ determines the cutting point in the string as 3. The substrings $[1 \ldots 3]$ and $[5 \ldots 8]$ are exchanged between parents. The remaining gene number 4 is then created as the weighted average of genes number

4 of both parents according to the value of $r$:

$$\begin{aligned} \text{gene 4 of offspring} &= (4 - 3.7) * (\text{gene 4 of parent 1}) \\ &+ (3.7 - 3) * (\text{gene 4 of parent 2}) \\ &= 0.3 * 102 + 0.7 * 26 = 49 \end{aligned} \tag{D.9}$$

The resulting offspring chromosome is :

**offspring :** *2 58 3* **49** 128 7 9 21

With this specialized operator, new genetic information is introduced in every reproduction so that the design space is satisfactorily explored to locate the optimum.

To compare the relative efficiencies of these three formulations (base-2 binary, Gray and integer) we considered again our problem of optimal location of exactly 8 masses in the laboratory truss. The objective function is expressed as in Eq. D.7.

The size of the population was set to $n_d = 50$ and the number of iterations to $n_{gen} = 50$ for a total number of analyses per run equal to $2,500$. The mutation rates were chosen as 1% for the base-2 binary and the Gray code. With this rate, each one of the 8 masses has a 7% chance of being displaced by mutation. For the integer formulation, since the mutation applies to decimal locations rather than bits, the mutation rate was set to 7%. The local mutation operator described previously was used in the last 10 generations with a probability of 15% per mass.

Since the outcome of a genetic search is essentially random, any comparison has to be based on a relatively large number of results. This implies a very large number of analyses and potentially enormous computational cost. For this reason and for the purpose of comparing our three formulations we used an approximate modal analysis using 20 natural mode shapes of the original structure (without any added mass). The exact analysis is performed only once at the beginning of the algorithm and the resulting eigenvectors are used to build approximate eigenproblems in all subsequent analyses. The approximate analysis of one configuration uses about 20 CPU milliseconds on an IBM 3090.

We performed 20 optimizations with each formulation. The distributions of residual frequency separation of the best individual of the final populations are plotted in figure D.10 for

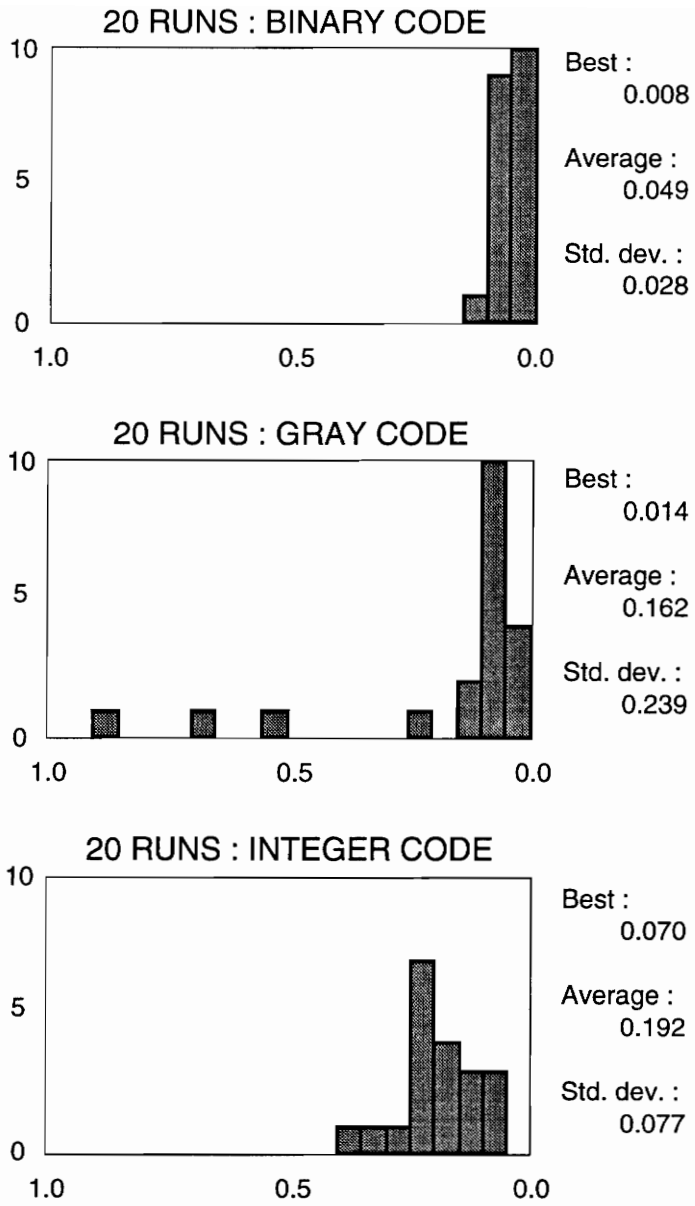


**Figure D.10. Distributions of frequency separation of best design; 20 optimization runs with each coding; the fitness of the best design is plotted versus the number of occurrences.**

each coding. The maximum, mean value and standard deviations of these results are listed next to each plot. Surprisingly, the base-2 binary code seems to perform better than the Gray code on this problem. Note, however, that a fair comparison would require optimizing the parameters

of the algorithm (mutation rate, population size, etc...) for each formulation before comparing their results. Unfortunately this is a very difficult task since there exists no deterministic way of evaluating optimum parameters for genetic algorithms. The integer formulation does not perform as well as the binary code but the difference in the quality of the final designs is insignificant when compared to the expected accuracy of the calculated frequencies. The integer coding also presents the advantage of being significantly easier to implement.

# Appendix E
# Truss Model Data

This appendix provides the detailed numerical data used in the Finite Element model. Direction vectors of the attachment holes, node coordinates and boundary conditions, member connectivities and properties and analytical-experimental correction factors are listed. All physical values are given in the MKSI unit system ($m$, $kg$, $s$, $N$).

## *E.1 Direction Vectors*

Directional cosines of the 9 available orientations for tuned dampers, with respect to the global axis system

| DIR | X | Y | Z |
|---|---|---|---|
| 1 | 1.00000 | 0.00000 | 0.00000 |
| 2 | 0.00000 | 1.00000 | 0.00000 |
| 3 | 0.00000 | 0.00000 | 1.00000 |
| 4 | 0.00000 | 0.70711 | 0.70711 |
| 5 | 0.00000 | -0.70711 | 0.70711 |
| 6 | 0.70711 | 0.50000 | 0.50000 |
| 7 | 0.70711 | -0.50000 | 0.50000 |
| 8 | -0.70711 | -0.50000 | 0.50000 |
| 9 | -0.70711 | 0.50000 | 0.50000 |

## *E.2 General Data*

```
NUMBER OF NODES    :  21
NUMBER OF MEMBERS  :  39
NUMBER OF SUPPORTS :  27
NUMBER OF DOFS     :  36
MEMBER MASS FLAG   :   0 (CONSISTENT, NON-UNIF)
```

## E.3 Grid Points Data

The coordinates in global axes of the grid points and the amount of lumped mass (in $kg$) at each node are given below (the lumped mass given here corresponds to the mass of the physical nodes only, the mass of the members is given further and is modeled using consistent matrices). Three support codes are also given for each node, and define whether each of the 3 degrees of freedom (in directions x, y, and z) is free (0) or locked (1).

| NODE | X COORD | Y COORD | Z COORD | CONC.MASS | SUPPORT |
|---|---|---|---|---|---|
| 1 | 0.000000 | 0.254000 | 0.000000 | 0.088620 | 0 0 0 |
| 2 | 0.000000 | 0.254000 | 0.254000 | 0.088620 | 0 0 0 |
| 3 | 0.000000 | 0.000000 | 0.254000 | 0.088620 | 0 0 0 |
| 4 | 0.179605 | 0.127000 | 0.127000 | 0.088620 | 0 0 0 |
| 5 | 0.179605 | 0.127000 | 0.381000 | 0.088620 | 0 0 0 |
| 6 | 0.179605 | -0.127000 | 0.381000 | 0.098270 | 0 0 0 |
| 7 | 0.359210 | 0.000000 | 0.254000 | 0.088620 | 0 0 0 |
| 8 | 0.359210 | 0.000000 | 0.508000 | 0.088620 | 0 0 0 |
| 9 | 0.359210 | -0.254000 | 0.508000 | 0.088620 | 0 0 0 |
| 10 | 0.538815 | -0.127000 | 0.381000 | 0.088620 | 0 0 0 |
| 11 | 0.538815 | -0.127000 | 0.635000 | 0.090970 | 0 0 0 |
| 12 | 0.538815 | -0.381000 | 0.635000 | 0.093320 | 0 0 0 |
| ---------- | WALL ENDS OF SUPPORT SPRINGS | ---------- | | | |
| 13 | -0.025400 | 0.254000 | 0.000000 | 0.000000 | 1 1 1 |
| 14 | 0.000000 | 0.279400 | 0.000000 | 0.000000 | 1 1 1 |
| 15 | 0.000000 | 0.254000 | 0.025400 | 0.000000 | 1 1 1 |
| 16 | -0.025400 | 0.254000 | 0.254000 | 0.000000 | 1 1 1 |
| 17 | 0.000000 | 0.279400 | 0.254000 | 0.000000 | 1 1 1 |
| 18 | 0.000000 | 0.254000 | 0.279400 | 0.000000 | 1 1 1 |
| 19 | -0.025400 | 0.000000 | 0.254000 | 0.000000 | 1 1 1 |
| 20 | 0.000000 | 0.025400 | 0.254000 | 0.000000 | 1 1 1 |
| 21 | 0.000000 | 0.000000 | 0.279400 | 0.000000 | 1 1 1 |

## E.4 Member Data

The following table lists the member connectivities, mechanical stiffnesses (in $N/m$), total mass (in $kg$), rotational mass inertia about an axis orthogonal to the longitudinal axis of the

member at the center of gravity (middle point) (in $kg\,m^2$), and the loss factor (non-dimensional). The members are modeled as non-uniform rod elements as described in Appendix B.

| MEMBER | NODES | | STIFFNESS | MASS | INERTIA | LOSS FACT |
|---|---|---|---|---|---|---|
| 1 | 1 | 2 | 0.2251E+08 | 0.1096E+00 | 0.5097E-03 | 0.1323E-02 |
| 2 | 1 | 3 | 0.1482E+08 | 0.1282E+00 | 0.1556E-02 | 0.1323E-02 |
| 3 | 2 | 3 | 0.2251E+08 | 0.1096E+00 | 0.5097E-03 | 0.1323E-02 |
| 4 | 1 | 4 | 0.2251E+08 | 0.1096E+00 | 0.5097E-03 | 0.1323E-02 |
| 5 | 2 | 4 | 0.2251E+08 | 0.1096E+00 | 0.5097E-03 | 0.1323E-02 |
| 6 | 3 | 4 | 0.2251E+08 | 0.1096E+00 | 0.5097E-03 | 0.1323E-02 |
| 7 | 2 | 5 | 0.2251E+08 | 0.1096E+00 | 0.5097E-03 | 0.1323E-02 |
| 8 | 3 | 5 | 0.2251E+08 | 0.1096E+00 | 0.5097E-03 | 0.1323E-02 |
| 9 | 3 | 6 | 0.2251E+08 | 0.1096E+00 | 0.5097E-03 | 0.1323E-02 |
| 10 | 4 | 5 | 0.2251E+08 | 0.1096E+00 | 0.5097E-03 | 0.1323E-02 |
| 11 | 4 | 6 | 0.1482E+08 | 0.1282E+00 | 0.1556E-02 | 0.1323E-02 |
| 12 | 5 | 6 | 0.2251E+08 | 0.1096E+00 | 0.5097E-03 | 0.1323E-02 |
| 13 | 4 | 7 | 0.2251E+08 | 0.1096E+00 | 0.5097E-03 | 0.1323E-02 |
| 14 | 5 | 7 | 0.2251E+08 | 0.1096E+00 | 0.5097E-03 | 0.1323E-02 |
| 15 | 6 | 7 | 0.2251E+08 | 0.1096E+00 | 0.5097E-03 | 0.1323E-02 |
| 16 | 5 | 8 | 0.2251E+08 | 0.1096E+00 | 0.5097E-03 | 0.1323E-02 |
| 17 | 6 | 8 | 0.2251E+08 | 0.1096E+00 | 0.5097E-03 | 0.1323E-02 |
| 18 | 6 | 9 | 0.2251E+08 | 0.1096E+00 | 0.5097E-03 | 0.1323E-02 |
| 19 | 7 | 8 | 0.2251E+08 | 0.1096E+00 | 0.5097E-03 | 0.1323E-02 |
| 20 | 7 | 9 | 0.1482E+08 | 0.1282E+00 | 0.1556E-02 | 0.1323E-02 |
| 21 | 8 | 9 | 0.2251E+08 | 0.1096E+00 | 0.5097E-03 | 0.1323E-02 |
| 22 | 7 | 10 | 0.2251E+08 | 0.1096E+00 | 0.5097E-03 | 0.1323E-02 |
| 23 | 8 | 10 | 0.2251E+08 | 0.1096E+00 | 0.5097E-03 | 0.1323E-02 |
| 24 | 9 | 10 | 0.2251E+08 | 0.1096E+00 | 0.5097E-03 | 0.1323E-02 |
| 25 | 8 | 11 | 0.2251E+08 | 0.1096E+00 | 0.5097E-03 | 0.1323E-02 |
| 26 | 9 | 11 | 0.2251E+08 | 0.1096E+00 | 0.5097E-03 | 0.1323E-02 |
| 27 | 9 | 12 | 0.2251E+08 | 0.1096E+00 | 0.5097E-03 | 0.1323E-02 |
| 28 | 10 | 11 | 0.2251E+08 | 0.1096E+00 | 0.5097E-03 | 0.1323E-02 |
| 29 | 10 | 12 | 0.1482E+08 | 0.1282E+00 | 0.1556E-02 | 0.1323E-02 |
| 30 | 11 | 12 | 0.2251E+08 | 0.1096E+00 | 0.5097E-03 | 0.1323E-02 |
| ---------- SUPPORT SPRINGS ---------- | | | | | | |
| 31 | 13 | 1 | 0.1488E+09 | 0.0000E+00 | 0.0000E+00 | 0.1824E-01 |
| 32 | 14 | 1 | 0.5728E+08 | 0.0000E+00 | 0.0000E+00 | 0.1824E-01 |
| 33 | 15 | 1 | 0.1240E+09 | 0.0000E+00 | 0.0000E+00 | 0.1824E-01 |
| 34 | 16 | 2 | 0.1488E+09 | 0.0000E+00 | 0.0000E+00 | 0.1824E-01 |
| 35 | 17 | 2 | 0.5728E+08 | 0.0000E+00 | 0.0000E+00 | 0.1824E-01 |

| | | | | | | |
|---|---|---|---|---|---|---|
| 36 | 18 | 2 | 0.1240E+09 | 0.0000E+00 | 0.0000E+00 | 0.1824E-01 |
| 37 | 19 | 3 | 0.1488E+09 | 0.0000E+00 | 0.0000E+00 | 0.1824E-01 |
| 38 | 20 | 3 | 0.5728E+08 | 0.0000E+00 | 0.0000E+00 | 0.1824E-01 |
| 39 | 21 | 3 | 0.1240E+09 | 0.0000E+00 | 0.0000E+00 | 0.1824E-01 |

## *E.5 Excitation and Response Data*

This table lists the locations and orientations of the excitation point (load cell) and the response pickup point (accelerometer) for each of the 3 first modes. Also listed are the definitions of the frequency windows for the acceleration limits.

| | DRIVING POINT | | RESPONSE PICKUP | | FREQUENCY WINDOWS | |
|---|---|---|---|---|---|---|
| MODE | NODE | DIR | NODE | DIR | FMIN | FMAX |
| 1 | 6 | 1 | 12 | 4 | 75.0 | 105.0 |
| 2 | 6 | 1 | 12 | 8 | 120.0 | 140.0 |
| 3 | 6 | 1 | 11 | 8 | 155.0 | 200.0 |

## *E.6 Analytical-Experimental Corrections*

In Chapter 5, the peak amplitudes $H_{peak}$ obtained analytically were applied a correction based on the model calibration. The correction is linear and the corrected value $H^{\star}_{peak}$ is defined by the equation

$$H^{*}_{peak} = AH_{peak} + B\,, \tag{E.1}$$

where A (non-dimensional) and B ($m/Ns^2$) are constant coefficients. The values of those coefficients depend on the mode considered and the type of analysis used; they are listed below.

| SEMI-ANALYTICAL APPROXIMATION | | |
|---|---|---|
| MODE | A | B |
| 1 | 0.9447 | -0.7116 |
| 3 | 1.2750 | -0.4611 |

FULL ORDER ANALYSIS

| MODE | A | B |
|---|---|---|
| 1 | 1.3680 | -0.7678 |
| 3 | 0.9486 | -0.5953 |

## *E.7 Natural Frequencies and Damping Ratios*

The natural frequencies and damping ratios of the first 10 modes for the truss with inherent damping only are listed below as obtained from the finite element analysis.

| MODE | W [RD/SEC] | FREQ [HZ] | DAMPING [%] |
|---|---|---|---|
| 1 | 631.041 | 100.433 | 0.162 |
| 2 | 814.776 | 129.676 | 0.151 |
| 3 | 1215.268 | 193.416 | 0.090 |
| 4 | 2787.212 | 443.599 | 0.093 |
| 5 | 3037.742 | 483.472 | 0.146 |
| 6 | 3411.686 | 542.987 | 0.148 |
| 7 | 3785.804 | 602.529 | 0.103 |
| 8 | 5030.331 | 800.602 | 0.083 |
| 9 | 5866.908 | 933.747 | 0.143 |
| 10 | 6542.271 | 1041.235 | 0.094 |

# Vita

Eric Ponslet was born in Brussels, Belgium, on the 29th of September, 1964. His interest in technology dates back to early days when he engaged in technical hobbies which would eventually lead him to the "Faculté des Sciences Appliquées", at the University of Brussels. He graduated in July 1987 with a degree in Mechanical and Electrical engineering (5 year program). His thesis work was devoted to the design and manufacture of an experimental articulated robot arm.

During the next year, he worked as an assistant in the newly created Department of Mechanical Engineering and Robotics of the same university under the guidance of Professor André Preumont. In 1989, he fulfilled his military duties in the Mechanical Engineering Department of the Royal Military Academy of Belgium.

In January 1990, he enrolled in the Ph.D. program in Aerospace Engineering at Virginia Tech. In the Summer of 1991, he was a visiting researcher in the Spacecraft Dynamics Branch at NASA Langley Research Center.